NPS-EC-01-008

NAVAL POSTGRADUATE SCHOOL
Monterey, California

Helicopter Payload Phase 1 Antenna Study

by

David C. Jenn

October 2001

Prepared for: SPAWAR PMW 189
San Diego, CA

NAVAL POSTGRADUATE SCHOOL
Monterey, California

Rear Admiral D. R. Ellison
Superintendent

R. Elster
Provost

This report was sponsored by SPAWAR PMW 189.

This report was prepared by:

REPORT DOCUMENTATION PAGE		Form Approved OMB No. 0704-0188

Public reporting burden for this collection of information is estimated to average 1 hour per response, including the time for reviewing instruction, searching existing data sources, gathering and maintaining the data needed, and completing and reviewing the collection of information. Send comments regarding this burden estimate or any other aspect of this collection of information, including suggestions for reducing this burden, to Washington headquarters Services, Directorate for Information Operations and Reports, 1215 Jefferson Davis Highway, Suite 1204, Arlington, VA 22202-4302, and to the Office of Management and Budget, Paperwork Reduction Project (0704-0188) Washington DC 20503.

1. AGENCY USE ONLY *(Leave blank)*	2. REPORT DATE	3. REPORT TYPE AND DATES COVERED
	September 1, 2001	Technical Report (January 2001 to September 2001)

4. TITLE AND SUBTITLE: Helicopter Payload Phase 1 Antenna Study	5. FUNDING NUMBERS
6. AUTHOR(S) David C. Jenn	
7. PERFORMING ORGANIZATION NAME(S) AND ADDRESS(ES) Naval Postgraduate School Monterey, CA 93943-5000	8. PERFORMING ORGANIZATION REPORT NUMBER NPS-EC-01-008
9. SPONSORING / MONITORING AGENCY NAME(S) AND ADDRESS(ES) SPAWAR PMW 189	10. SPONSORING / MONITORING AGENCY REPORT NUMBER

11. SUPPLEMENTARY NOTES The views expressed in this thesis are those of the author and do not reflect the official policy or position of the Department of Defense or the U.S. Government.

12a. DISTRIBUTION / AVAILABILITY STATEMENT	12b. DISTRIBUTION CODE
Distribution authorized to U.S Government Agencies and their contractors. Other requests for this document shall be referred to Superintendent, Naval Postgraduate School, Code N006, Monterey, CA 93943-5000 via the Defense Technical Information Center, 8725 John J. Kingman Road, STE 0944, Fort Belvoir, VA 22060-6218.	C

13. ABSTRACT

This study examines the performance of a communications antenna at various locations on an unmanned helicopter. The suitability of a location is determined by the quality of the antenna pattern, primarily field of view, which is defined as the range of angles over which the antenna gain is constant enough and/or sufficient enough to permit signal reception regardless of the direction of flight. The antenna performance when installed on the helicopter was simulated using the method of moments code PATCH and physical optics code APATCH. The simulated pattern data for the installed antenna was compared to that of the free standing antenna, which is used as a baseline from which to determine the effects of the antenna placement on signal reception. Antennas examined included (1) a short monopole and (2) a hemispherical pattern similar to the pattern of commercially available wideband annular slot antennas. The frequency range of interest is from 100 MHz to 1200 MHz.

14. SUBJECT TERMS	15. NUMBER OF PAGES
method of moments, physical optics, computational electromagnetics, antennas	68
	16. PRICE CODE

17. SECURITY CLASSIFICATION OF REPORT	18. SECURITY CLASSIFICATION OF THIS PAGE	19. SECURITY CLASSIFICATION OF ABSTRACT	20. LIMITATION OF ABSTRACT
Unclassified	Unclassified	Unclassified	UL

Table of Contents

1.0 Introduction

1.1 Background

The main role of the Helicopter is reconnaissance using a combination of sensors, primarily infrared and electro-optical (EO/IR) systems and a laser target designator. Data links on board are used to receive and send flight control commands as well as downloading and uploading sensor information. Microwave data links and many of the sensors require antennas. Antennas on the Helicopter have special design requirements, for example, small size and light weight. The location of the antennas are limited and therefore the field of view (antenna pattern coverage) is a primary design consideration. Figure 1 shows the locations of antennas (as of March 2001). The placement of an additional communications antenna should not adversely impact the performance of other onboard systems, yet the location must allow adequate communication system performance.

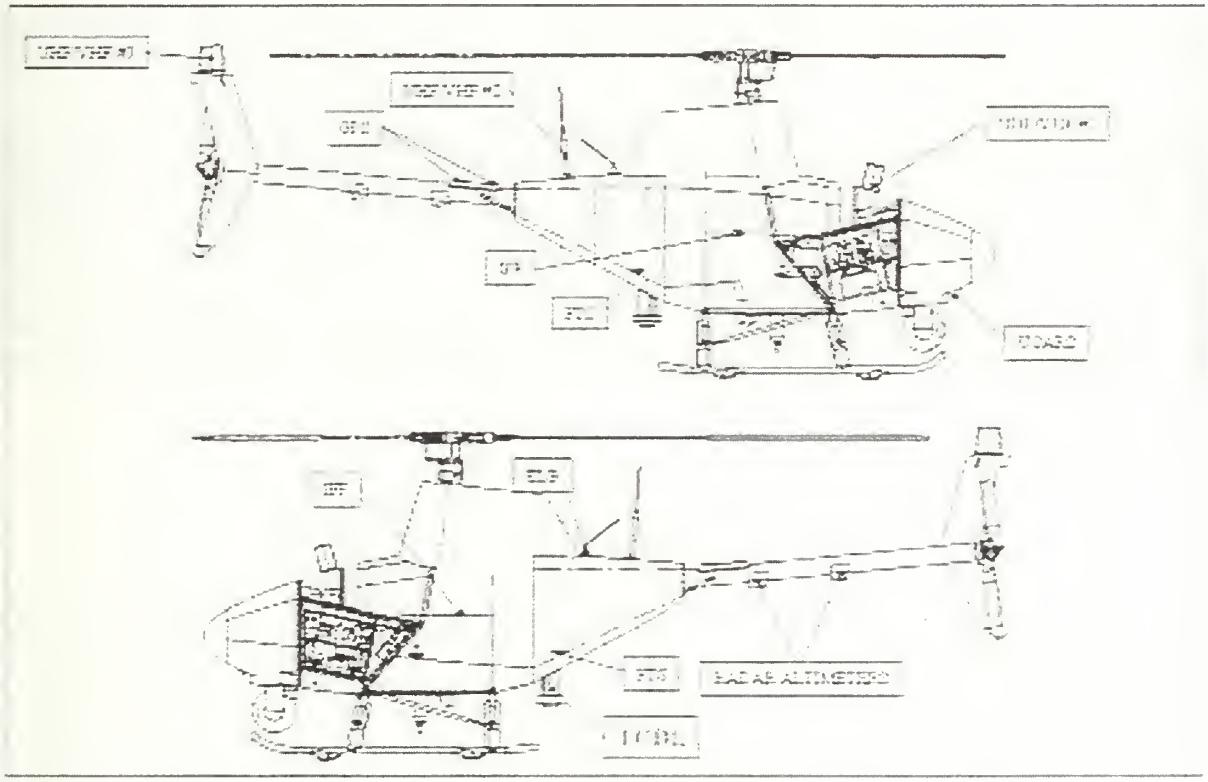

Figure 1: Proposed helicopter antenna locations (as of March 1, 2001).

There are several commercial of the shelf (COTS) systems that are under consideration for the payload. Although the systems are designed for ground based direction finding (DF), they should be suitable for use on a variety of helicopters. The systems employ small vertically polarized "disk-shaped" antennas about 15 inches in diameter with omni-directional azimuth patterns.

1.2 Objective

The objective of this study is to determine the optimum antenna placement given the available locations on the helicopter. The suitability of a location is determined by the quality of the antenna pattern, primarily field of view, which is defined as the range of angles over which the antenna gain is constant enough and/or sufficient enough to permit signal reception regardless of the direction of flight. The frequency range of interest is from 100 MHz to 1200 MHz.

1.3 Technical Approach

An analysis and simulation of the antenna installed on the helicopter was conducted using computational electromagnetics (CEM) codes. The simulated pattern data for the installed antenna was compared to that of the free standing antenna, which is used as a baseline from which to determine the effects of the antenna placement on signal reception. If the installed antenna pattern deviates significantly from the baseline antenna pattern, then the reception is potentially degraded. Furthermore, if DF is to be performed, then pattern deviations can lead to increased rms error. The antenna pattern is an indication of the DF system sensitivity as discussed in Appendix A.

Exactly what constitutes "significant degradation" of the pattern cannot be identified yet, primarily because the ability of receiver systems to respond to pattern nulls is not known, and therefore, the antenna's gain specification is not known. This report will consider a 10 dB reduction to be significant, and for the reader's convenience the pattern grids are spaced in 10 dB increments. With regard to DF, gain is not the only measure of antenna performance. Since the DF is based on phase sampling, phase errors introduced by the antenna's environment can also reduce DF capability. However, the effects of small phase errors can be eliminated by calibrating the system after it is installed on the helicopter.

2.0 Technical Background

2.1 Issues With Regard to Electromagnetic Modeling of the Antenna and helicopter

The electromagnetic modeling of antennas and complex structures is well understood and many codes exist to predict antenna performance. Although rigorous methods exist, they are usually limited in practice by computer memory and CPU speed. A rigorous method is one that is shown mathematically to converge to the "correct" value when properly applied. The rigorous methods are generally based differential or integral equations derived from Maxwell's equations and the boundary conditions. The integral or differential equation is converted to a set of simultaneous linear equations that can be solved using standard matrix methods.

Finite element methods (FEM) [1] and the method of moments (MM) [2] fall into the category of rigorous codes. They are applied by first discretizing the antenna and any surrounding structures to be modeled into subdomains. The subdomains are usually triangular facets for MM and tetrahedra for FEM. The currents on all subdomains are determined by solving a set of simultaneous equations. Therefore interactions between all currents on the body are included. Once the currents have been determined, the radiation integrals [3] can be used to find the fields.

For MM the size of the matrix is determined by the number of triangle edges. For a converged solution the general rule of thumb is that the triangle edges should not exceed 0.1λ, where λ is the wavelength. Thus computer memory and processing time can limit the size of an antenna problem that can be analyzed. Today's computers can handle bodies that are electrically small to moderate in size (10 to 20 wavelengths, depending on the amount of detail in the model).

Because of the computer limitations, approximate methods are applied to electrically large problems. For large bodies the traditional "high-frequency techniques" can be applied. The total field at an observer's location can be considered a superposition of fields that arrive by various propagation paths as depicted in Figure 2. They include:

1) direct
2) reflection (single and multiple reflections)
3) diffraction
4) surface waves

The rays are depicted as emanating from the antenna in the transmitting mode, however, by reciprocity, the same ray paths exist on receive. The scattering mechanisms such as diffraction make it possible to receive a signal when the direct line-of-sight to the antenna is blocked. Even if the line of sight is not completely blocked, multiple signal paths may exist, making constructive or destructive interference possible (commonly referred to as multipath). Multipath can lead to phase errors that degrade direction finding in phase comparison systems.

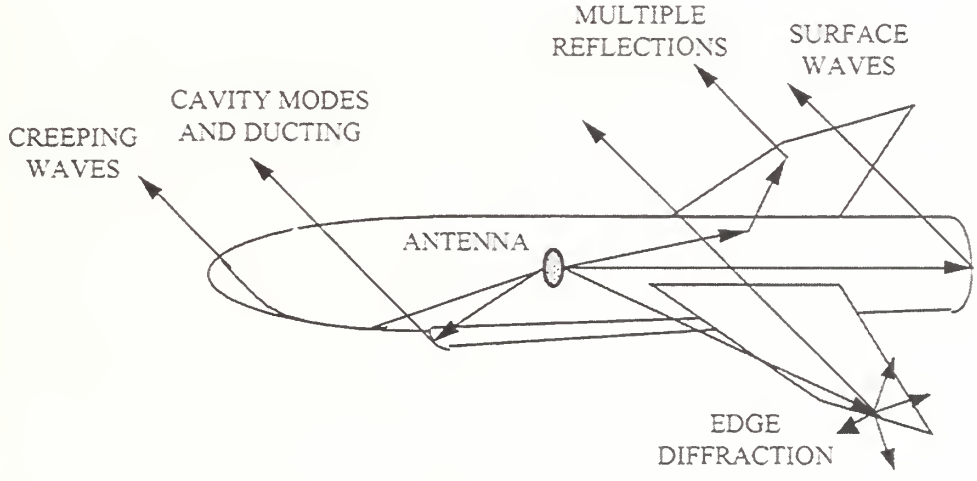

Figure 2: Illustration of several scattering mechanisms that may occur when the antenna is installed on the helicopter.

The antenna investigation was comprised of the following steps:

1. Develop a CAD model for the helicopter.
2. Develop a CAD model for the antenna.
3. Verify the antenna models by comparison with measured or published data.
4. Generate data for the antenna installed on helicopter.
5. Investigate the performance as a function of antenna location and frequency.

2.2 Candidate Computational Electromagnetics Codes

Computational electromagnetics (CEM) codes can be divided into two broad categories. The first category are those used to perform detailed antenna design and analysis. Codes in this category must be able to predict the effects of subtle geometric and material variations on the antenna performance. They are generally used in the early stages of the antenna design process to avoid multiple iterations of expensive prototyping.

The second category of computer codes are those used to predict the antenna's performance when it is in its operational environment; that is, when installed on the helicopter with other objects near it or in its field of view. These codes must be able to adequately model the interfering objects, an ability that generally occurs at the expense of the detailed antenna modeling capability. This is not due to any shortcoming in the electromagnetic theory, but it is a computational limitation imposed by the need for computer memory or practical computation times. In the second case, the impact on system performance is usually described by the change in the antenna pattern relative to what it would be in the isolated environment.

This research requires CEM codes of the second type. The performance of the antenna on a complex structure is of interest. (Complex structures are those with curved surfaces, edges, protrusions, and composite materials.) Several frequency domain codes are applicable to this problem. They are broadly grouped into the categories of approximate and rigorous methods. The codes and their capabilities are summarized in Table 1.

The frequencies of interest for the antenna analysis range from 100 MHz to 1200 MHz, and therefore the helicopter spans both the "low-frequency" (electrically small) and "high-frequency" (electrically large) regimes. For the low frequency region the MM code PATCH [4] is used. The accuracy of PATCH has been validated for a wide range of antenna and scattering problems.

Approximate codes ignore the higher order coupling, or approximate the higher order contributions by a series of correction terms. An example of this type of code is APATCH [5] which combines the physical optics approximation (PO) with the shooting and bouncing ray (SBR) technique to estimate multipath effects. SBR is a hybrid method that is used extensively in the calculation of the radar cross section (RCS) of large targets at high frequencies. It combines geometrical optics (GO) and physical optics, and can be supplemented by the physical theory of diffraction (PTD). Current distributions are determined from the trajectories of rays in a dense bundle. The current distributions can be used to:

1. initiate secondary rays to evaluate multiple reflections,
2. compute PTD fringe currents for edge diffraction contributions, and
3. compute the far scattered fields.

Currently this technique is the most accurate and flexible for computing the scattering that occurs from large complex bodies such as aircraft with engine inlets and cockpits. APATCH is the preferred code because of the inclusion of higher order scattering mechanisms, and its compatibility with computer aided design (CAD) software.

Code Name	Type	Advantages	Disadvantages
PATCH (Sandia Labs)	rigorous (MM)	• surface impedance • wide range of excitations • open source code • limited CAD interface	• computer limitations on both the high and low ends • no dielectrics • antenna/platform near field coupling included
FERM (Lincoln Labs)	rigorous (MM)	• all frequencies • surface impedance • wide range of excitations • multiple matrix solvers	• no directed CAD interface • limited geometry generator • no source code distribution • no longer supported (no updates)
NEC-BSC (Ohio State)	approximate (GO &GTD)	• ray tracing with higher order bounces • GO/GTD ray interaction • geometry viewer • limited to high frequencies	• no direct CAD interface • crude geometry and antenna models • some scattering mechanisms missing • limited dynamic range
APATCH (Demaco/SAIC) soon to be URBANA	approximate (PO & SBR)	• interfaces directly with CAD software • detailed target models possible • antenna gain tables • arrays of elemental radiators	• relatively high frequency • crude antenna models • antenna/platform near field coupling not included
FEKO (EMSS)	approximate (MM/hybrid)	• rigorous MM for low frequencies • hybrid approach for high frequencies • all types of material (electric & magnetic)	• expert system (steep learning curve) • limited antenna models • complicated antennas can be derived from collections of simple antennas
FASANT (U. of de Alcala)	approximate (GO &GTD)	• limited CAD interface • self contained PC software • GUI/menu driven • includes geometry generator and mesher	• new release – untried software • crude/simple antenna types • post-processing options appear to be limited

MM = method of moments
SBR = shooting and bouncing rays
PO = physical optics
GO = geometrical optics
GTD = geometrical theory of diffraction
ACAD = advanced computer aided design

Table 1: Summary of capabilities of candidate CEM codes.

2.3 Computer Aided Design (CAD)

Facet models can be generated using a computer aided design program named ACAD (Advanced Computer Aided Design) [6]. ACAD can read files in the IGES (International Graphics Exchange Standard) format, and therefore is capable of using databases generated by all of the major commercial CAD programs such as AutoCad or Versacad. The antenna and helicopter configurations are relatively easy to change using a CAD program, which simplifies investigations into the effect of antenna location and body material composition on antenna performance.

ACAD provides users with the ability to create and modify geometry in two- or three-dimensions. Users can choose to model geometry with wire frames, surfaces, or solids. ACAD is the primary tool used by Lockheed Fort Worth Company's Advanced Programs for configuration and subsystem design of new and existing aircraft programs. At the heart of the ACAD system is the associative database. In an associative database, geometry is linked together in a relational structure that remembers parent/child dependencies. This type of database enables rapid modifications of geometry, since modifying one geometric element automatically adjusts its dependencies based on a set of predefined rules. For instance, changing a control spline of a fuselage will automatically regenerate any surfaces built with the spline. In turn, any geometry that is associated to the fuselage surface (i.e., plane/curve and surface intersections, fillets) will automatically regenerate.

The helicopter and antenna models were built using ACAD. The auto-meshing capability was used to generate facet model files which could be translated and then ported to PATCH and APATCH for use in the pattern calculations.

2.4 Antenna Requirements

Several common measures of passive antenna performance are gain, pattern shape (field of view), input voltage standing wave ratio (VSWR), polarization, and bandwidth. For active antennas employing pre-amplification, signal-to-noise ratio (SNR) is a more accurate indicator of antenna performance than gain. Ground-based DF systems generally deal with radiation sources on the ground or on low flying aircraft. Therefore the desired pattern coverage is omni-directional (equal gain) in azimuth with the highest gain in the direction of the horizon (i.e., high gain at low elevations).

A common antenna used in a ground based application is the vertical monopole [7]. Pattern cuts for such an antenna are depicted in Figure 3. However for airborne installation a lower profile antenna is preferred. An ideal antenna type for the helicopter is an annular slot in a ground plane [7]. Most COTS antennas are of the annular slot type. Their patterns are more "hemispherical" than those in Figure 3 (i.e., without the deep null).
Referring to Figure 3, principal plane cuts (elevation and azimuth) are shown for a vertically polarized antenna setting on the ground and pointing up. Azimuth generally corresponds to compass angle and has values from 0 to 360 degrees measured in a clockwise direction from North (positive x axis). The elevation angle is measured from the horizon (0 degrees) to the zenith (directly above, 90 degrees). The elevation cuts shown are for two orthogonal planes, for example, north-south and east-west for a ground-based system.

For an airborne system looking at the ground the antenna pattern would be inverted. The aircraft coordinate system in straight and level flight is a convenient reference, as shown in Figure 4 for the helicopter. Azimuth has values from 0 to 360 degrees, as on the ground, but elevation varies from 0 degrees on the horizon to –90 degrees directly down. The highest gain values are still on the horizon, where the slant ranges to the emitters are greatest. The low gain directly below the aircraft is not a severe problem because of the relatively short range to the ground. Also, antennas installed on the aircraft may not have a null as deep as the one shown in Figure 3.

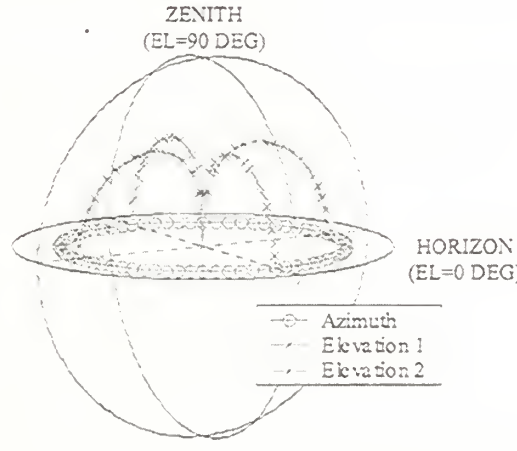

Figure 3: Azimuth and elevation cuts for a typical vertically polarized antenna setting on the ground and looking up (decibel scale).

Referring to Figure 5, the more convenient designations of pitch, roll and yaw planes are defined. The elevation cut for $\phi = 0^\circ$ and 180° (x-z plane) is called the pitch plane. The elevation cut for $\phi = 90^\circ$ and 270° (y-z plane) is called the roll plane. The azimuth cut for $\theta = 90^\circ$ (x-y plane) is also called the yaw plane. As the names indicate, pattern cuts in these planes represent rotations about the pitch, roll and yaw axes, respectively.

Figure 5 shows typical pitch, roll and yaw cuts in polar form for a dipole antenna rotated 20° from vertical in the pitch plane. Also shown is the direction of the θ component of the electric field vector. Note that vertically polarized vectors on the horizon are orthogonal at $\theta = 0^\circ$. Therefore the pattern levels are not equal along the z axis (i.e., the gain curves do not intersect). All patterns shown in this report are for θ polarization.

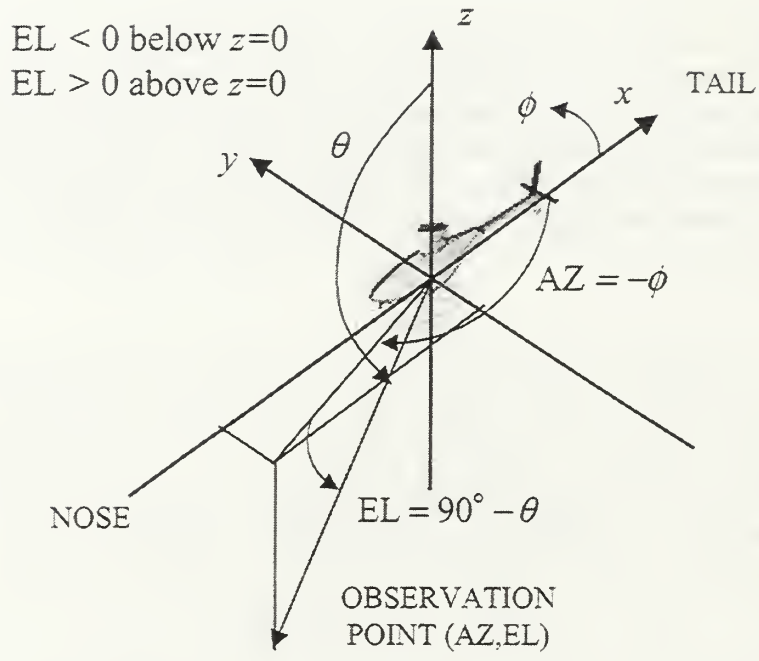

Figure 4: Azimuth and elevation coordinates referenced to the helicopter in straight and level flight.

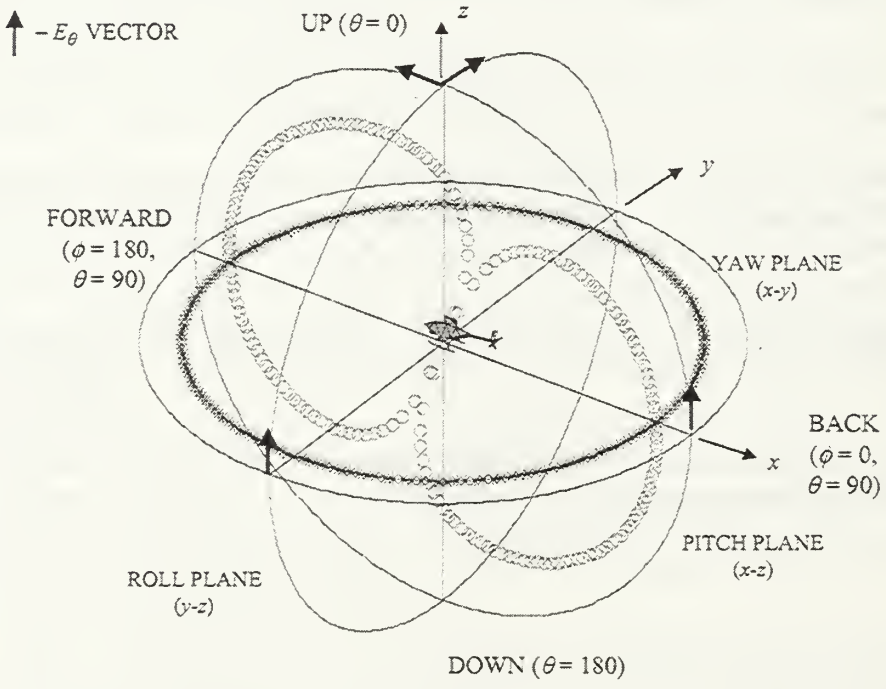

Figure 5: Illustration of pitch (o), roll (÷) and yaw (*) patterns in the helicopter coordinate system.

Direction finding systems operate over extremely wide bandwidths. For example, the Titan MA-445C antenna covers 2 MHz to 2000 MHz. The antenna parameters change somewhat as a function of frequency. The changes may be more significant when the antenna is installed on the helicopter, because there is little or no ground plane. The effects of a small ground plane include broadening of the antenna beam, higher backlobes, and increased cross polarization. These changes can lead to increased interference and noise, but they can also lead to increased field of view by broadening the beamwidth. Aircraft structures like the landing skids will be in the near field of the antenna, potentially modifying the pattern. At low frequencies in the band, ripples in the gain pattern might occur while at high frequencies shallow dips or notches could appear.

The directivity is the maximum value of the directive gain, which is identical to the gain if the antenna is lossless. For the purpose of comparing radiation patterns the losses will be neglected, and therefore the terms gain and directivity are used interchangeably.

The directivity D_o is the maximum value of [4]

$$D(\theta,\phi) = \frac{4\pi}{\Omega}\left|\bar{E}_{\text{norm}}(\theta,\phi)\right|^2$$

where Ω is the beam solid angle in steradians

$$\Omega = \int_0^{2\pi}\int_0^{\pi} \left|\bar{E}_{\text{norm}}(\theta,\phi)\right|^2 \sin\theta \, d\theta \, d\phi$$

and $\left|\bar{E}_{\text{norm}}(\theta,\phi)\right|$ is the magnitude of the normalized electric field pattern (i.e., the normalized radiation pattern)

$$\left|\bar{E}_{\text{norm}}(\theta,\phi)\right| = \frac{\left|\bar{E}(R,\theta,\phi)\right|}{\left|\bar{E}_{\max}(R,\theta,\phi)\right|}$$

For the method of moments calculations, the electric field

$$\bar{E}(R,\theta,\phi) = \hat{\theta}E_\theta(R,\theta,\phi) + \hat{\phi}E_\phi(R,\theta,\phi)$$

is obtained from PATCH and a second gain calculation program is used to evaluate the integral numerically. APATCH automatically calculates the directivity of the antenna as part of the scattered pattern normalization process. The directivity is defined in the far field, where $E_R(R,\theta,\phi) = 0$ and E_θ and E_ϕ have a $1/R$ dependence, which divides out leaving $\bar{E}_{\text{norm}}(\theta,\phi)$ independent of R.

A simple model for a low gain antenna (with negligible power in the sidelobes) is a single beam with half power widths Θ and Φ in two orthogonal principal planes, as shown in Figure 6. The beam solid angle is approximately $\Omega \approx \Theta\Phi$ giving a directivity of $D_o \approx \frac{4\pi}{\Phi\Theta}$ rad. The directivity of a dipole is 1.6 (≈ 2 dB) and 3.2 (≈ 4 dB) for a monopole over an infinite ground plane.

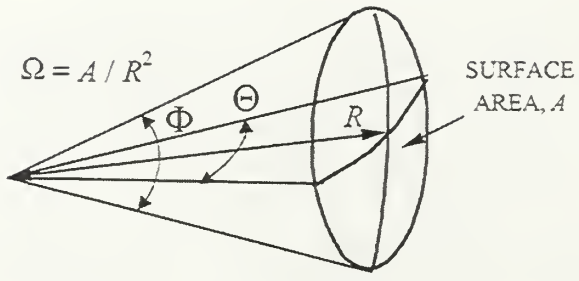

Figure 6: Approximate antenna model.

3.0 Antenna Models

3.1 Generic Monopole Antenna

Two vertically polarized antenna models were used in the analysis. The first is a simple vertical monopole over a ground plane. Although neither the COTS systems under consideration uses a single monopole in the 100 to 1200 MHz band, it is a standard antenna and serves as a good reference for evaluating the performance of other antenna types. It is also a good problem for comparing the two codes.

Many different methods are used to match the monopole over a wide bandwidth, but the pattern remains very similar to the one depicted in Figure 3. The PATCH model is shown in Figure 7 and patterns obtained from PATCH in Figures 8 through 10 for infinite and finite ground planes at two frequencies. The dimensions shown in the figure are in meters. For an infinite ground plane there is no radiation in the back direction (up in the case of the helicopter). Note that at 300 MHz the finite disk is an ineffective ground plane; the radiation in the back direction is as large as the radiation in the forward direction. At 600 MHz the ground plane behavior of the disk is improved.

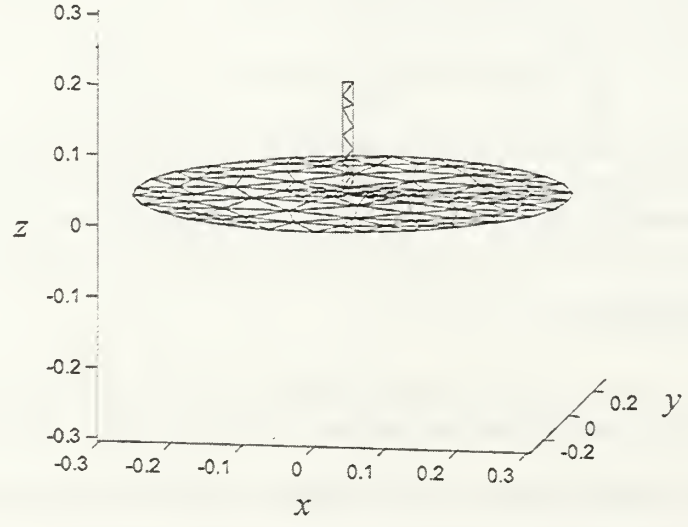

Figure 7: MM patch model of a monopole over a disk ground plane.

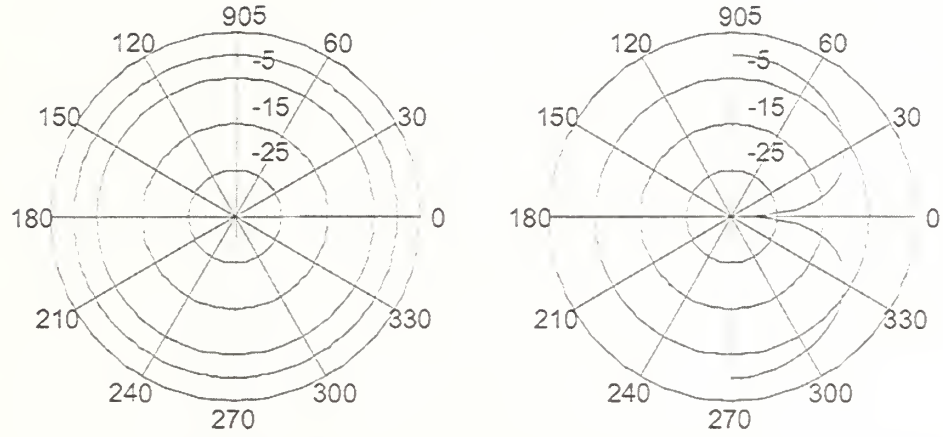

Figure 8: Normalized azimuth (left) and elevation (right) patterns of the monopole over an infinite ground plane at 300 MHz. θ is measured from the normal the monopole axis.

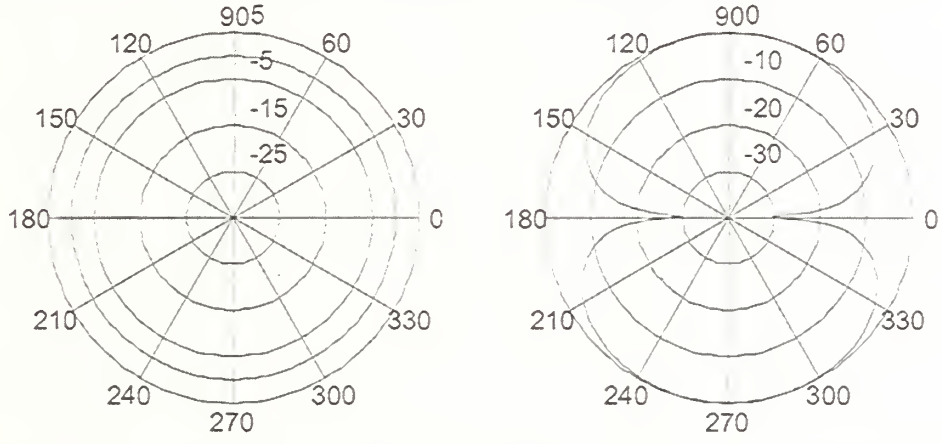

Figure 9: Normalized azimuth (left) and elevation (right) patterns of the monopole over a finite ground plane at 300 MHz. θ is measured from the normal the monopole axis.

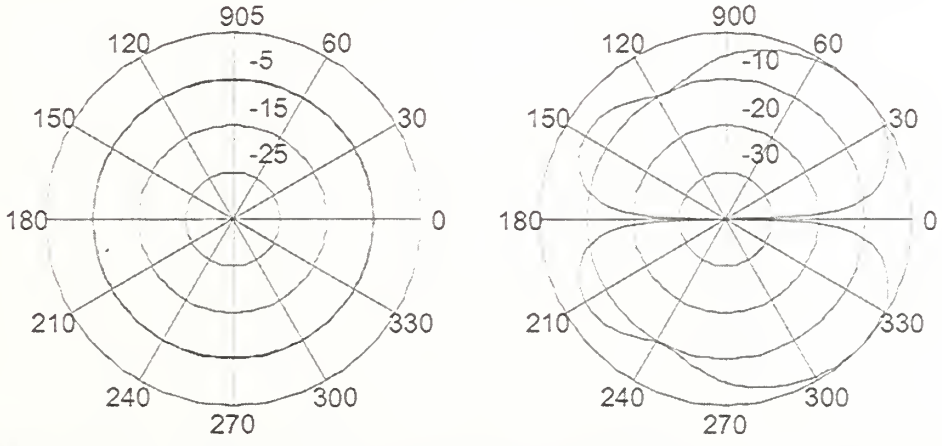

Figure 10: Normalized azimuth (left) and elevation (right) patterns of the monopole over a finite ground plane at 600 MHz. θ is measured from the normal the monopole axis.

3.2 Hemispherical Antenna Patterns

In order to obtain wide bandwidths, the antennas are actually packages of several receiving structures that yield contiguous coverage over a wide frequency band. Primarily, they contain combinations of slots that provide nearly hemispherical antenna patterns over the entire frequency band. The measured patterns for an antenna manufactured by Delfin Titan Systems is shown in Figure 11 for several frequencies. The measurements were taken with the antenna setting on the ground, facing up. Therefore the back radiation level is unknown. The measured data was taken in only one elevation plane. It is expected that the pattern in the other principal elevation plane is very close to that of the first elevation plane shown on the right in Figure 11.

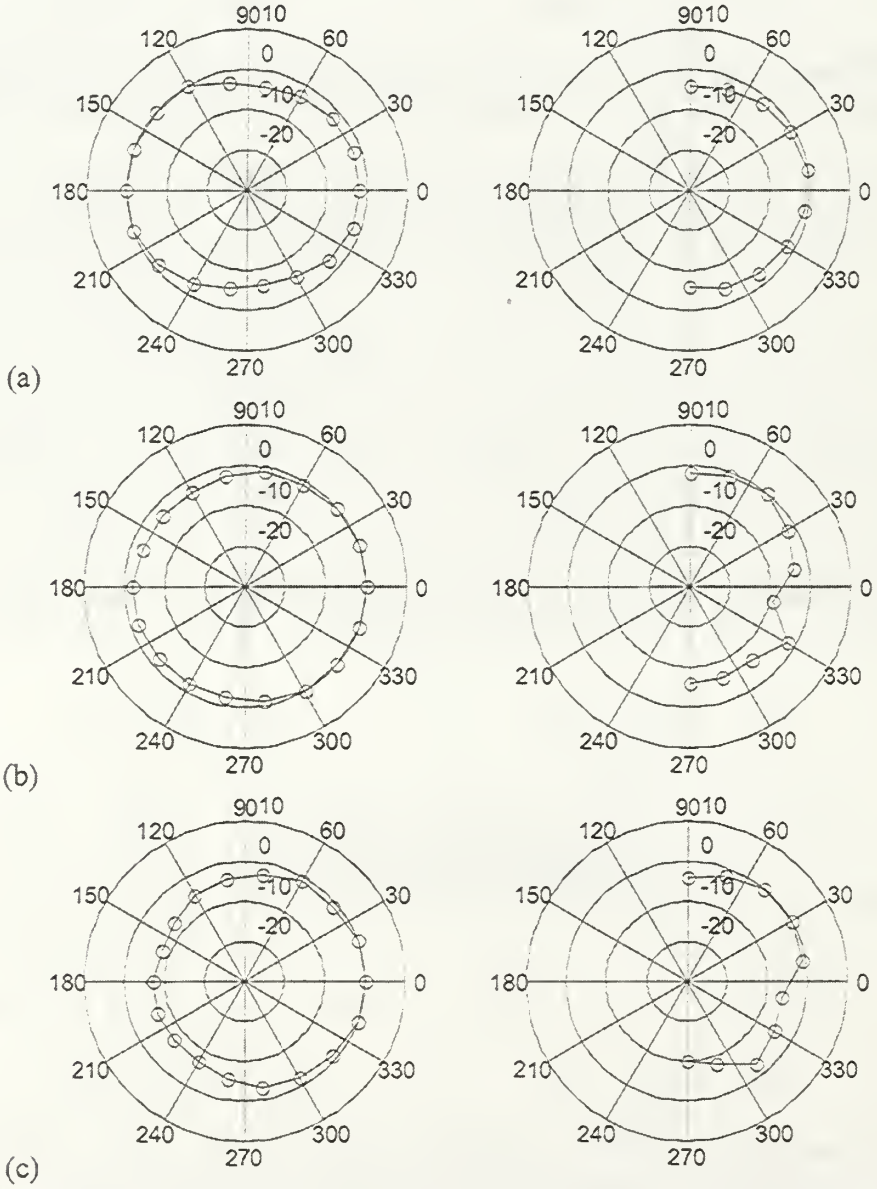

Figure 11: Normalized measured azimuth (left) and elevation (right) patterns for the Delfin antenna at (a) 200 MHz, (b) 600 MHz, and (c) 1100 MHz.

A computationally simple model that can mimic the behavior of the Delfin antenna is the array of three orthogonal wires shown in Figure 12. The voltages applied to each of the dipoles can be adjusted to provide a good approximation to the measured antenna data. Computed patterns for the approximate antenna over an infinite ground plane are shown in Figure 13.

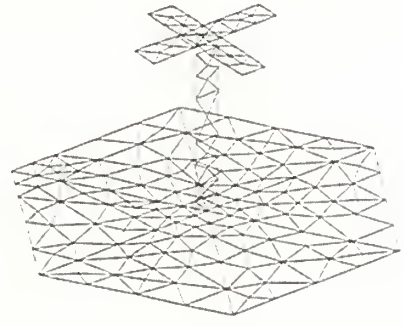

Figure 12: Approximate model of the Delfin antenna consisting of a vertical monopole and two horizontal crossed dipoles.

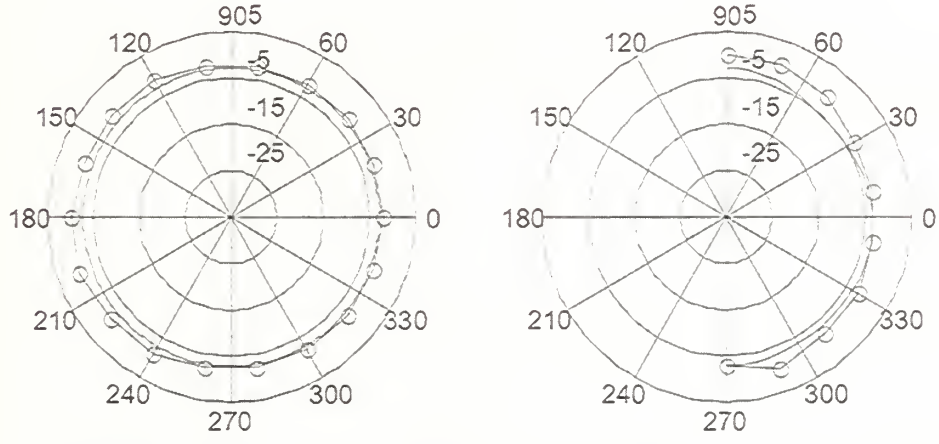

Figure 13: Comparison of the measured (circles) and approximate model on an infinite ground plane patterns for 200 MHz. Azimuth (left) and elevation (right).

Initial calculations using the model in Figure 12 showed that the pattern was extremely sensitive to the ground plane size and shape. Patterns for the antenna model on the helicopter were dramatically different than those on the infinite ground plane. The reason is probably due to the highly unbalanced nature of the model and the manner in which it is fed against the vehicle body. The Delfin antenna is a balanced antenna with very little near field coupling, and therefore it is not expected to experience this problem. Since the Delfin will not couple significantly to nearby structure, the isolated free-space radiation pattern can be used when it is installed on the helicopter. A general hemispherical pattern shape that approximates the measured data is

$$E_\theta = \begin{cases} |\cos\theta|^N + a, & |\theta| < 90^\circ \\ b|\cos\theta|^M + a|\sin\theta|^P, & |\theta| \geq 90^\circ \end{cases} \quad (1)$$

where θ is the angle from the antenna normal. The pattern is basically a cosine on a pedestal, where the exponents M, N and P control the directivity of the pattern and a is the pedestal height. Figure 14 shows the pitch, roll, and yaw plane patterns of the above function.

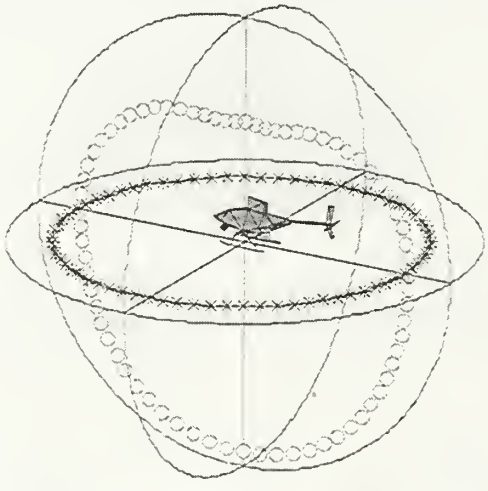

Figure 14: Illustration of pitch (o), roll (+) and yaw (*) patterns for the hemispherical antenna in the helicopter coordinate system.

4.0 Helicopter CAD Model

The helicopter CAD model was generated from front, top and side photographs of the aircraft. Therefore the dimensions are only approximate. The model includes the EO/IR globe, and the landing winch and skids. Three views of the model are shown in Figure 15. The main and tail rotors are not included. Previous studies have shown that they are not significant scatterers for antenna locations on the bottom side of the aircraft [8]. This conclusion is supported by sample calculations presented in Appendix B.

The ACAD automatic meshing feature allows rapid modification of the model when the antenna position is changed. After the meshed is generated, the model is written in the ACAD ".facet" file format. Then the file is translated into a format that can be read by either PATCH or APATCH, depending on which code is being used.

For the analysis of the helicopter various mesh densities were investigated. At low frequencies the MM code PATCH is used. All of the propagation mechanisms shown in Figure 2 are automatically included. When PATCH is employed, adhering to the 0.1λ edge guideline assures that the magnitude and phase of the current crossing the edge is approximately constant. If the radius of curvature of a surface is much less than a wavelength, then nothing is gained by using a finer mesh if only to give a tighter fit to the surface. An example is an electrically thin wing with

a rounded leading edge. At low frequencies the rounded edge can be accurately modeled by a sharp edge and the double-sided wing surface by a single surface sheet.

Figure 15: Helicopter model views.

At low frequencies the skids and struts are represented by flat strips. This is a good approximation when the diameter of the struts is small compared to the wavelength. As shown in Figure 16, there is an equivalent flat strip width w for a cylinder radius of radius a [9]. Using this "thin wire" approximation avoids having to mesh the entire surface area of the cylinder, thereby reducing the number of triangles by about 75%. The mesh model has about 4200 edges, with an average edge length of 0.125 m, which is 0.1λ at 240 MHz. Increasing the number of edges to 6000 only reduced the average edge length to about 0.1 m, or a frequency limit of about 300 MHz.

Above 200 MHz the helicopter is more than 4 wavelengths long, and that is large enough to use the high-frequency code APATCH. APATCH uses the physical optics approximation for the currents on a triangle. The directions of specular reflections are determined by the surface orientation and curvature, and therefore it is important that the mesh conform to the surface. A major difference in the models is the way the landing structure is handled. In the high frequency model the landing structure is comprised of circular cylinders. When the facet model is generated, the circular cross sections of the cylinders are segmented into polygons. The number of sides in the polygon is the number of flat sides making up the cylinder.

Edge diffractions are included in APATCH calculations when an ".edge" file is provided. A special APATCH utility is used to generate the ".edge" file from the ACAD ".facet" file.

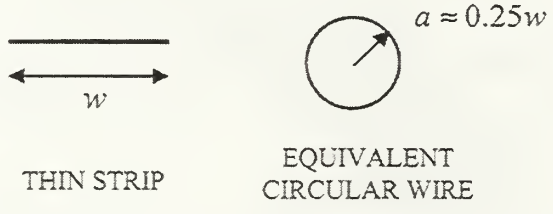

Figure 16: Equivalent thin strips and wires that is valid at low frequencies $w < 0.1\lambda$

5.0 Monopole Antenna Patterns at Various Locations

5.1 Introduction

The monopole antenna patterns were calculated for several frequencies and antenna locations. The locations are designated A, B and C. Location A is just in front of the landing skid frame (Figure 17), location B is midway between the landing skid frame and the EO/IR globe (Figure 29), and location C is in front of the EO/IR globe (Figure 38). All three points are on the center line of the vehicle ($y = 0$) in order to obtain equal views of the left and right sides of the aircraft.

Five frequencies in the band between 100 MHz and 1200 MHz were examined: 130 MHz, 275 MHz, 460 MHz, 810 MHz, and 960 MHz.

5.2 Antenna Location A

The first antenna location (designated as location A) is on the centerline just in front of the skids. Figure 17 shows a vertical monopole at the location. Patterns were computed using both

PATCH and APATCH for 130, 275 and 460 MHz. At 810 and 960 MHz only APATCH was used. All of the APATCH calculations include edge diffraction, even though edge diffraction did not significantly change the patterns. A typical examples illustrating the effects of diffraction are shown in Figure 18.

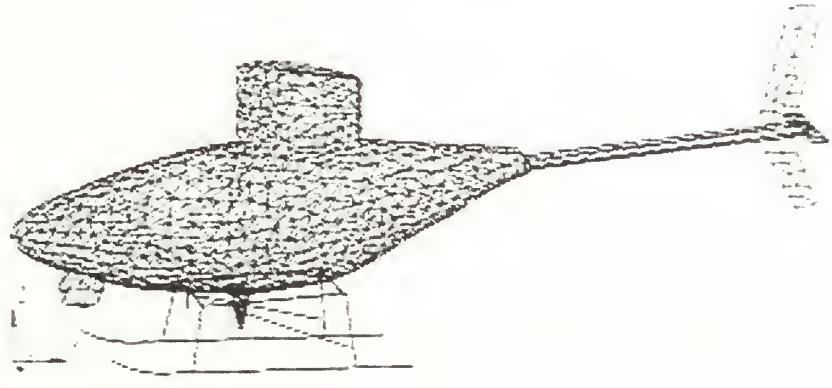

Figure 17: Antenna location A, just in front of the top horizontal skid strut.

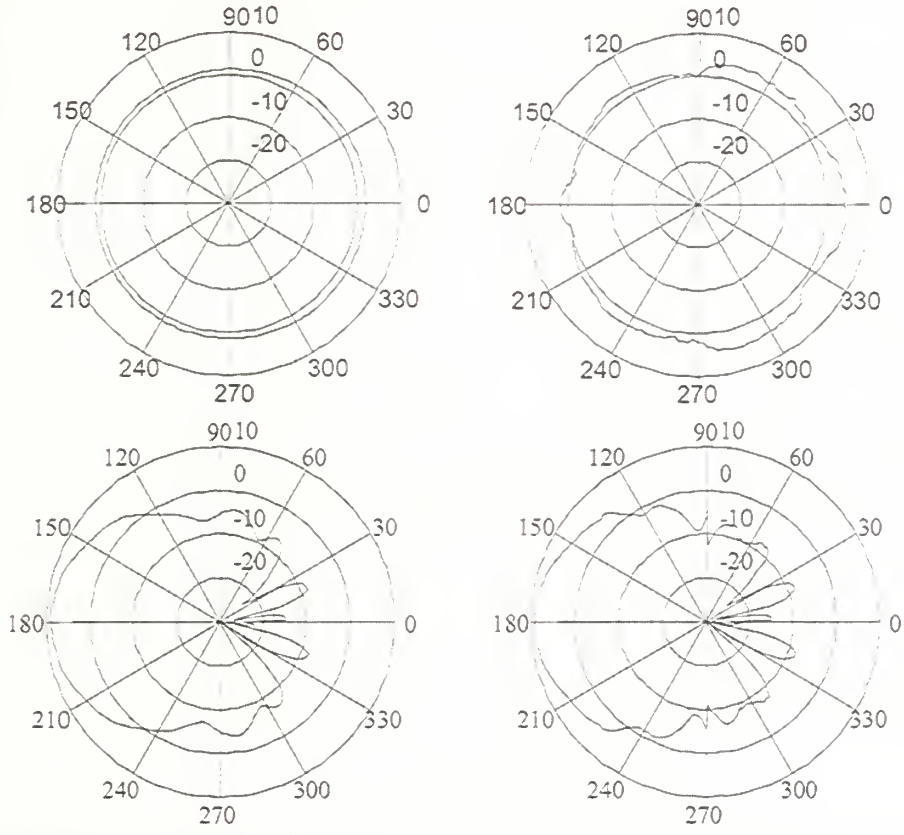

Figure 18: Sample comparisons of APATCH patterns with and without diffraction. Top: 130 MHz yaw (azimuth) and bottom: 810 MHz roll patterns. (Left: without diffraction and right: with diffraction).

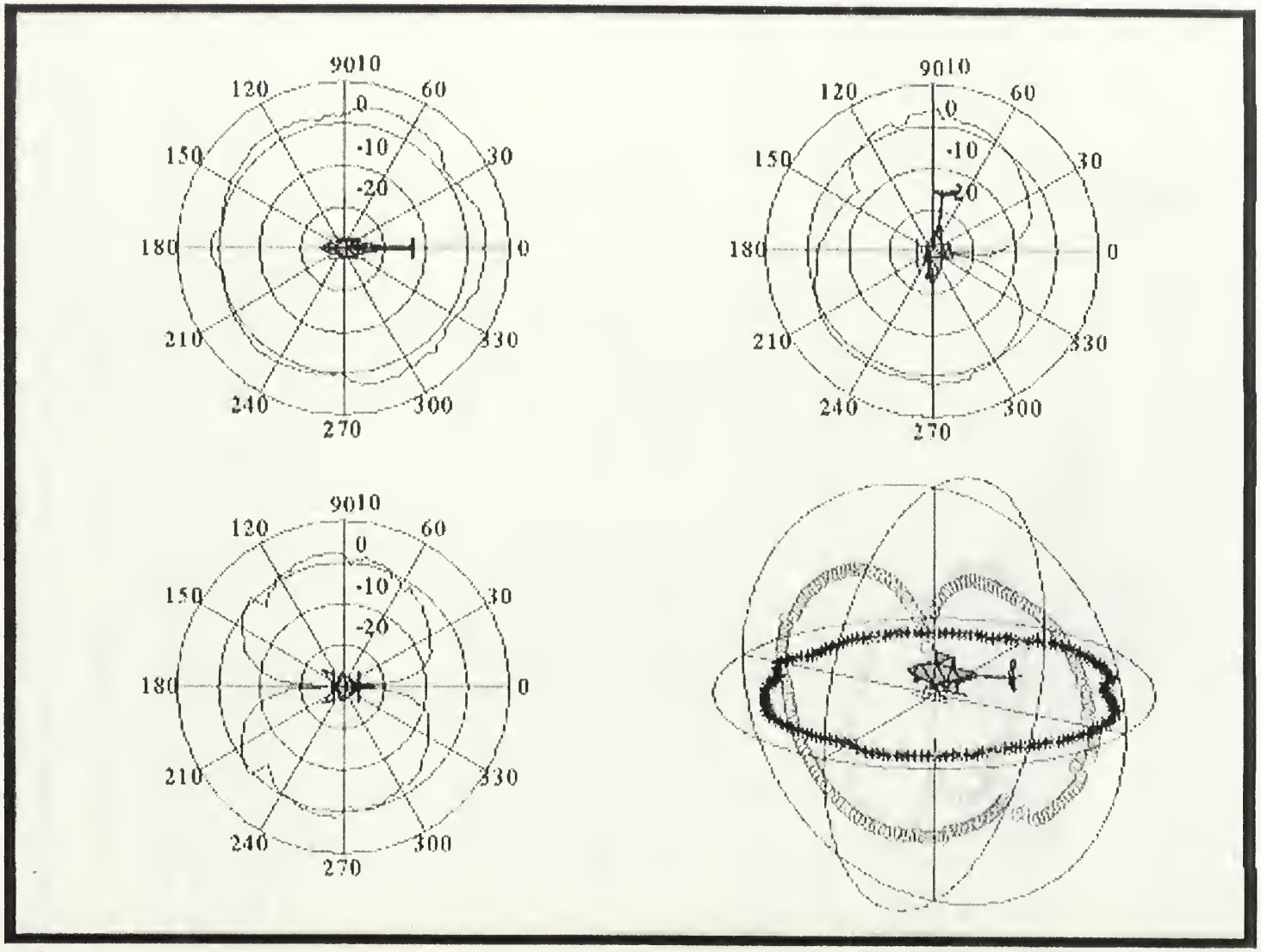

Figure 19: Yaw, pitch, roll and composite APATCH patterns for 130 MHz, antenna location A.

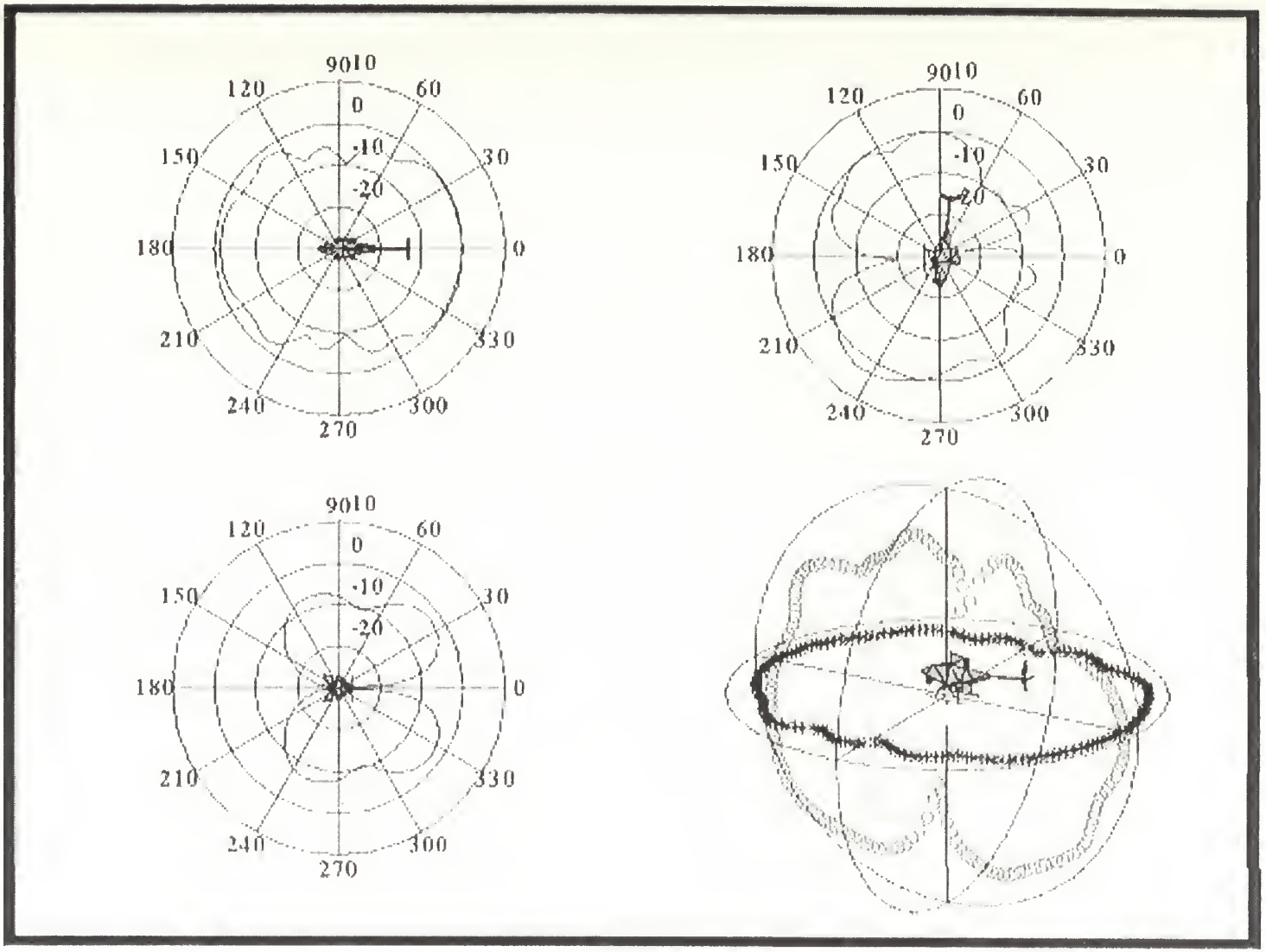

Figure 20: Yaw, pitch, roll and composite PATCH patterns for 130 MHz, antenna location A.

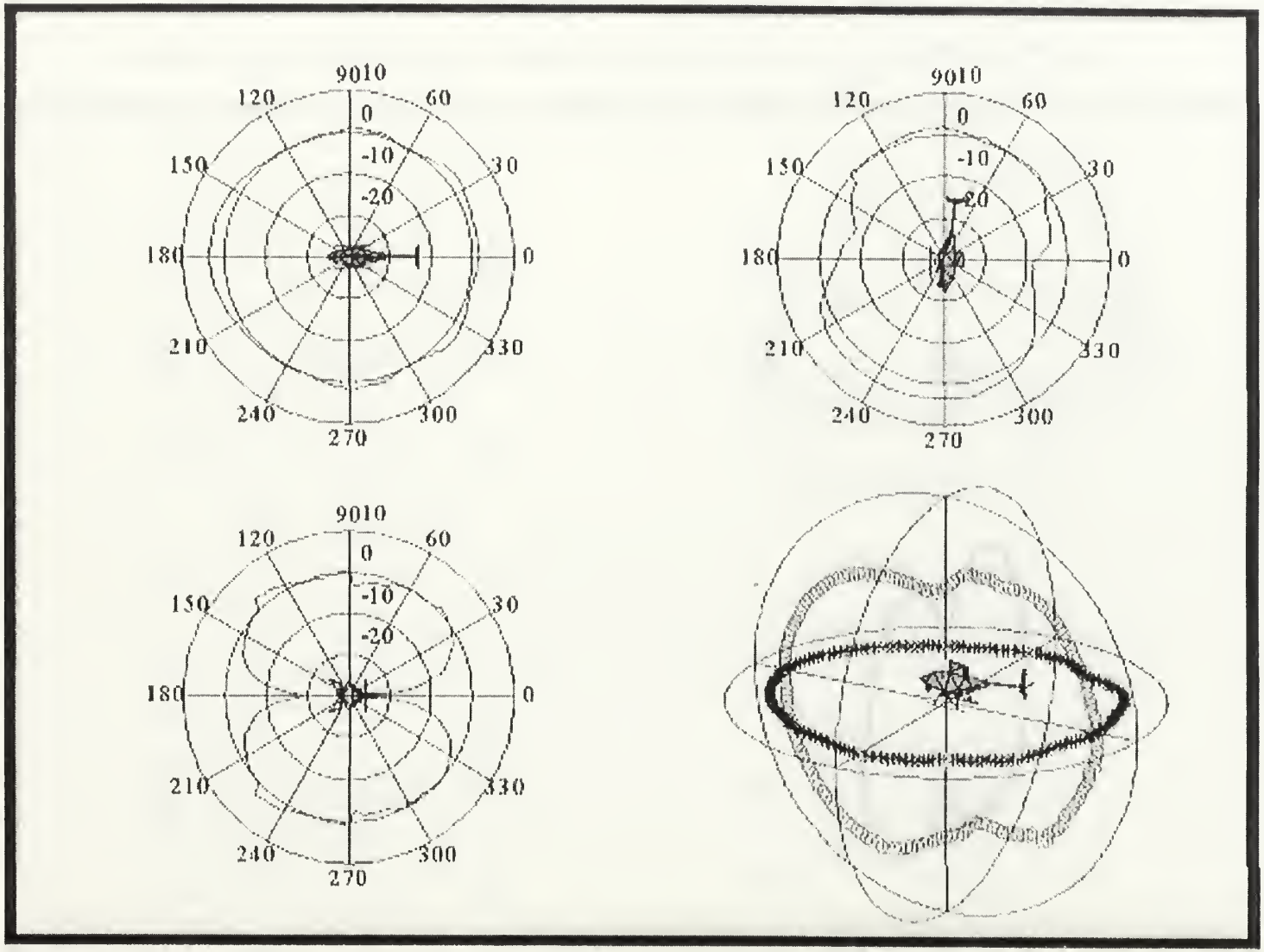

Figure 21: Yaw, pitch, roll and composite APATCH patterns for 275 MHz, antenna location A.

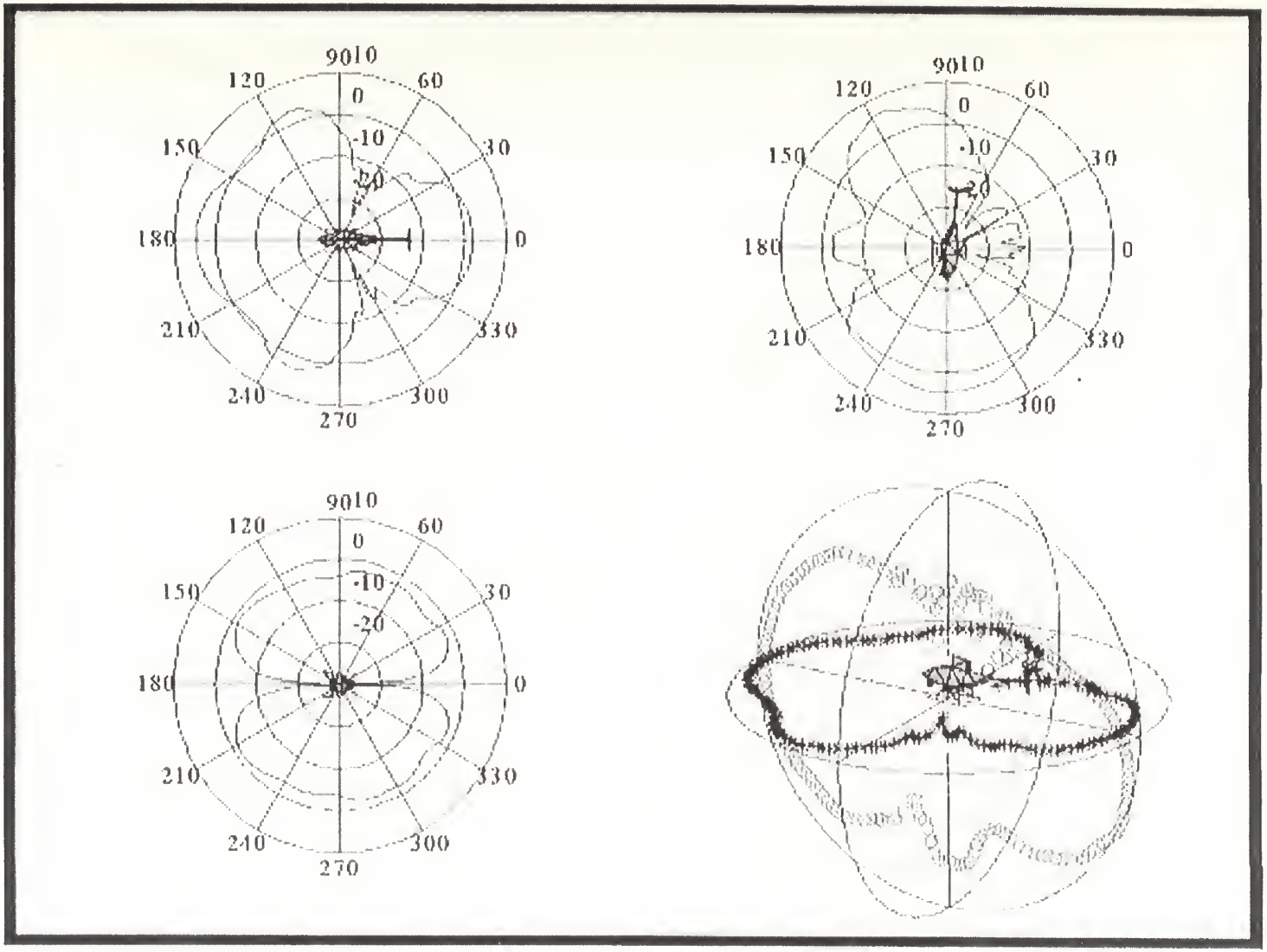

Figure 22: Yaw, pitch, roll and composite PATCH patterns for 275 MHz, antenna location A.

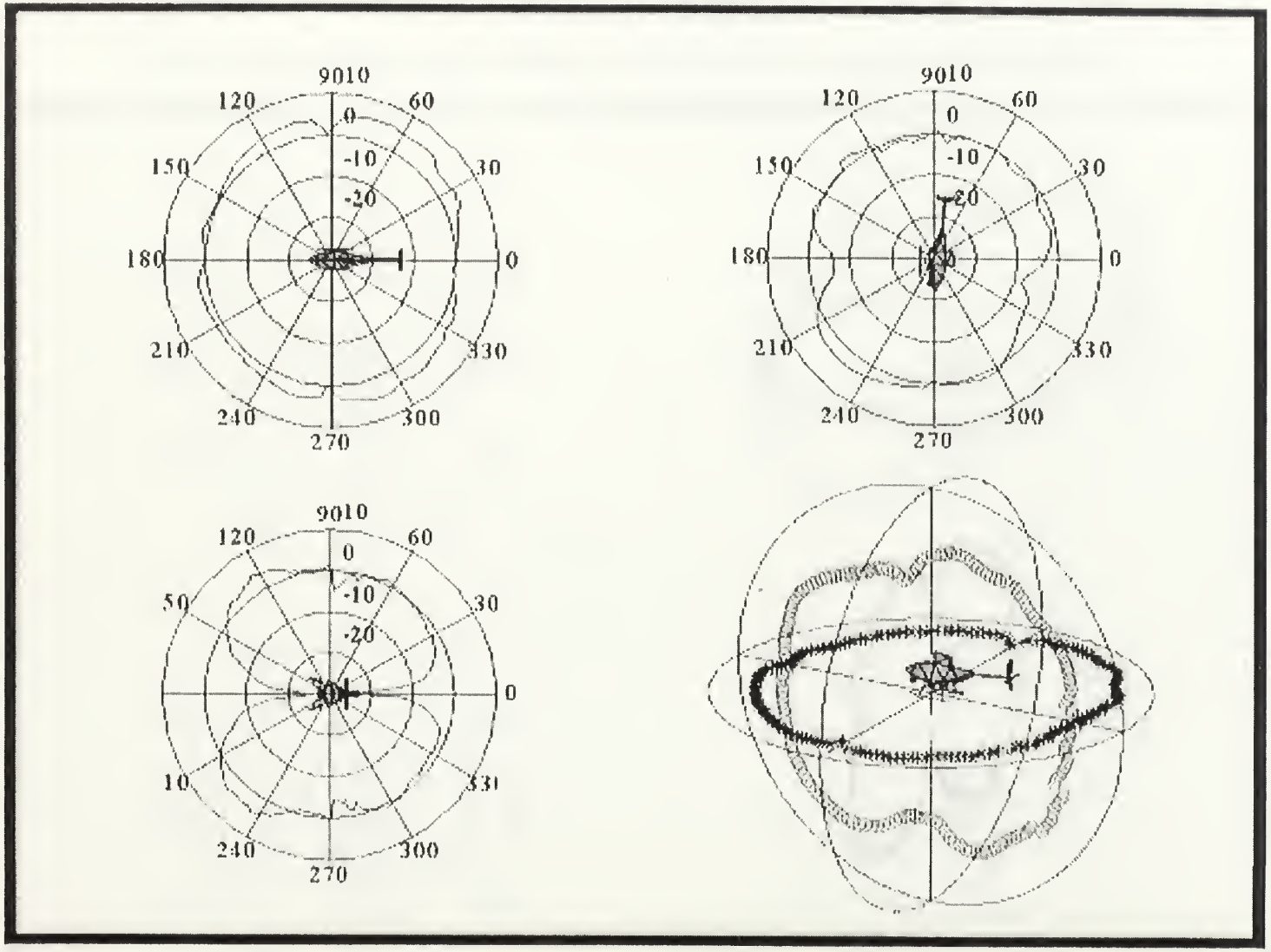

Figure 23: Yaw, pitch, roll and composite APATCH patterns for 460 MHz, antenna location A.

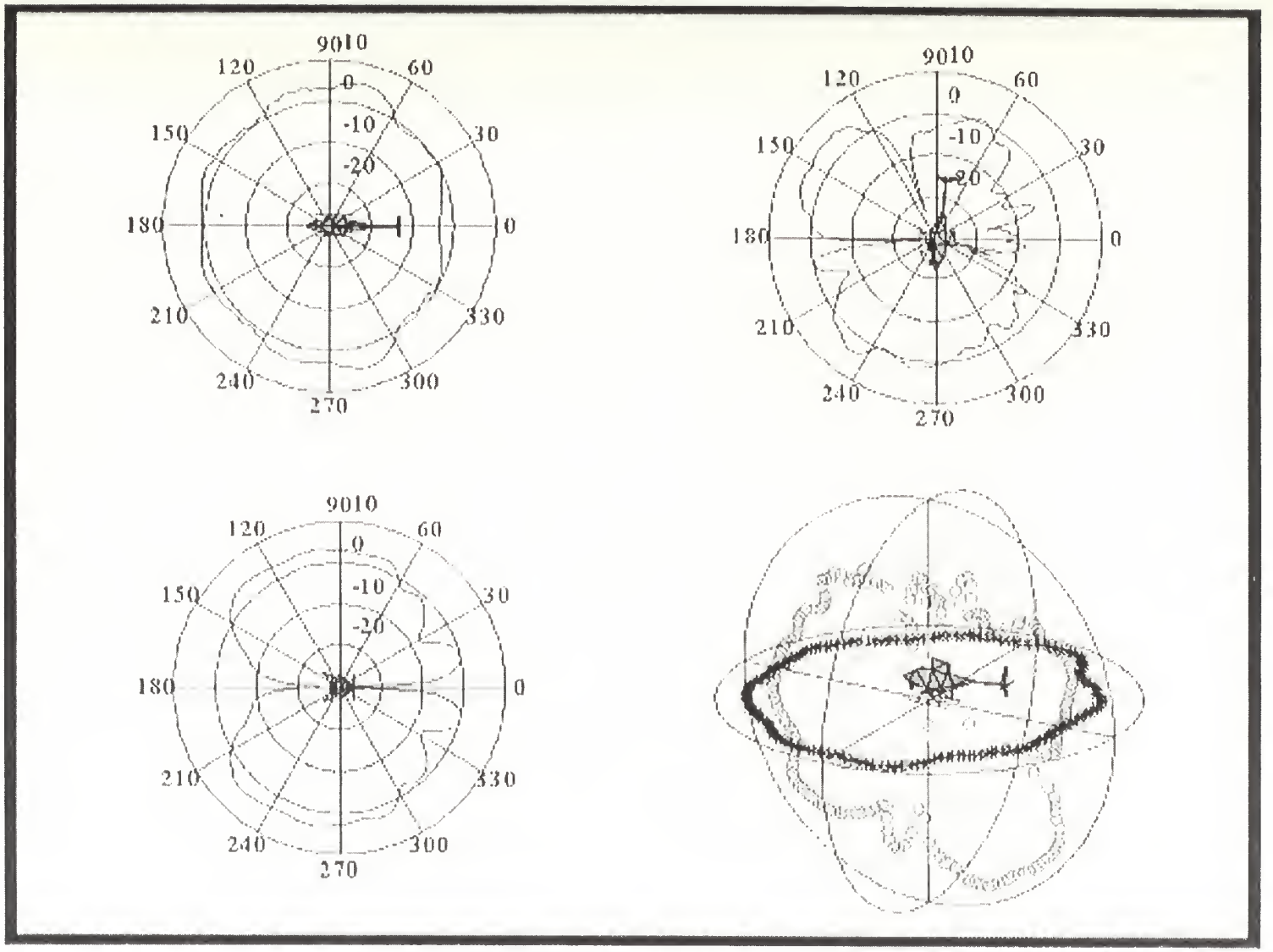

Figure 24: Yaw, pitch, roll and composite PATCH patterns for 460 MHz, antenna location A

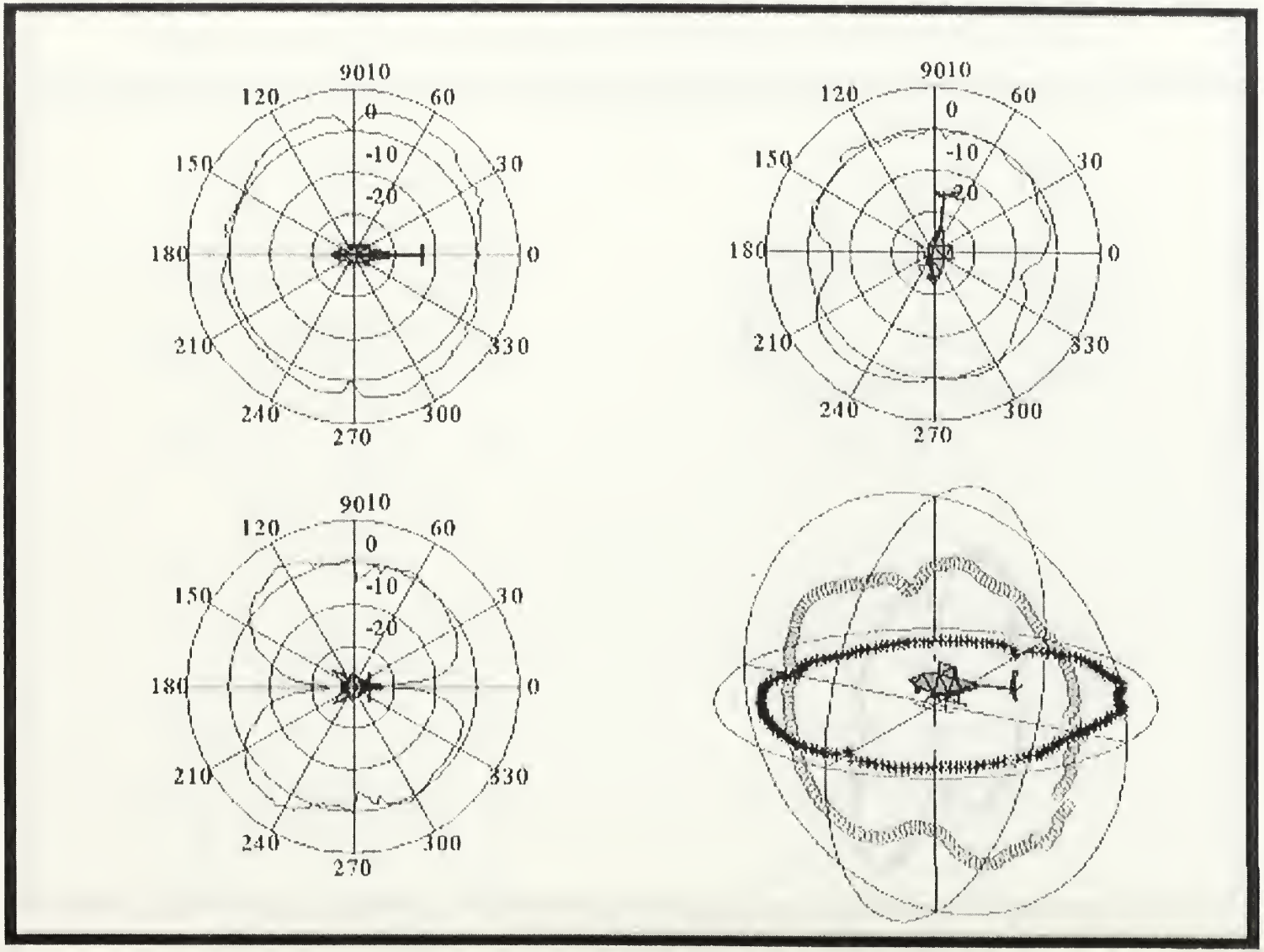

Figure 25: Yaw, pitch, roll and composite APATCH patterns for 810 MHz, antenna location A.

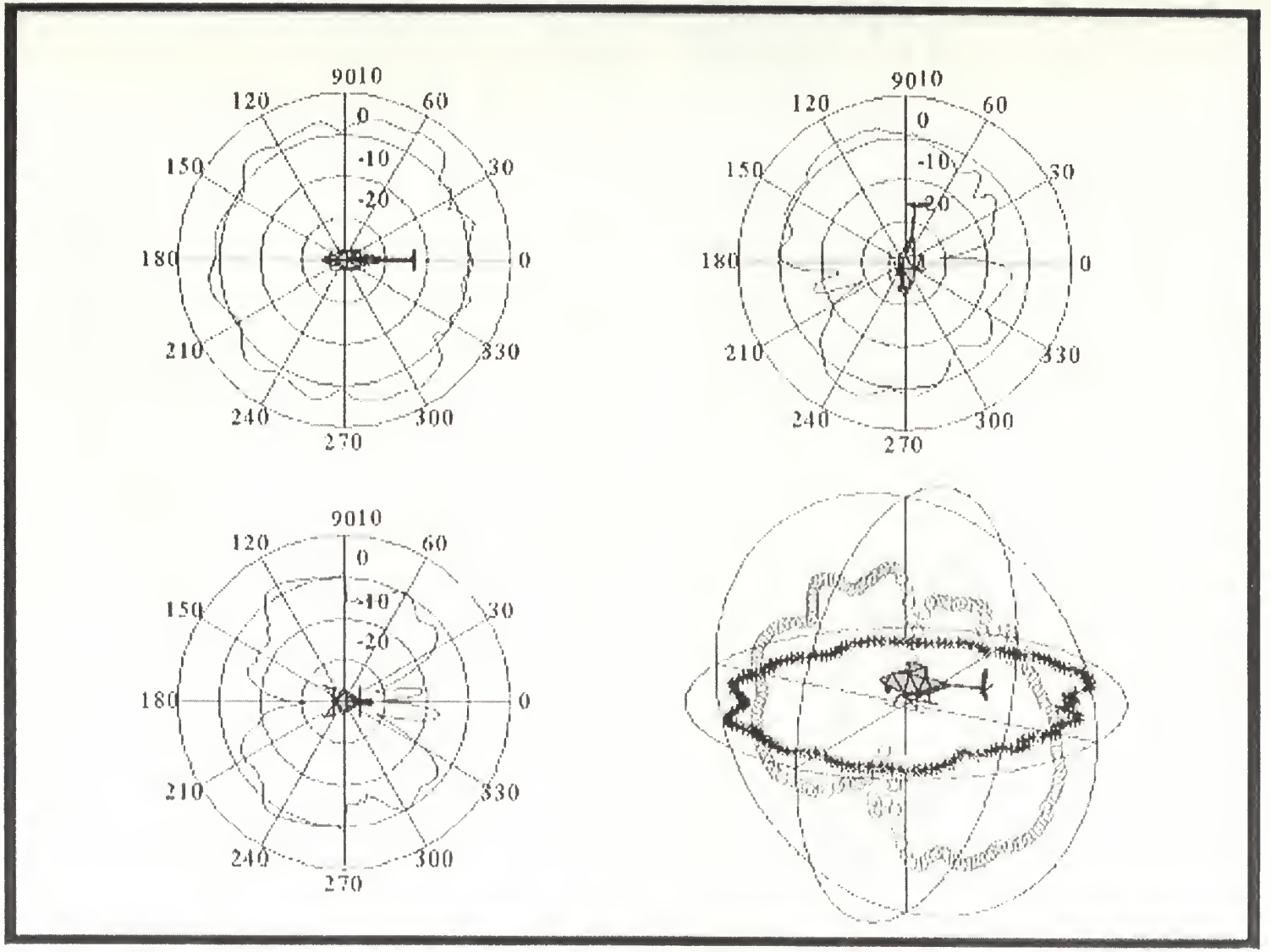

Figure 26: Yaw, pitch, roll and composite APATCH patterns for 960 MHz, antenna location A.

An examination of the plots leads to the following conclusions:

1. There is generally good agreement between PATCH and APATCH, even at low frequencies where the limitations imposed by PO and PTD are violated. The APATCH results degrade gracefully as the frequency is decreased.
2. The PATCH patterns begin to degrade at about 300 MHz. At this frequency the average edge length is 0.125 m and 0.1λ limitation is violated. The number of edges in the model is about 4200 and the run time approximately 2 hours on a 500 MHz PC.
3. The addition of diffraction to APATCH calculations did not yield any dramatic changes in the pattern data.

One of the largest deviations of the pattern shape from the baseline occurred at 275 MHz in the azimuth plane (Figure 22). The ripple in the pattern is due to scattering from the vertical supports for the skids. The simple multipath model shown in Figure 27 accounts for the pattern shape. Figure 28 shows the pattern computed using the multipath model (circles). The forward scattering adds constructively with the direct radiation from the antenna causing a slight enhancement of the gain at $\delta = \pm 90^{\circ}$. In the rear hemisphere (toward the tail) the pattern has more severe degradation, probably due to the angled parts of the support structure and blockage by the winch. Note that at the low frequencies the winch diameter is only a small fraction of a wavelength. It can have a behavior similar to a director in a Yagi Uda array (causing an increase in gain in its direction, rather than a reduction in gain).

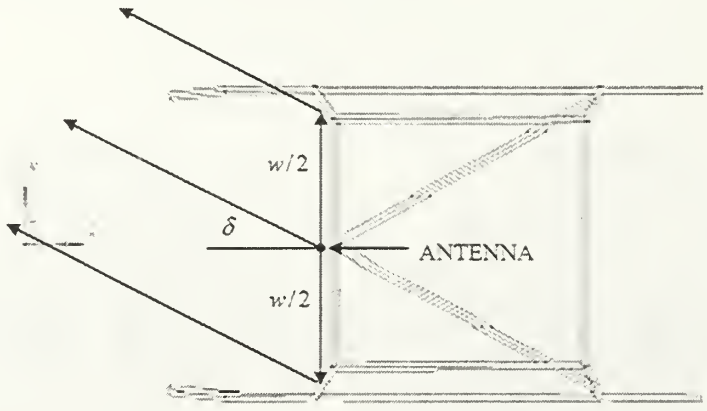

Figure 27: Simple multipath model for reflection from the vertical supports (top view).

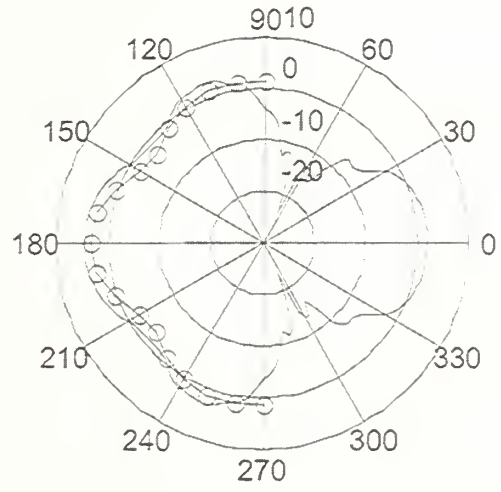

Figure 28: Pattern calculated from the simple multipath model of Figure 27 (circles).

The patterns for the two highest frequencies are shown in Figures 25 and 26. The data was generated using APATCH. There was not enough computer memory to use PATCH and get a converged result. At the high frequencies, more ripples are noticeable in the patterns. The constructive and destructive interference from structure scattering occurs more rapidly with the change in angle, because separation distances are longer in terms of the wavelength.

In summary, the antenna patterns at location A are good in the forward lower hemisphere (except in the direction of the monopole axis). A few frequencies would suffer drop outs in the rear lower hemisphere due to obstruction and scattering from the vertical members of the landing structure.

5.3 Antenna Location B

The second antenna location (designated as location B) is on the centerline midway between the EO/IR globe and skids. Figure 29 shows a vertical monopole at the location. Both APATCH and PATCH patterns are shown for the frequencies of 130, 275 and 460 MHz. Only APATCH are shown for 810 and 960 MHz.

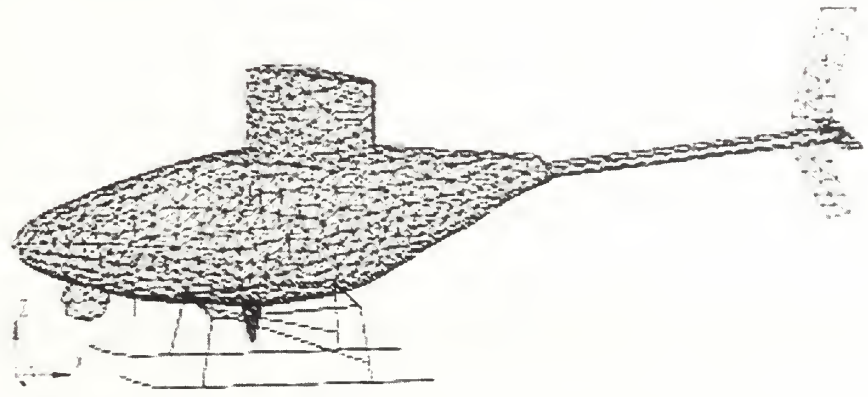

Figure 29: Antenna location B between the EO/IR globe and landing structure.

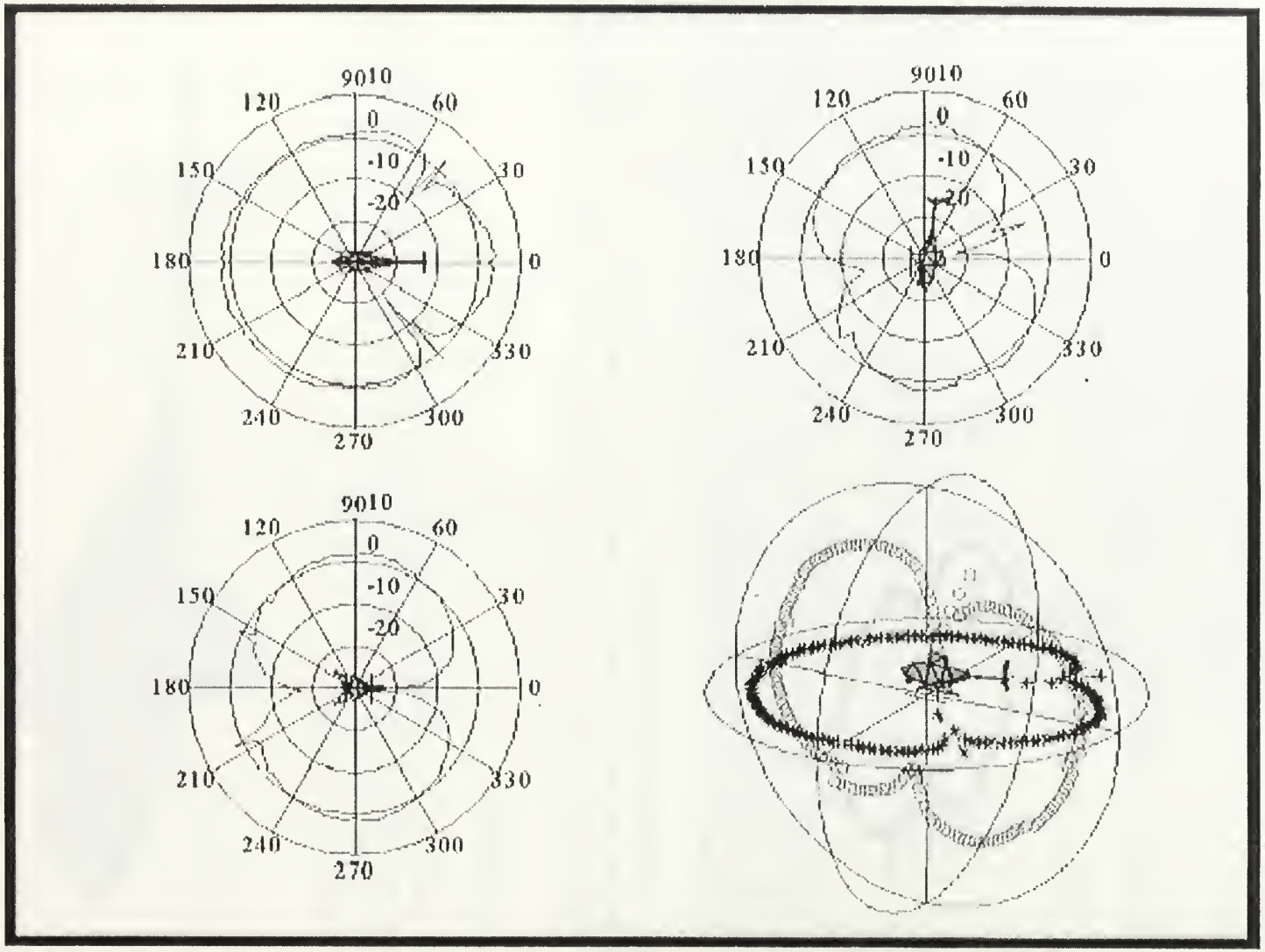

Figure 30: Yaw, pitch, roll and composite APATCH patterns for 130 MHz, antenna location B.

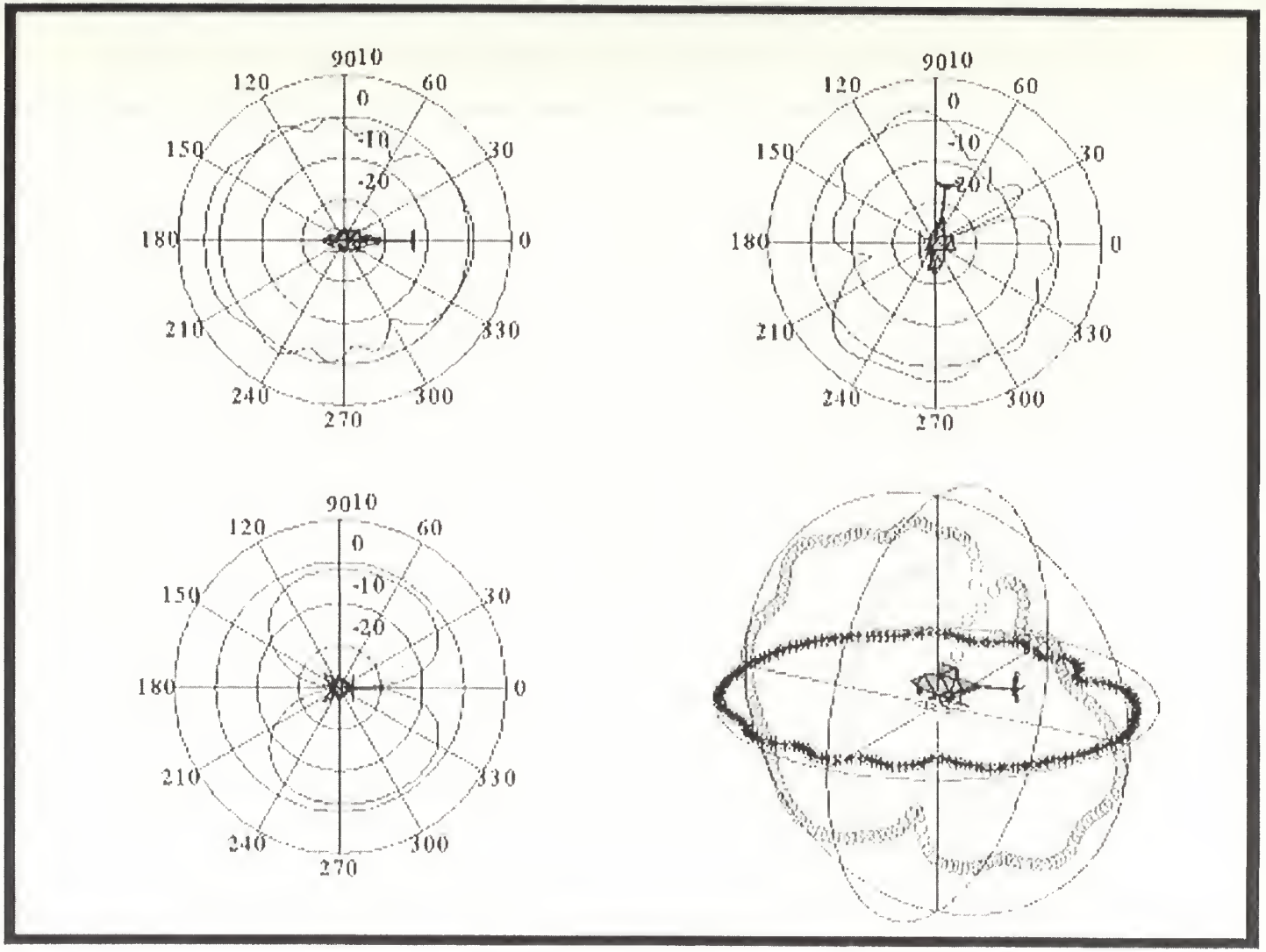

Figure 31: Yaw, pitch, roll and composite PATCH patterns for 130 MHz, antenna location B.

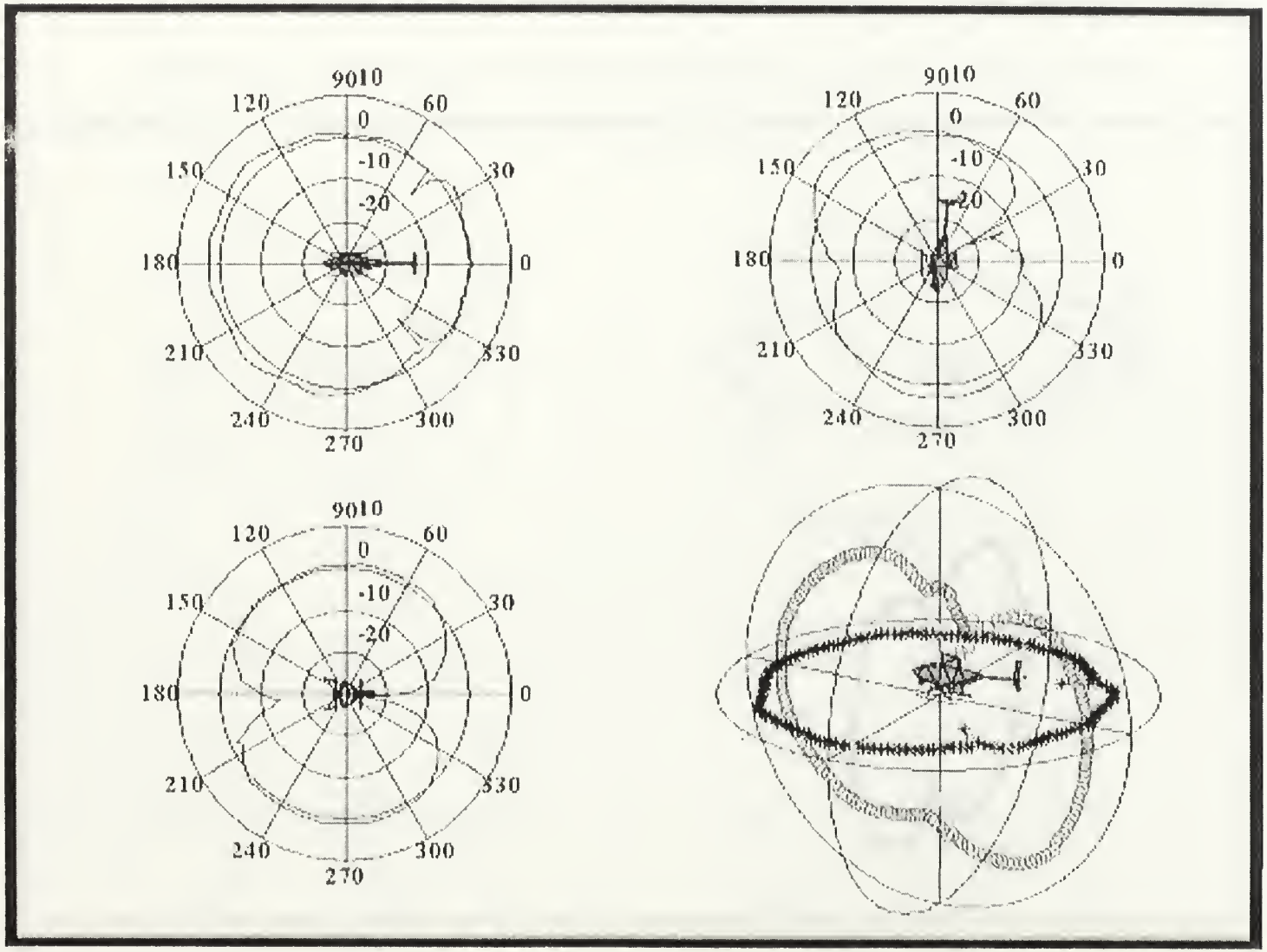

Figure 32: Yaw, pitch, roll and composite APATCH patterns for 275 MHz, antenna location B.

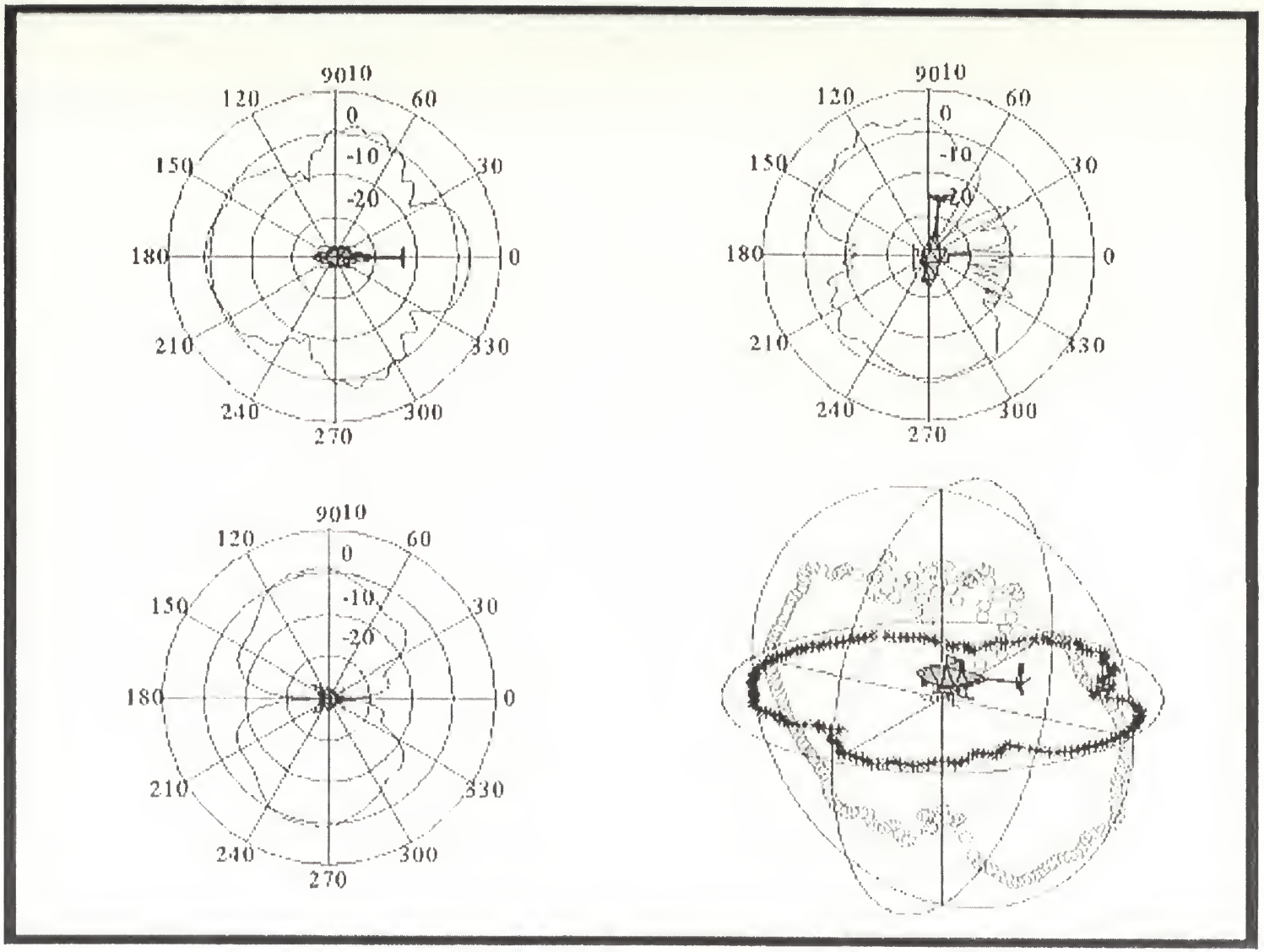

Figure 33: Yaw, pitch, roll and composite PATCH patterns for 275 MHz, antenna location B.

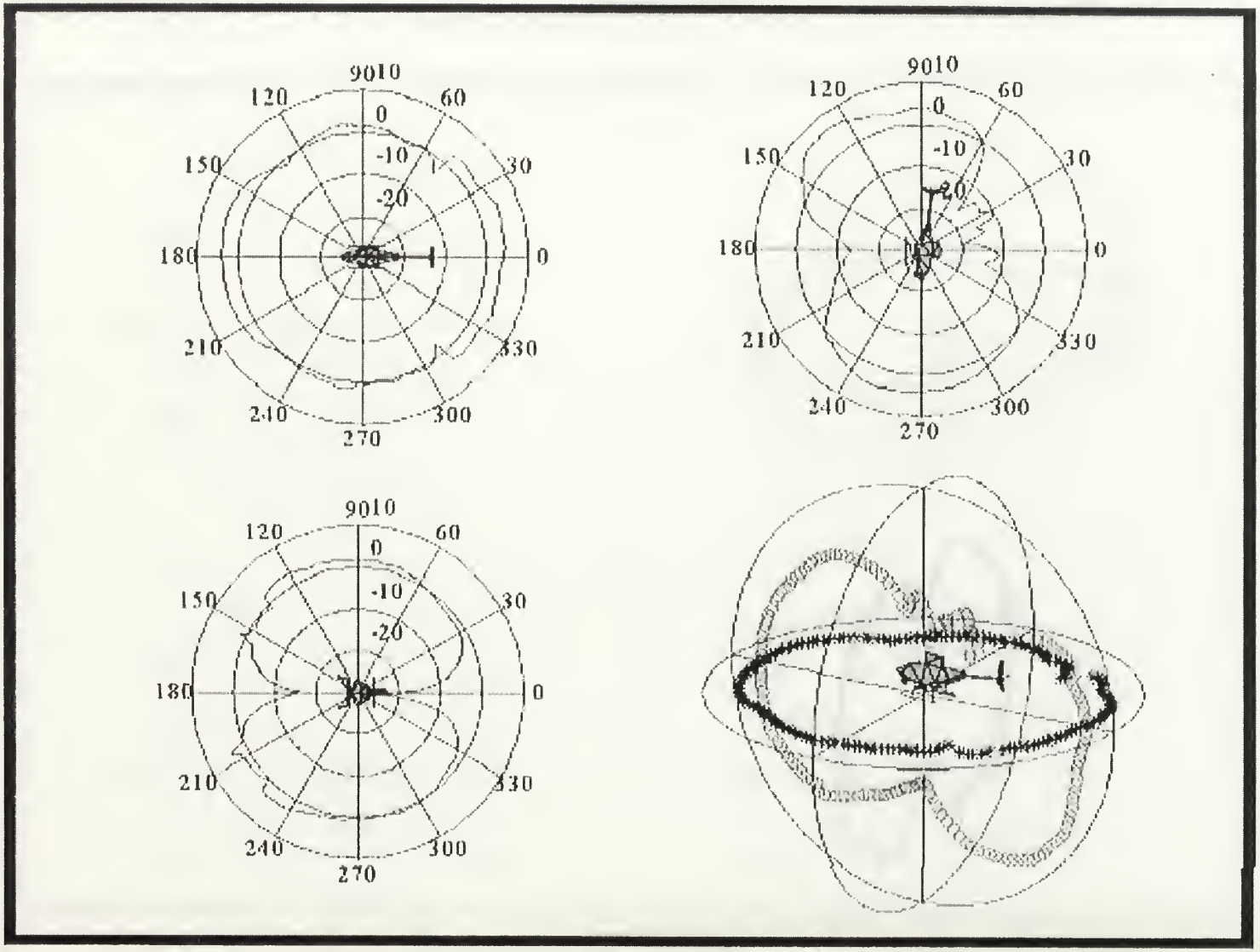

Figure 34: Yaw, pitch, roll and composite APATCH patterns for 460 MHz, antenna location B.

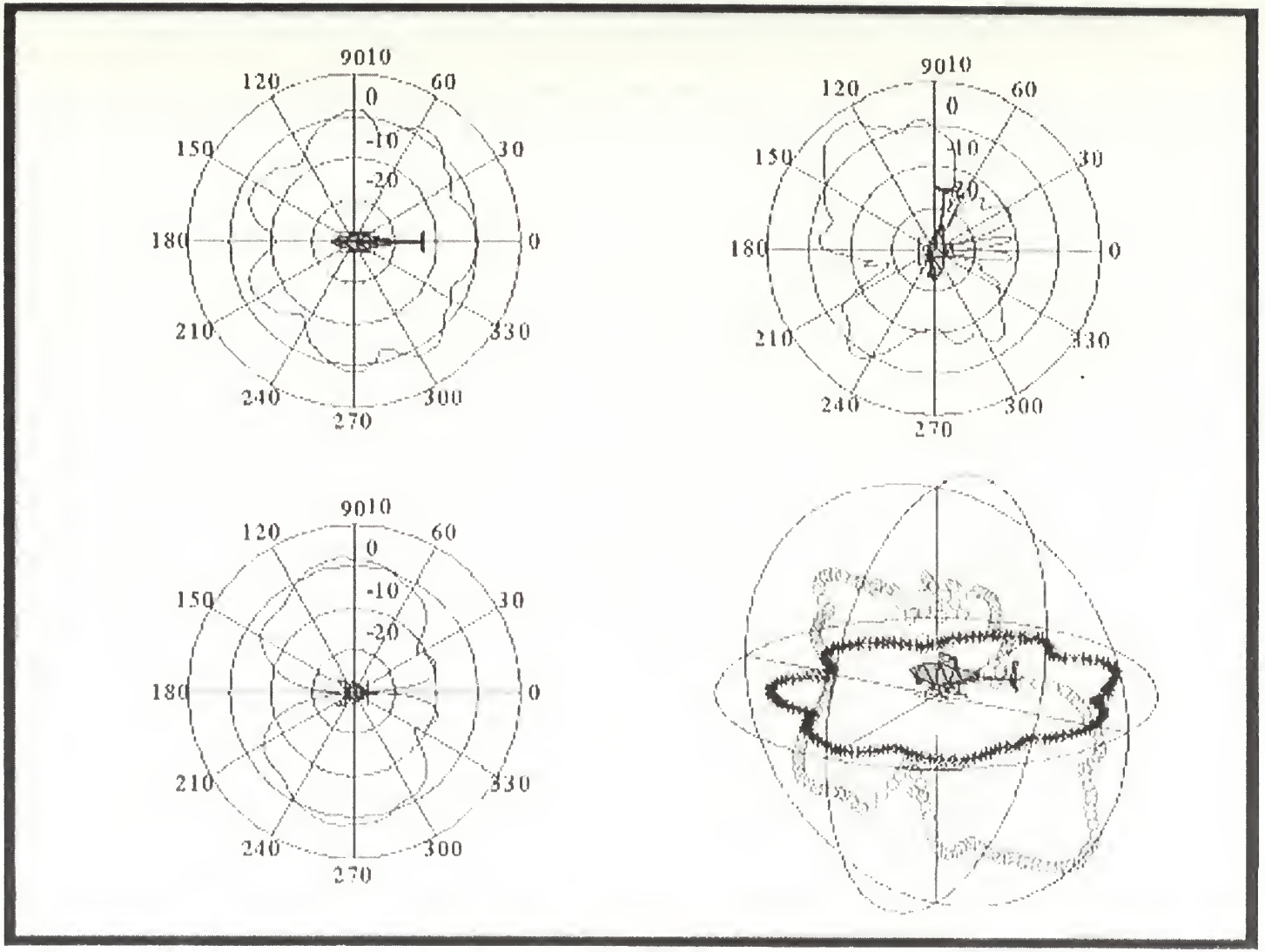

Figure 35: Yaw, pitch, roll and composite PATCH patterns for 460 MHz, antenna location B.

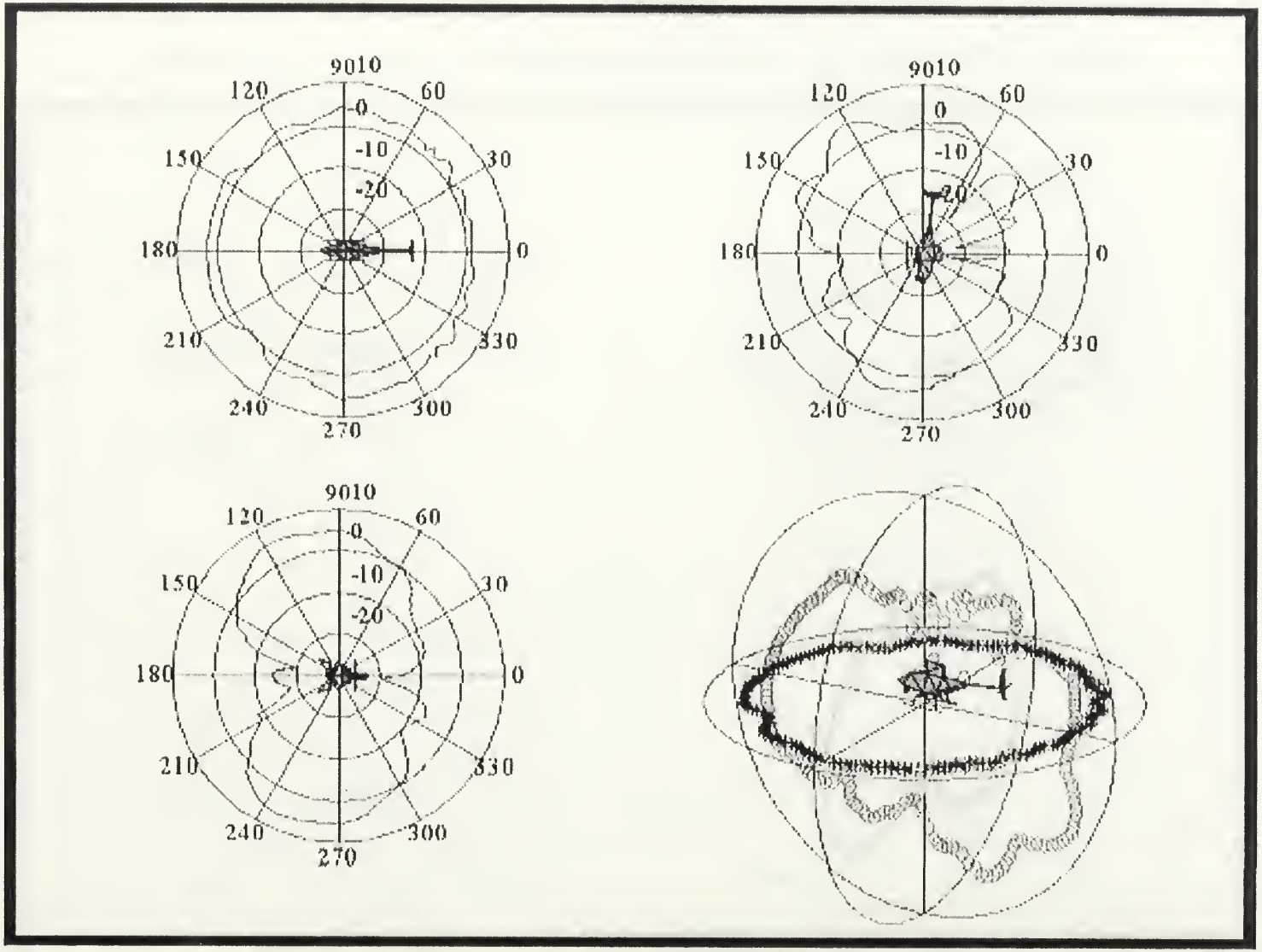

Figure 36: Yaw, pitch, roll and composite APATCH patterns for 810 MHz, antenna location B.

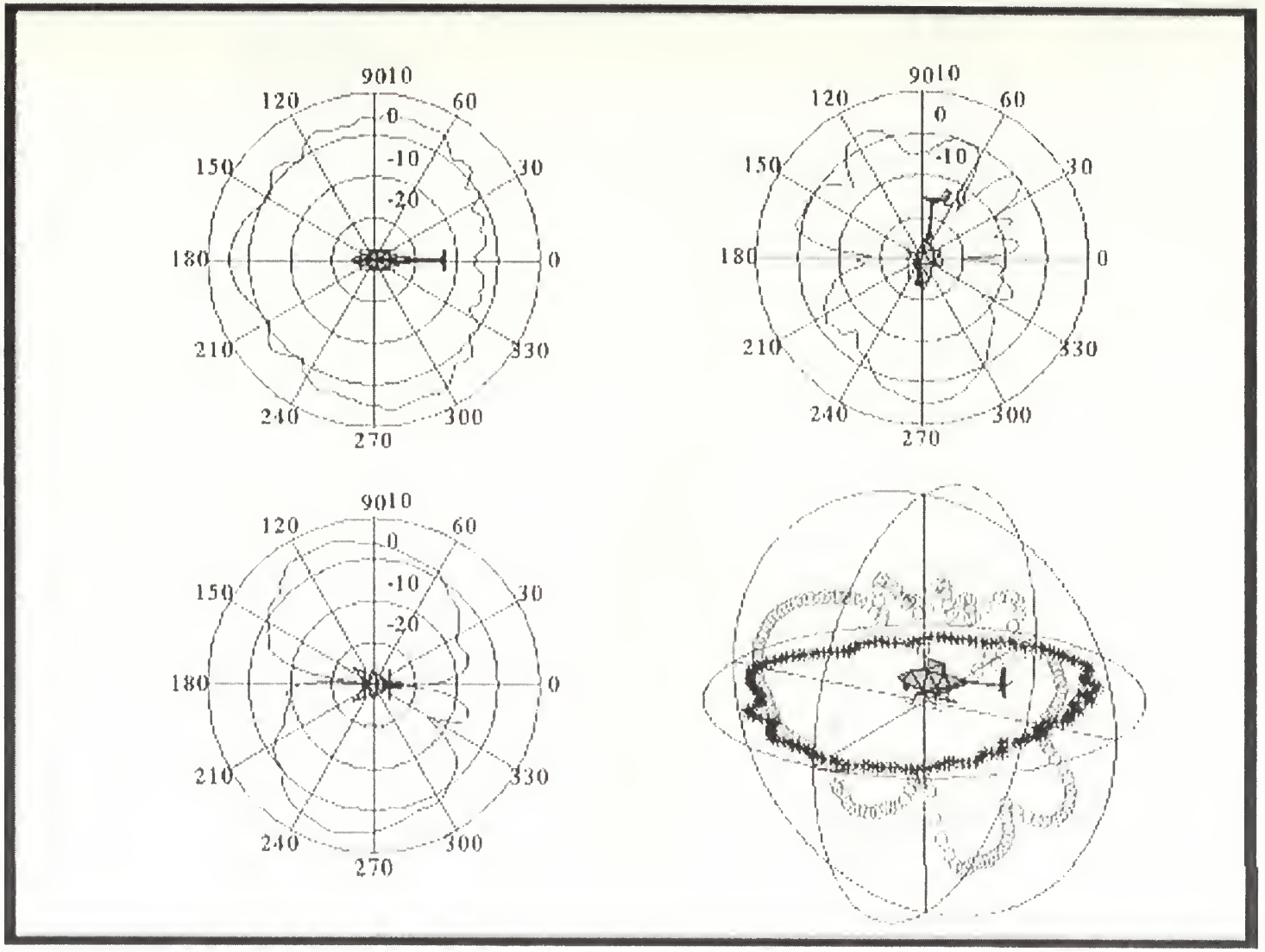

Figure 37: Yaw, pitch, roll and composite APATCH patterns for 960 MHz, antenna location B.

An examination of the data indicates that there is no dramatic difference between the patterns for locations A and B. However, the following points are noted:

1. The azimuth pattern coverage for location B is not quite as good in the rear hemisphere (tail direction) as it is for antenna location A.
2. More radiation appears directed in the upper hemisphere (above the aircraft) in the forward direction, than was the case for the antenna at location A.
3. The pitch plane pattern null is a little deeper and points more toward the horizon than for location A. This is undesirable for the longer slant ranges for sources just below the horizon.

5.4 Antenna Location C

The third antenna location (designated as location C) is on the centerline in front of the EO/IR globe. Figure 38 shows a vertical monopole at the location. As in the previous two cases PATCH and APATCH are used for the three lowest frequencies and APATCH for the two high frequencies.

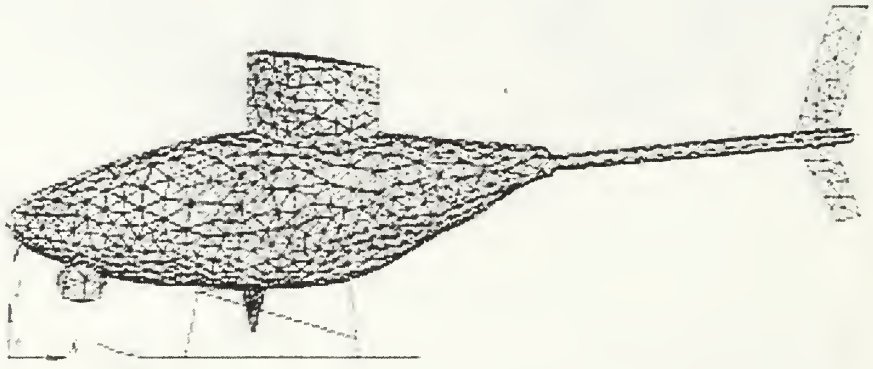

Figure 38: Antenna location C in front of the EO/IR globe.

The pattern data for location C shows that the radiation in the lower forward hemisphere is low relative to the other two antenna locations. This is because the monopole null is pointed toward the horizon. The pitch plane patterns have very deep nulls and more ripple than antenna locations A and B. Also, the pitch plane patterns show that there is significantly more radiation in the upper forward hemisphere, most likely due to mounting the monopole on the rounded nose, which is not an effective ground plane.

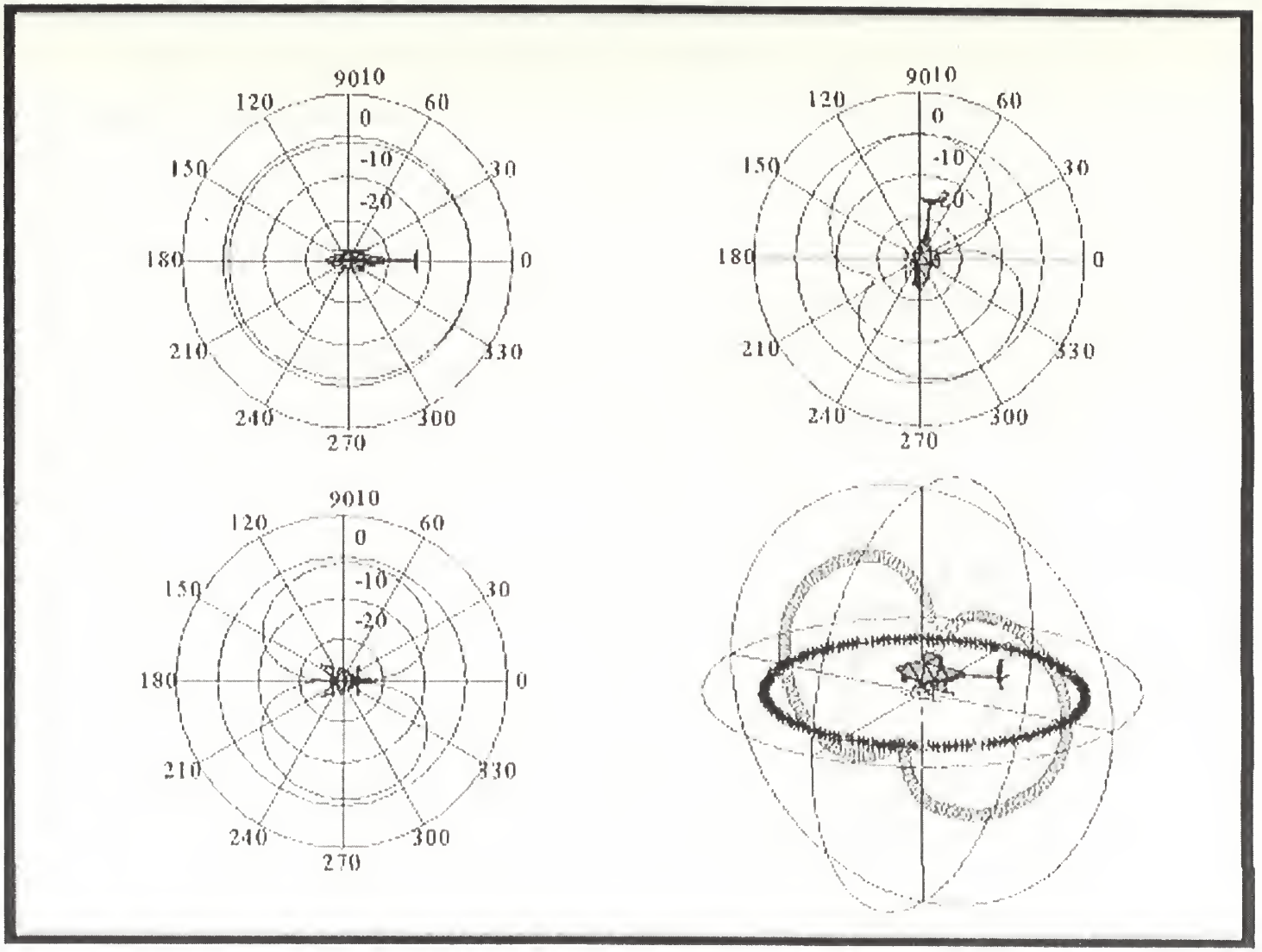

Figure 39: Yaw, pitch, roll and composite APATCH patterns for 130 MHz, antenna location C.

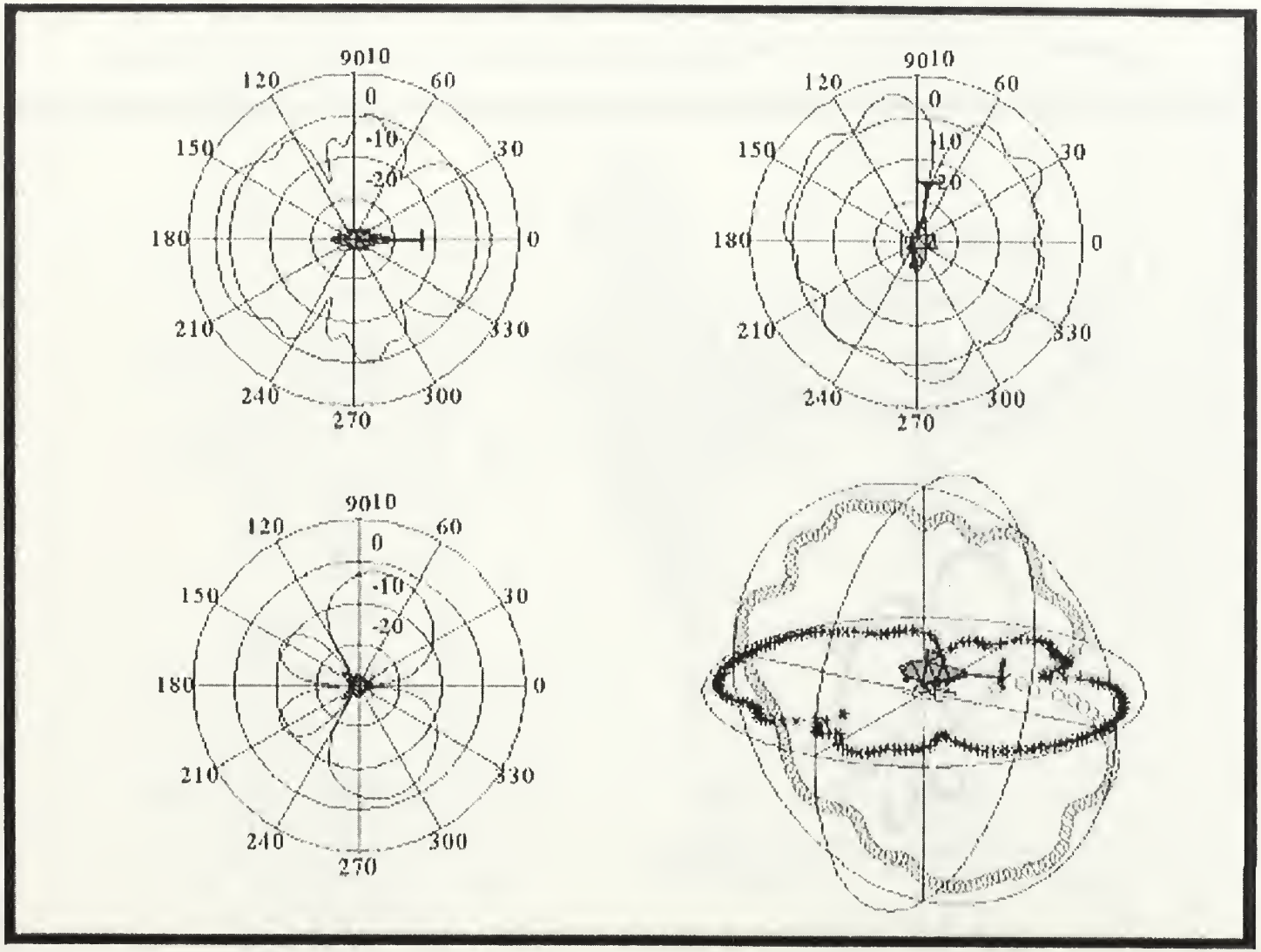

Figure 40: Yaw, pitch, roll and composite PATCH patterns for 130 MHz, antenna location C.

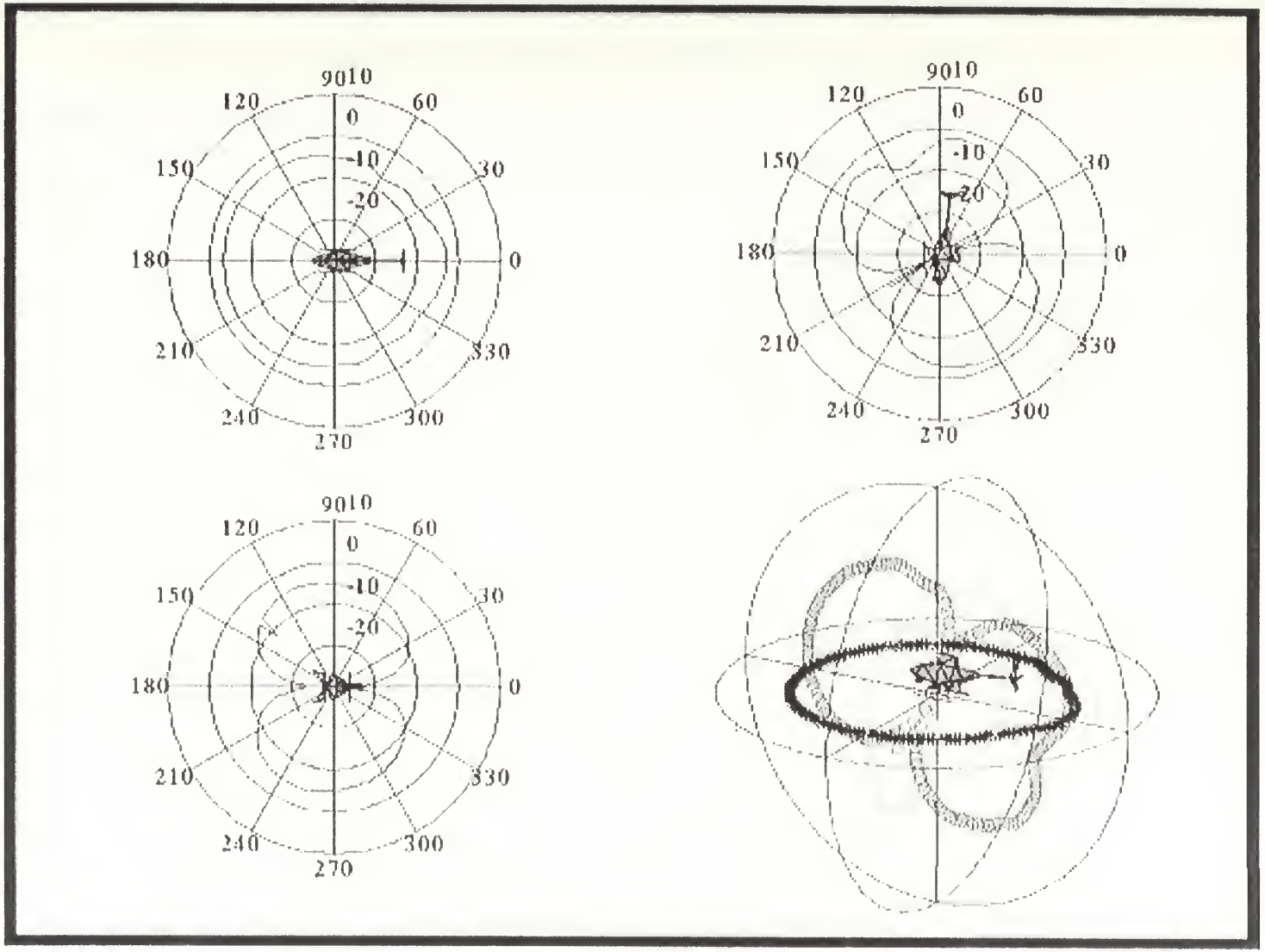

Figure 41: Yaw, pitch, roll and composite APATCH patterns for 275 MHz, antenna location C.

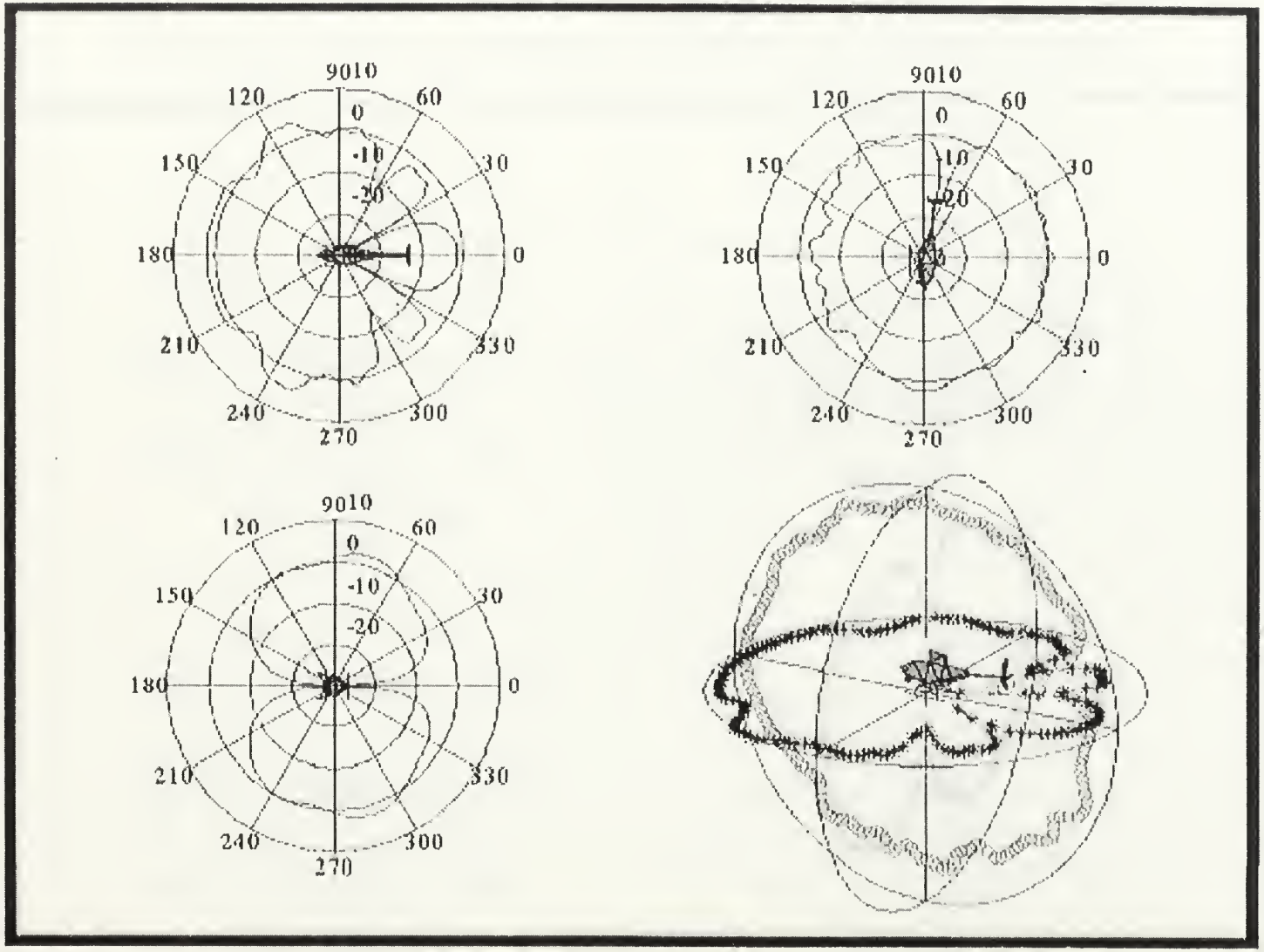

Figure 42: Yaw, pitch, roll and composite PATCH patterns for 275 MHz, antenna location C.

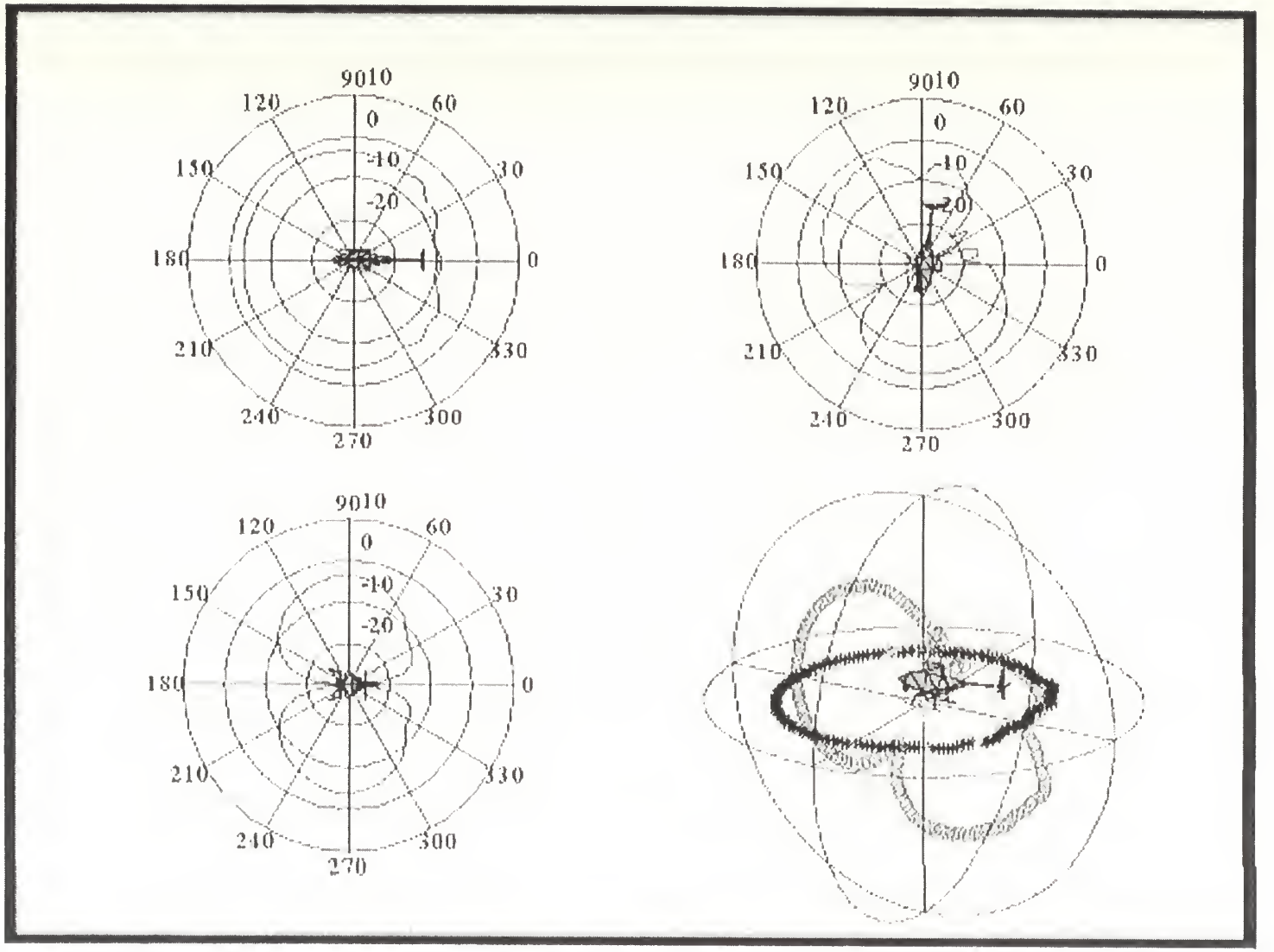

Figure 43: Yaw, pitch, roll and composite APATCH patterns for 460 MHz, antenna location C.

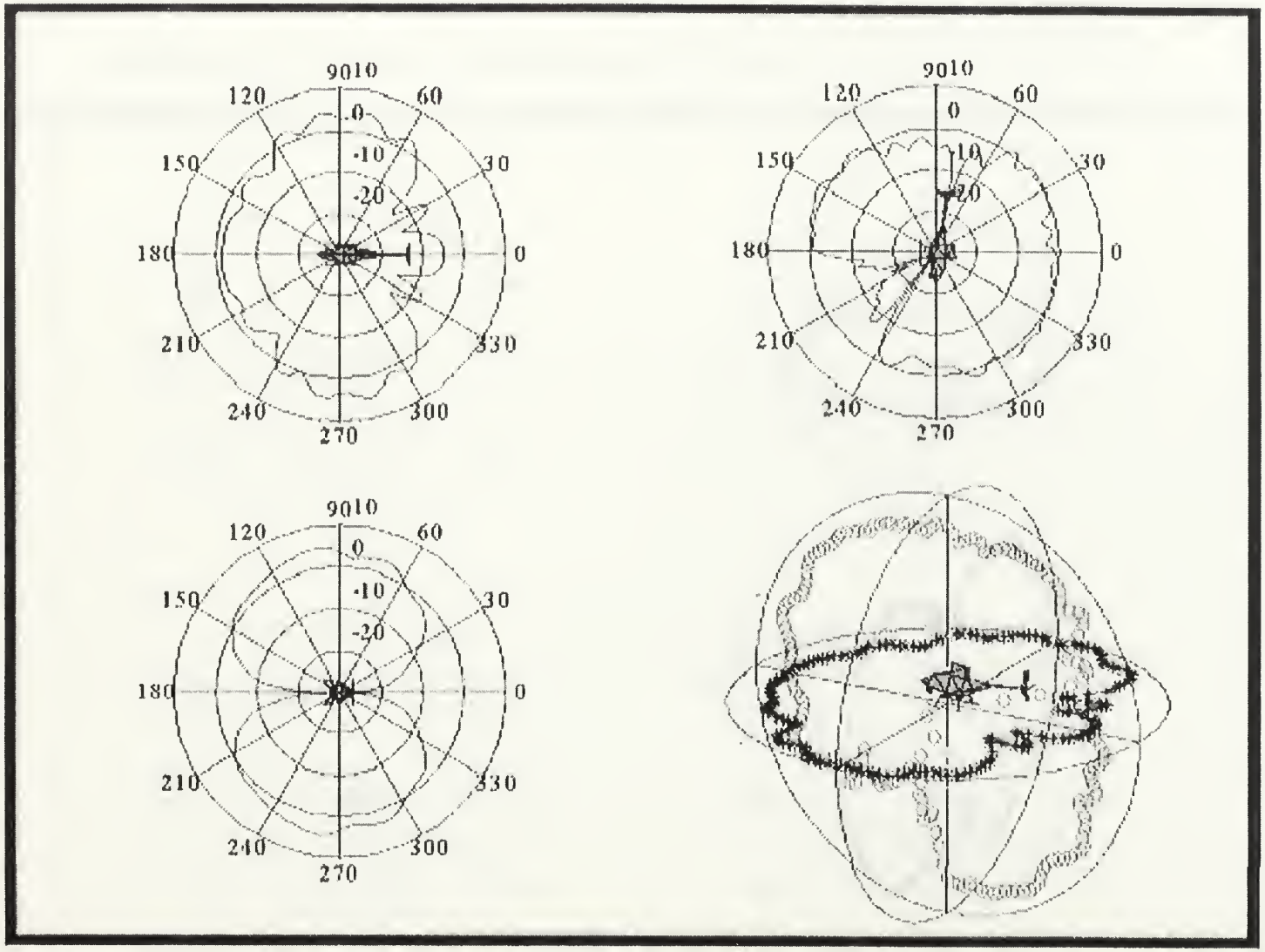

Figure 44: Yaw, pitch, roll and composite PATCH patterns for 460 MHz, antenna location C.

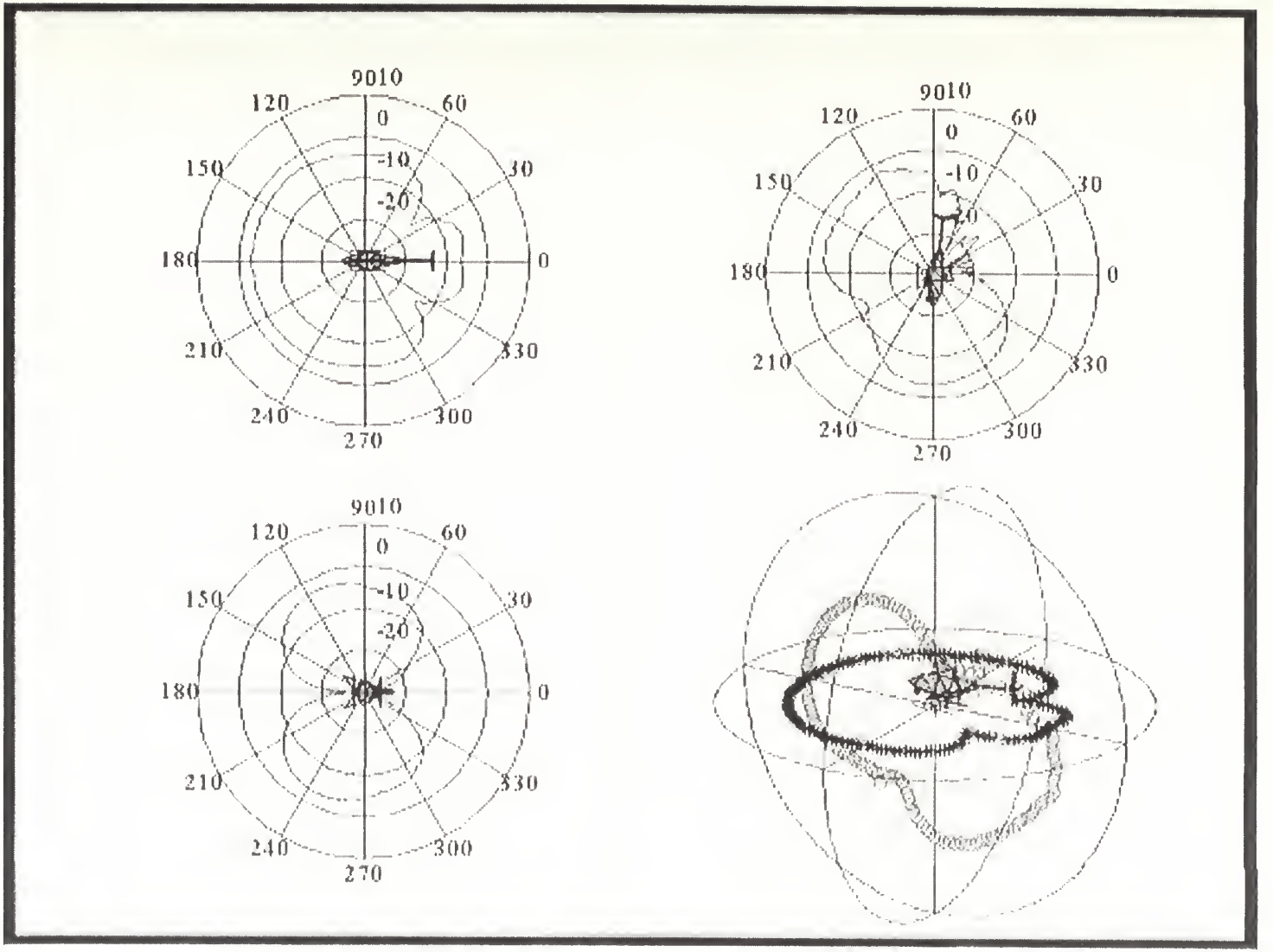

Figure 45: Yaw, pitch, roll and composite APATCH patterns for 810 MHz, antenna location C.

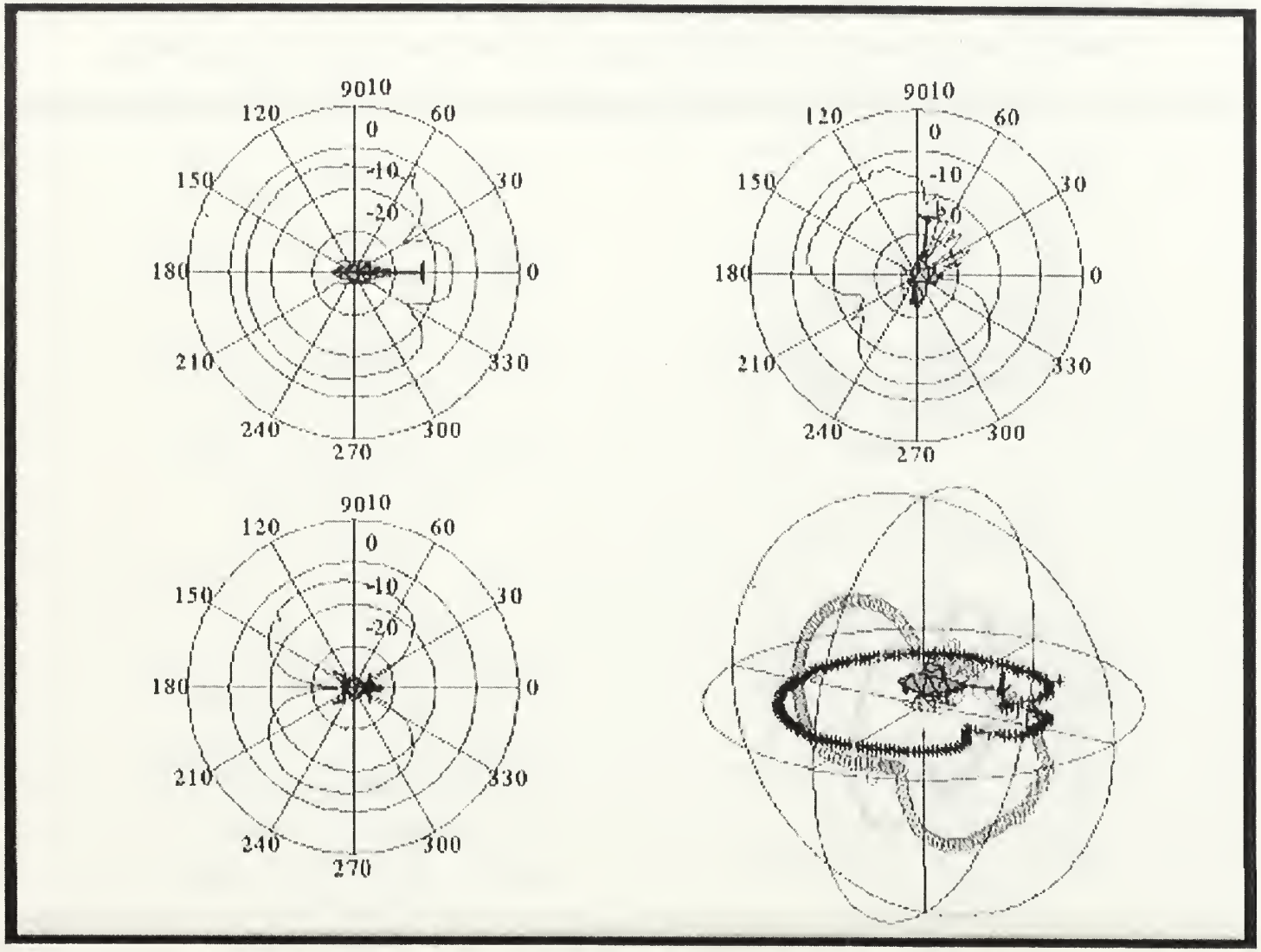

Figure 46: Yaw, pitch, roll and composite APATCH patterns for 960 MHz, antenna location C.

6.0 Hemispherical Antenna Patterns at Various Locations

6.1 Introduction

Pattern calculations for the hemispherical antenna described in Section 3.2 are presented in this section. Only APATCH is used. APATCH's tabular input mode is used for the antenna: the pattern data is provided in an external file generated using Equation (1) with $N = P = 3$, $M = 20$, $a = 0.3$ and $b = 0.05$. The amplitude of the shooting and bouncing rays are adjusted according to the pattern value in the direction of the ray. Edge diffraction is included in all cases.

6.2 Antenna Location A

Antenna location A is shown in Figure 17. Patterns are shown in Figures 47 through 51. There are no major holes in the coverage for this location.

6.3 Antenna Location B

Antenna location B is shown in Figure 29. Patterns are shown in Figures 52 through 56. As for location A, there are no major holes in the coverage.

6.4 Antenna Location C

Antenna location C is shown in Figure 38. Patterns are shown in Figure 57 through 61. There are no large holes in the coverage, however, the radiation in the rear hemisphere is reduced relative to locations A and B.

7.0 Summary and Conclusions

Radiation patterns for five frequencies were calculated for two antenna types installed on the helicopter at three locations. The results for two computer codes were compared for a monopole. The rigorous method of moments code PATCH was used only for the three lowest frequencies because of computer memory limitations (strictly speaking, its results are converged for only the two lowest frequencies). APATCH is an approximate code that was used at all frequencies. Although the two lowest frequencies "mildly" violate the limitations of APATCH, the pattern data was in good agreement with PATCH for the monopole (i.e., within a couple of dB). Edge diffraction was included in all APATCH calculations even though it did not appear to have a significant impact on the pattern data.

The manufacturers of the two systems considered for this application do not give gain or pattern specifications for their antennas. An evaluation of the antenna location was based on the overall change in patterns of the installed antenna relative to those when it is isolated in free space. The following observations are noted:

- Patterns for hemispherical antennas near the nose (location C) had significant radiation upward and reduced radiation in the back direction toward the horizon.

- The EO/IR globe did not seem to affect the patterns as adversely as the winch.
- The most significant source of scattering appears to be the vertical components of the landing support structure.
- Using the 10 dB points as a limit for good reception, locations A and B have good patterns at most azimuth angles for elevation angles below –30 degrees (i.e., good reception within a cone of 60 degree half angle centered on the vertical).
- Of the three positions, location B appears to have the best overall performance. It provides a large flat surface area for mounting the antenna that is sufficiently far from obstructions.
- The predicted detection ranges in Appendix C can be extended by using an antenna with a higher gain on the horizon.

8.0 References

[1] J. Volakis, A. Chatterjee and L. Kempel, *Finite Element Method for Electromagnetics*, IEEE Press, 1998.

[2] R. Harrington, *Field Computation by Moment Methods*, MacMillan, 1968.

[3] C. Balanis, *Antenna Theory*, Wiley, 1982.

[4] W. Johnson, D. Wilton, and R. Sharpe, *Patch Code Users' Manual*, Sandia Laboratory Report SAND87-2991, May 1988.

[5] *APATCH Ver 2.1 Users Manual*, DEMACO Inc., 100 Trade Center Drive, Champaign, IL, 61820.

[6] *ACAD Users Manual*, Lockheed-Martin, Fort Worth, TX, 76108.

[7] H. Jasik, editor, *Antenna Engineering Handbook*, McGraw-Hill, 1961.

[8] T. Firestone, K. Cybert, D. Reuster and M. McKaughan, "The Effects of Rotor Modulation on a Sikorsky HH-60J Helicopter HF Communication Antenna," *17th Annual Review of Progress in Applied Computational Electromagnetics*, March 19-23, 2001.

[9] E. A. Wolff, *Antenna Analysis*, Wiley and Sons, 1966.

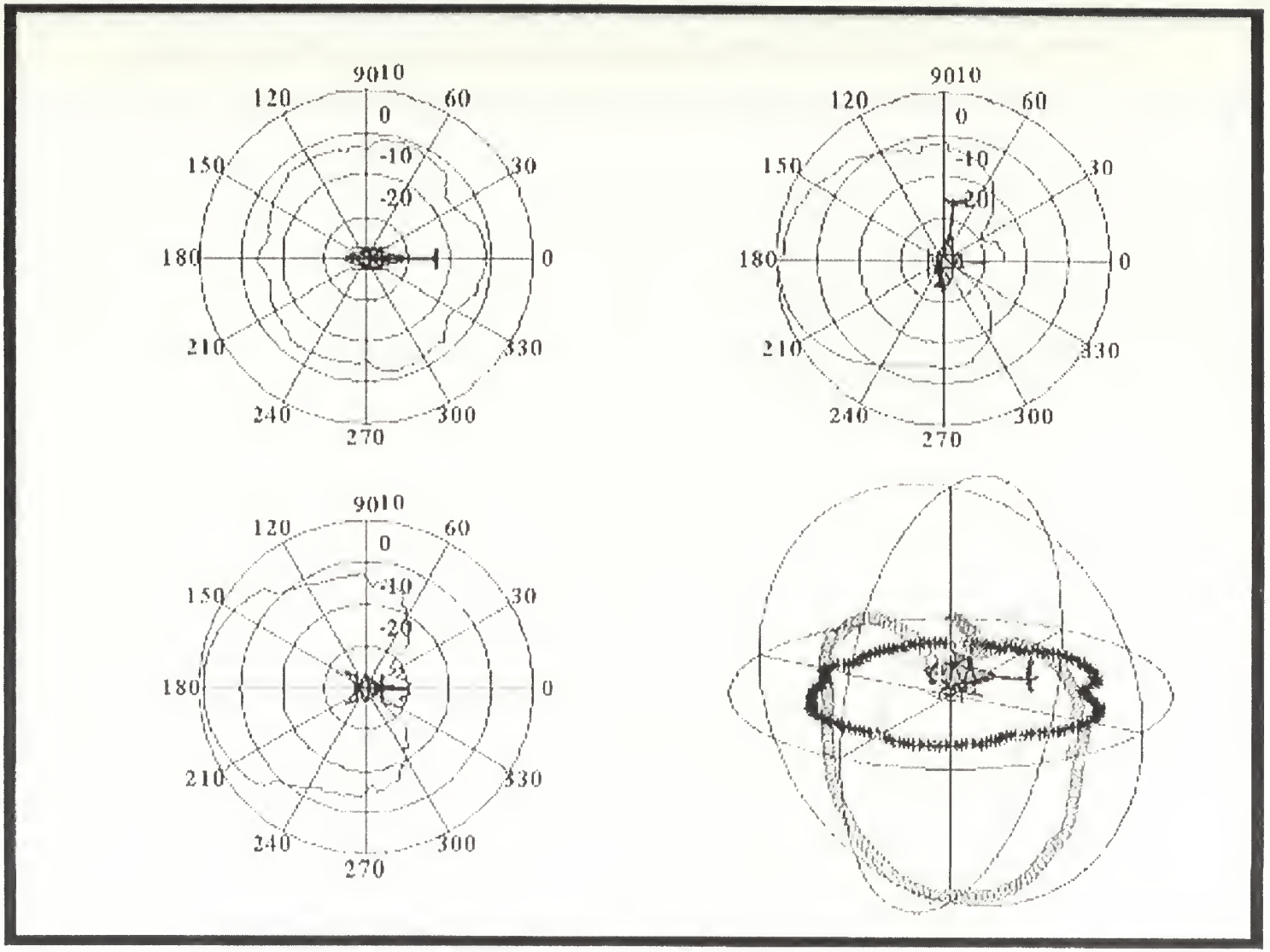

Figure 47: Yaw, pitch, roll and composite APATCH patterns for 130 MHz, antenna location A.

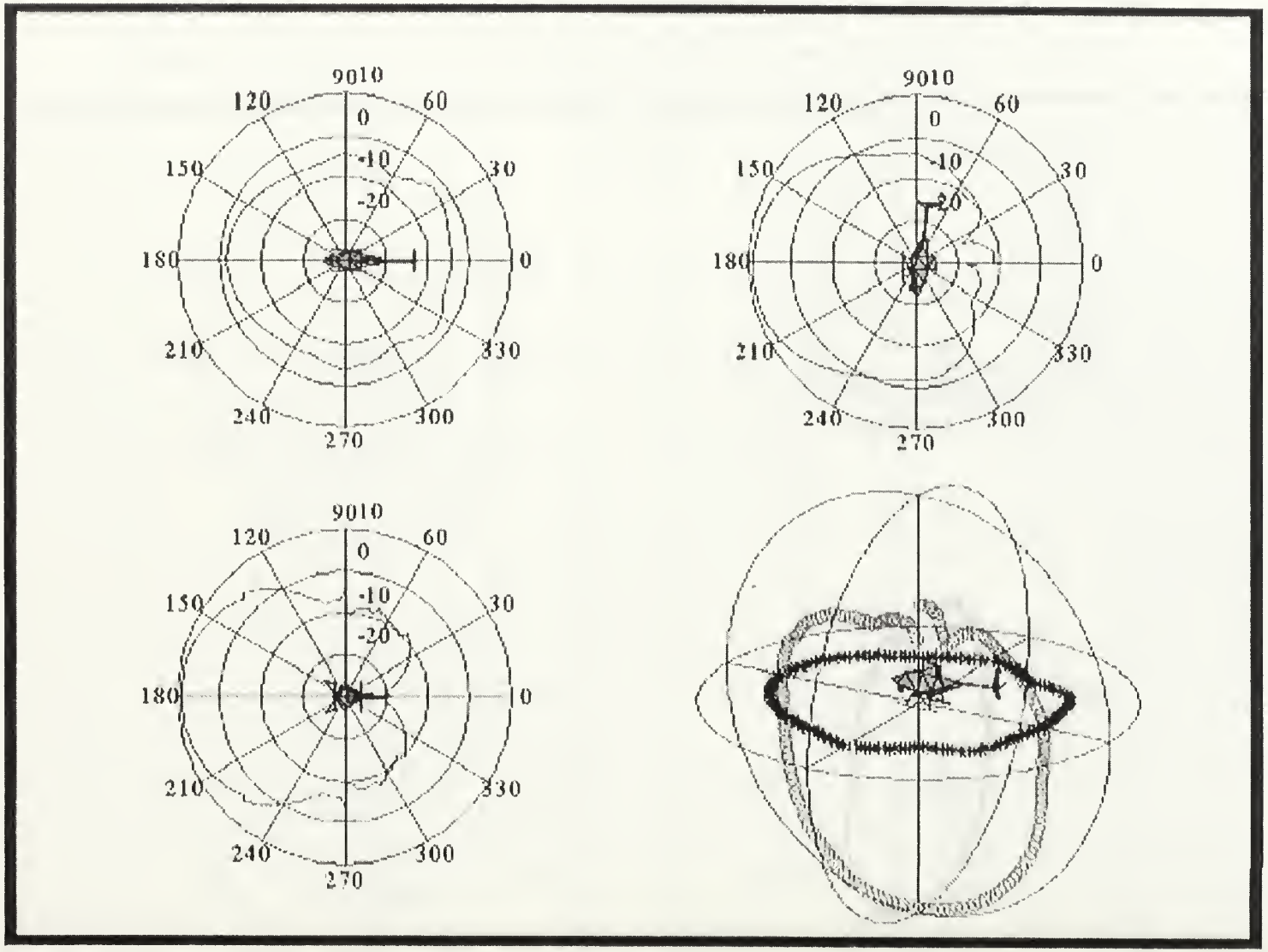

Figure 48: Yaw, pitch, roll and composite APATCH patterns for 275 MHz, antenna location A.

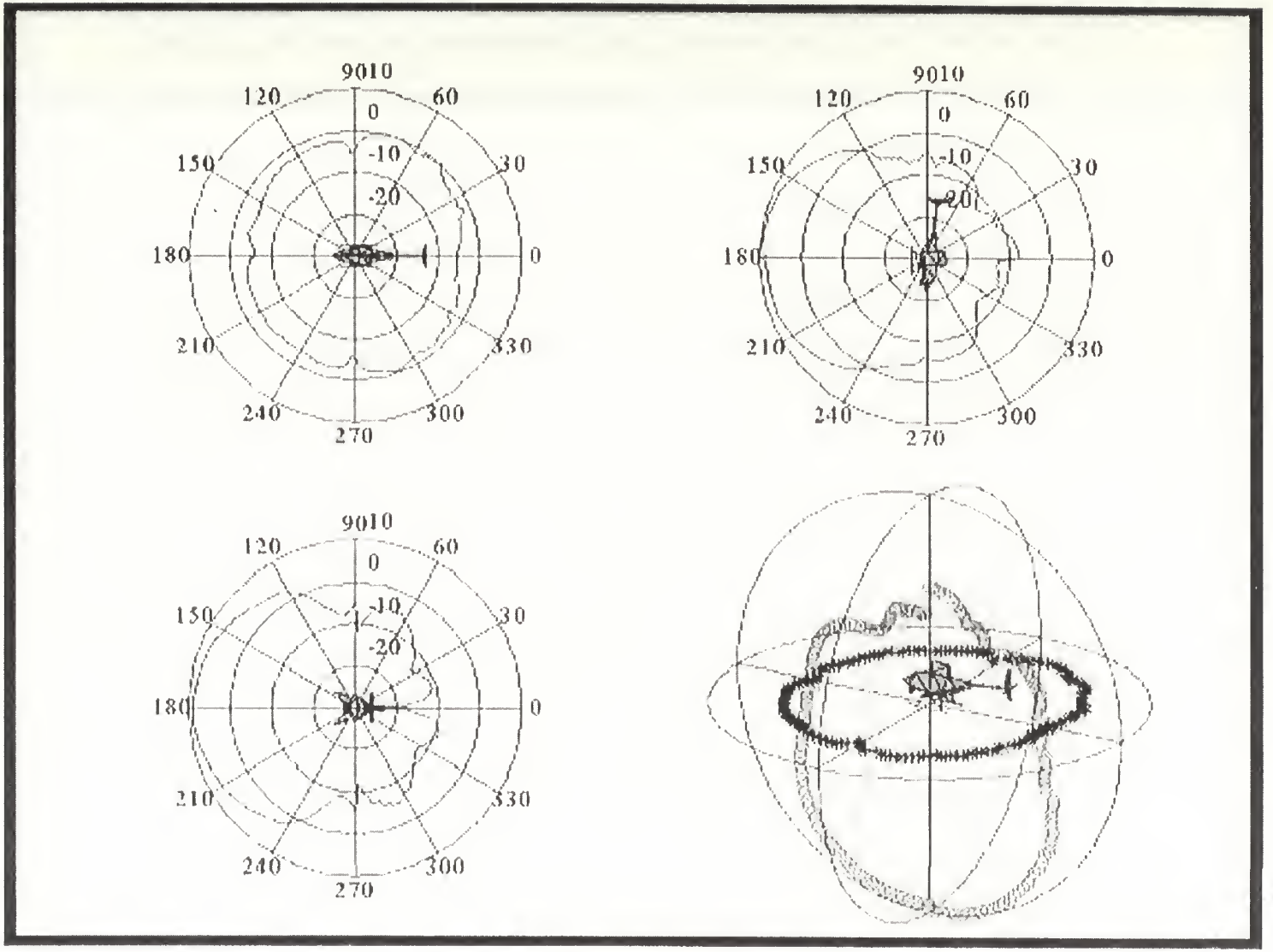

Figure 49: Yaw, pitch, roll and composite APATCH patterns for 460 MHz, antenna location A.

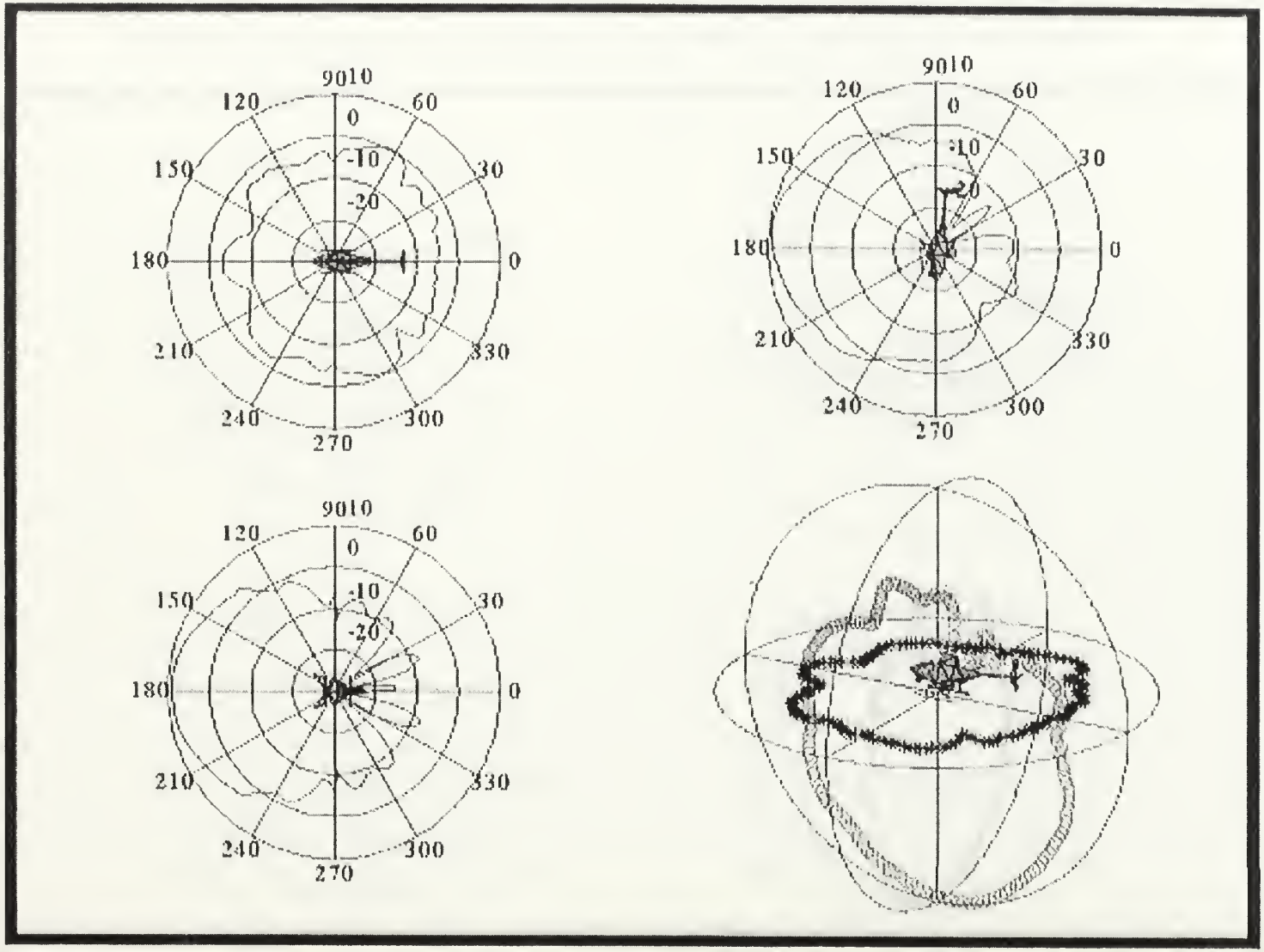

Figure 50: Yaw, pitch, roll and composite APATCH patterns for 810 MHz, antenna location A.

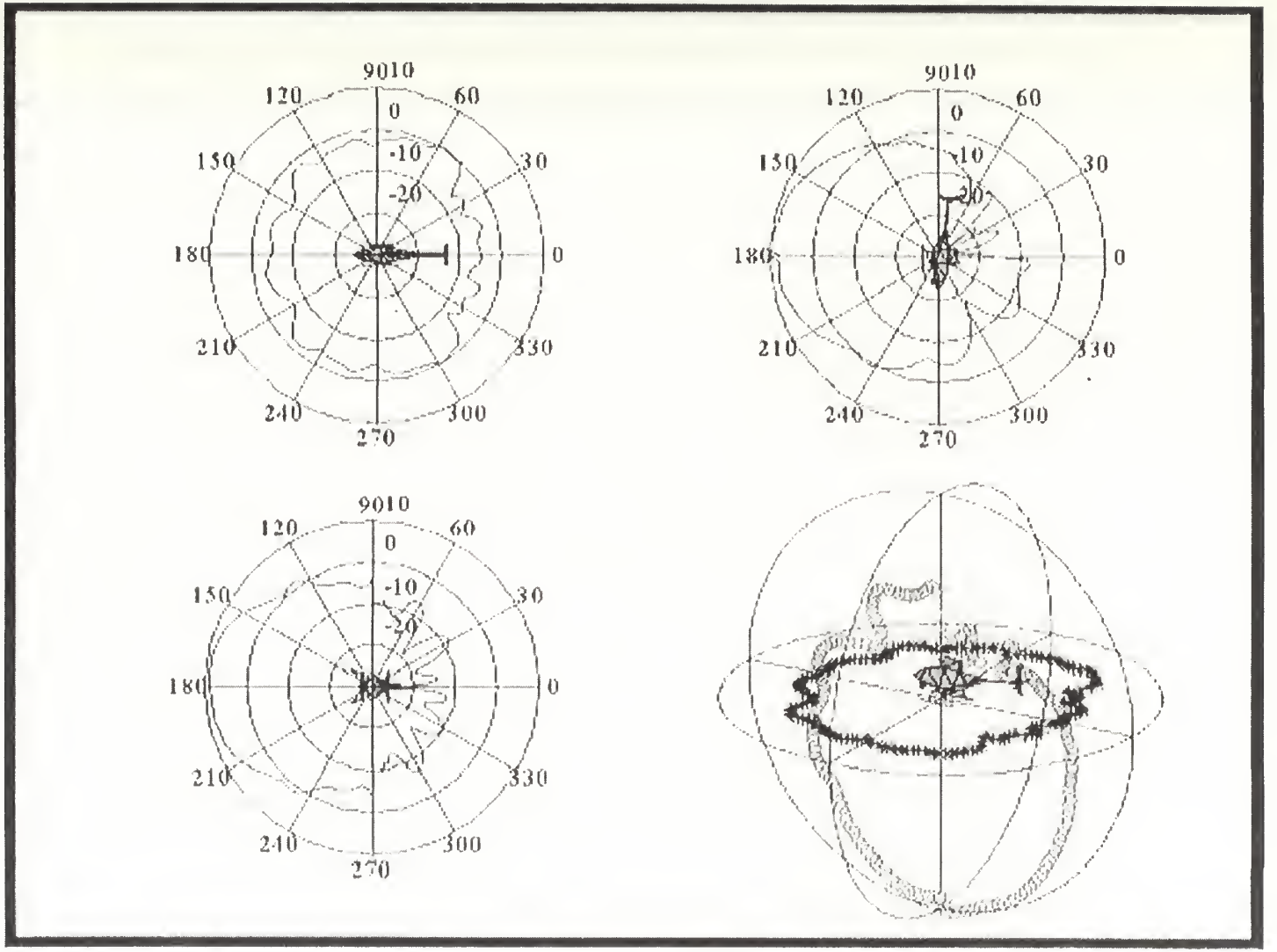

Figure 51: Yaw, pitch, roll and composite APATCH patterns for 960 MHz, antenna location A.

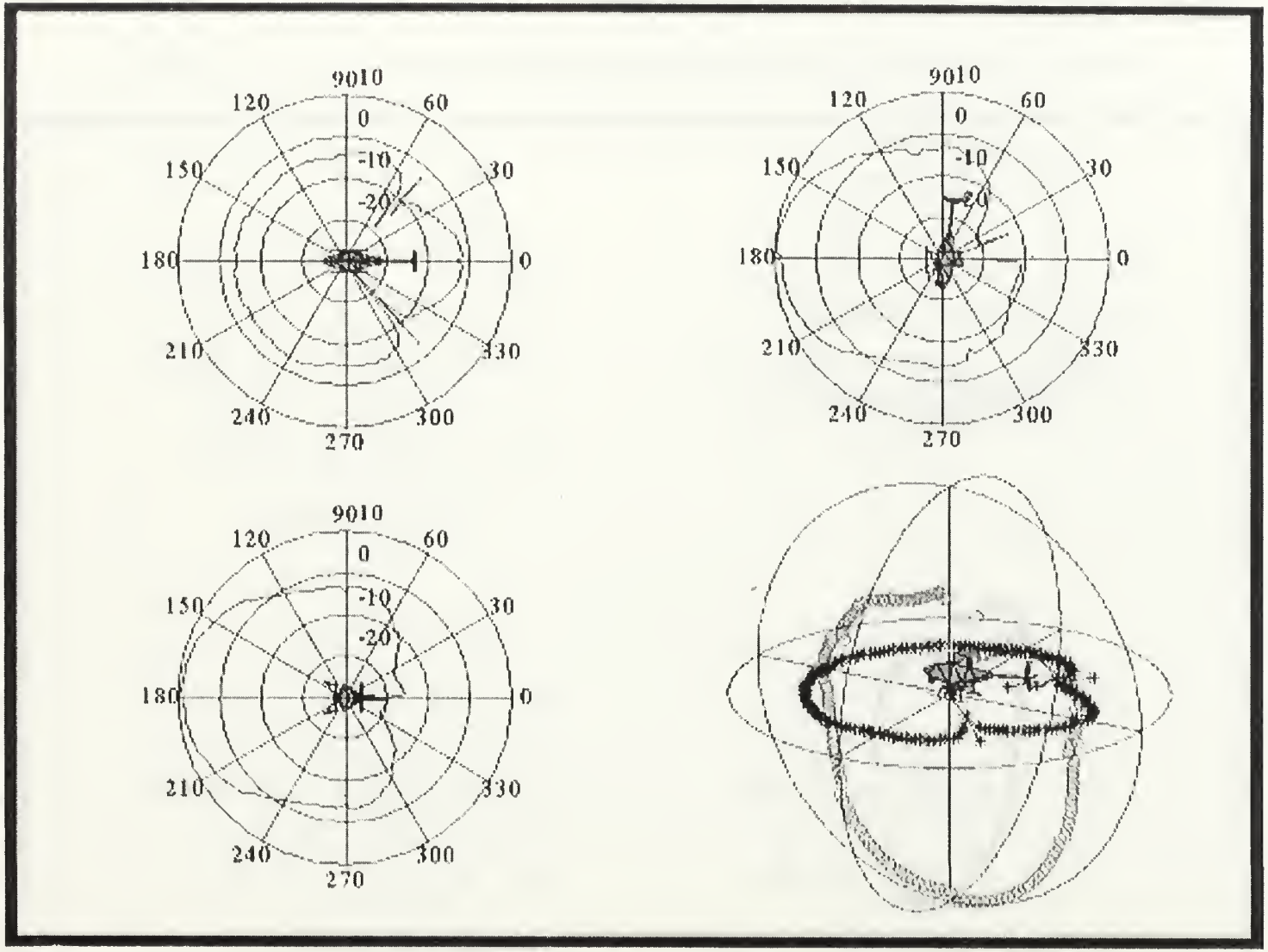

Figure 52: Yaw, pitch, roll and composite APATCH patterns for 130 MHz, antenna location B.

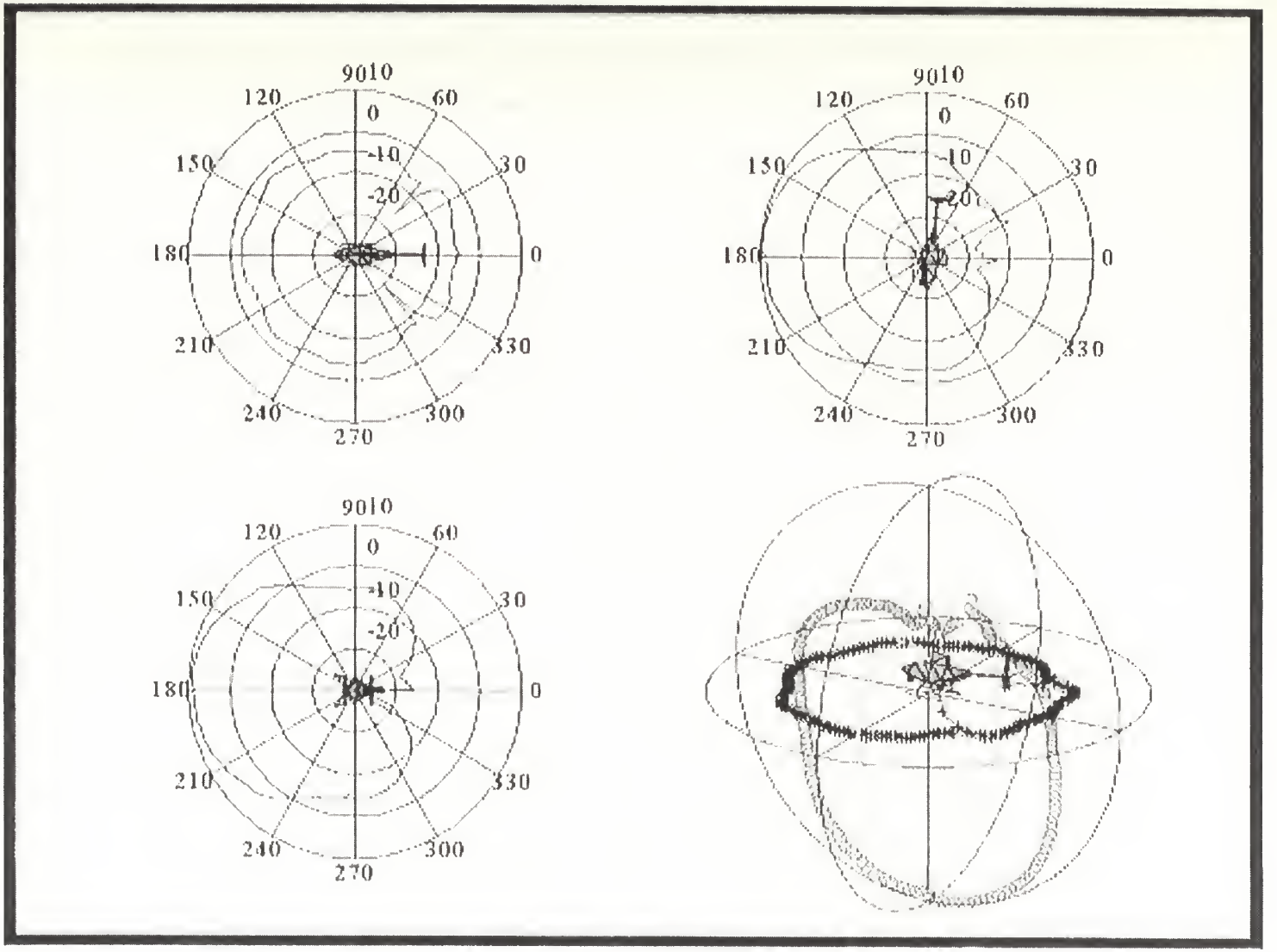

Figure 53: Yaw, pitch, roll and composite APATCH patterns for 275 MHz, antenna location B.

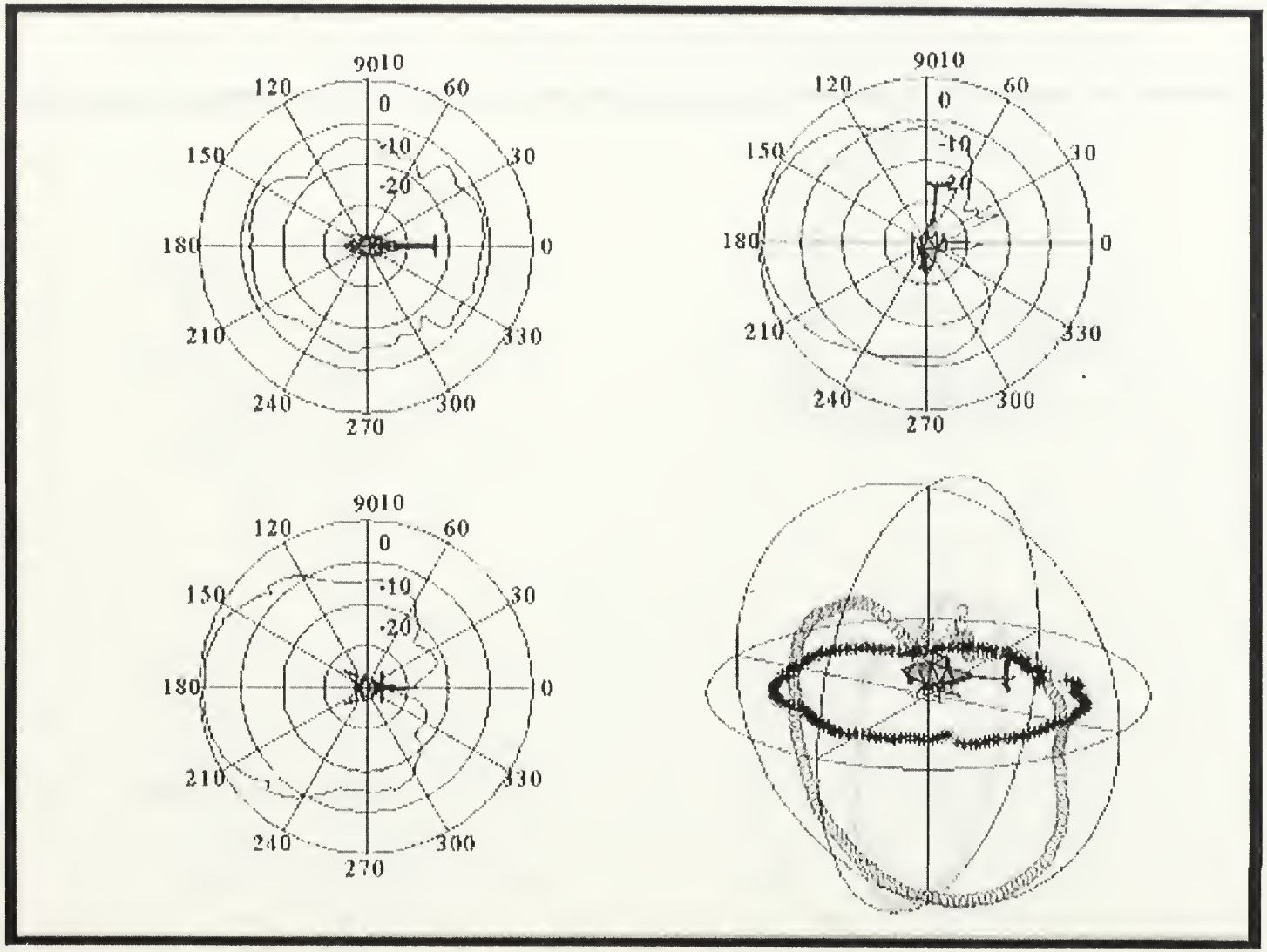

Figure 54: Yaw, pitch, roll and composite APATCH patterns for 460 MHz, antenna location B.

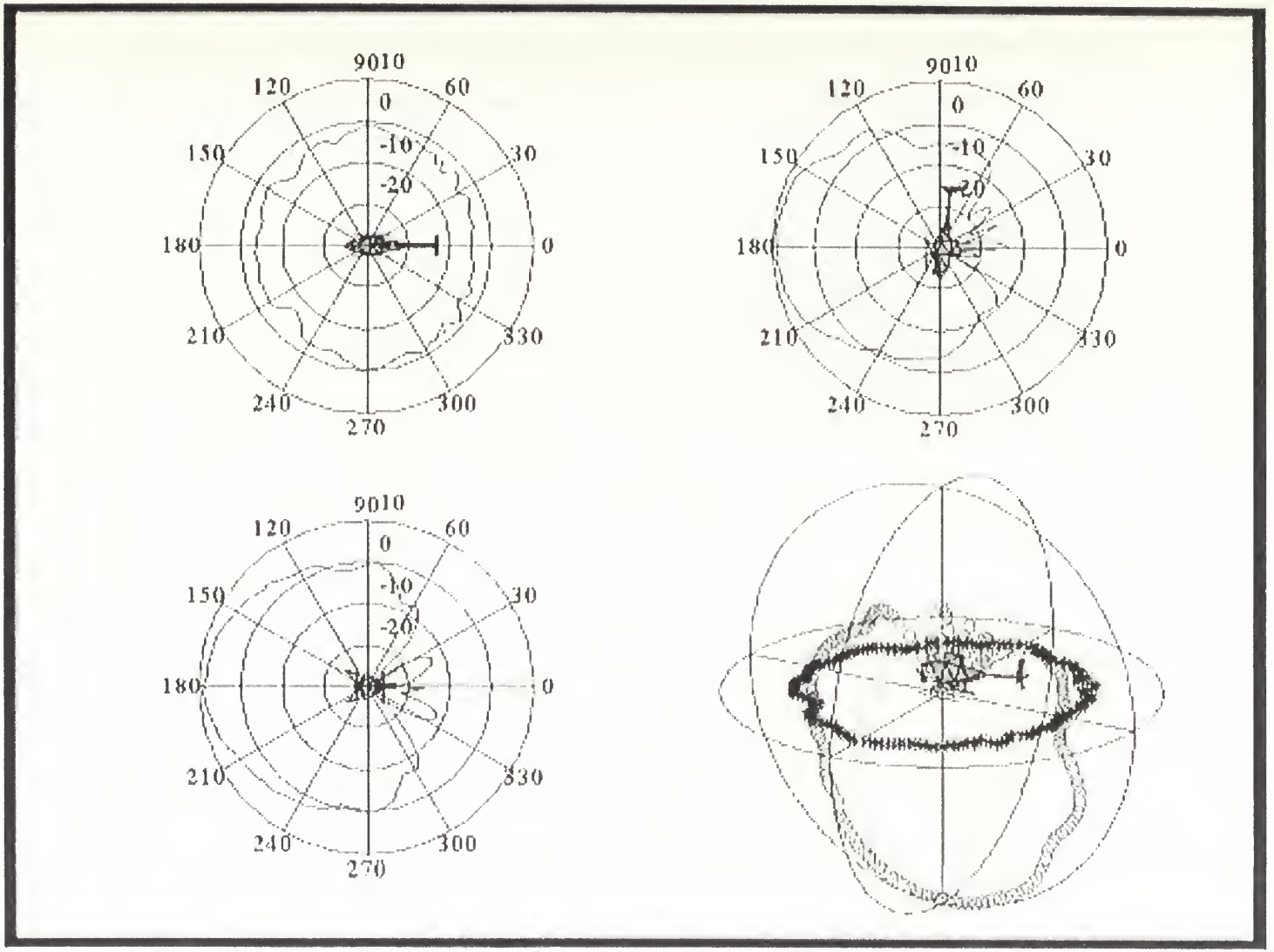

Figure 55: Yaw, pitch, roll and composite APATCH patterns for 810 MHz, antenna location B.

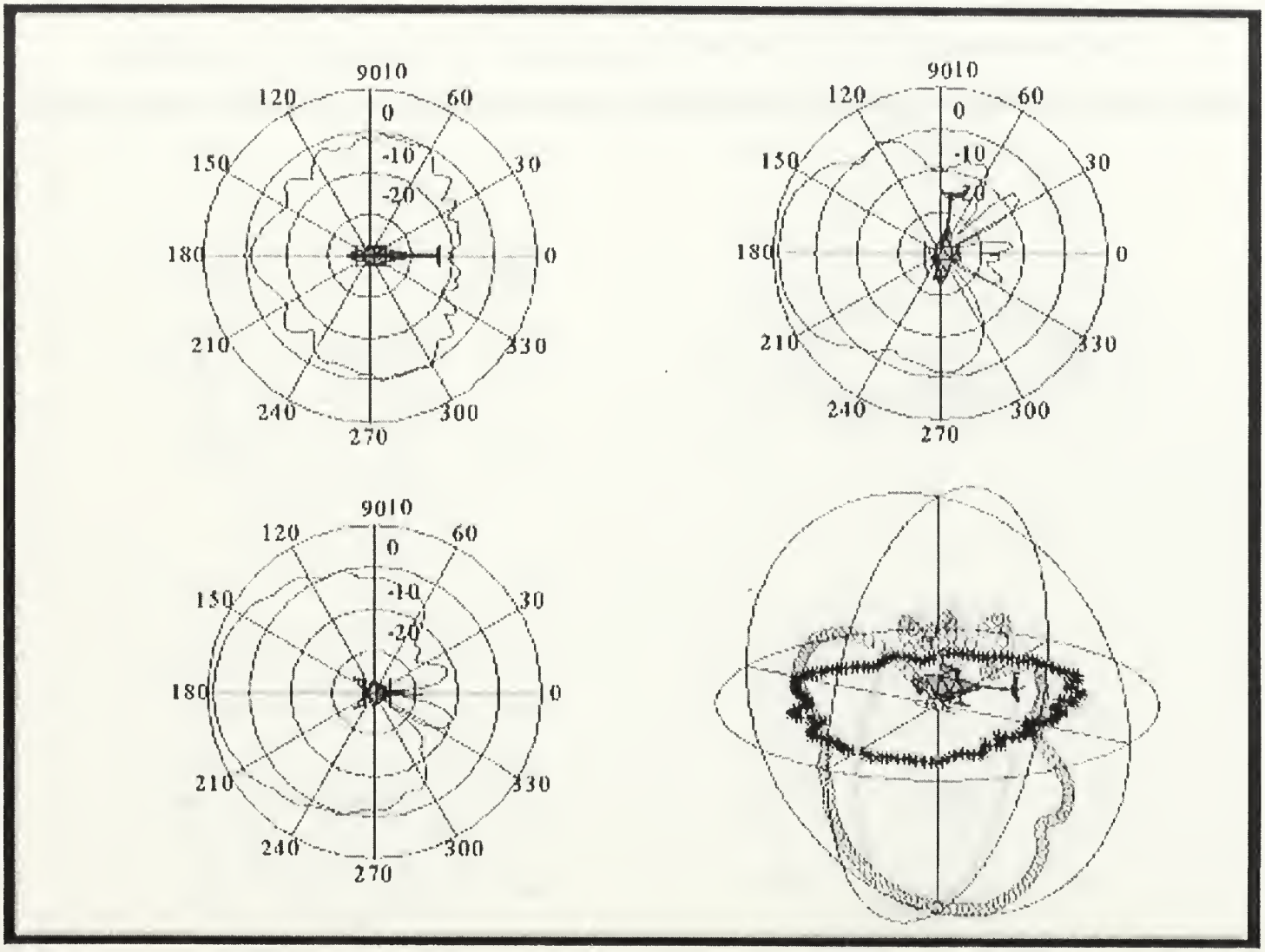

Figure 56: Yaw, pitch, roll and composite APATCH patterns for 960 MHz, antenna location B.

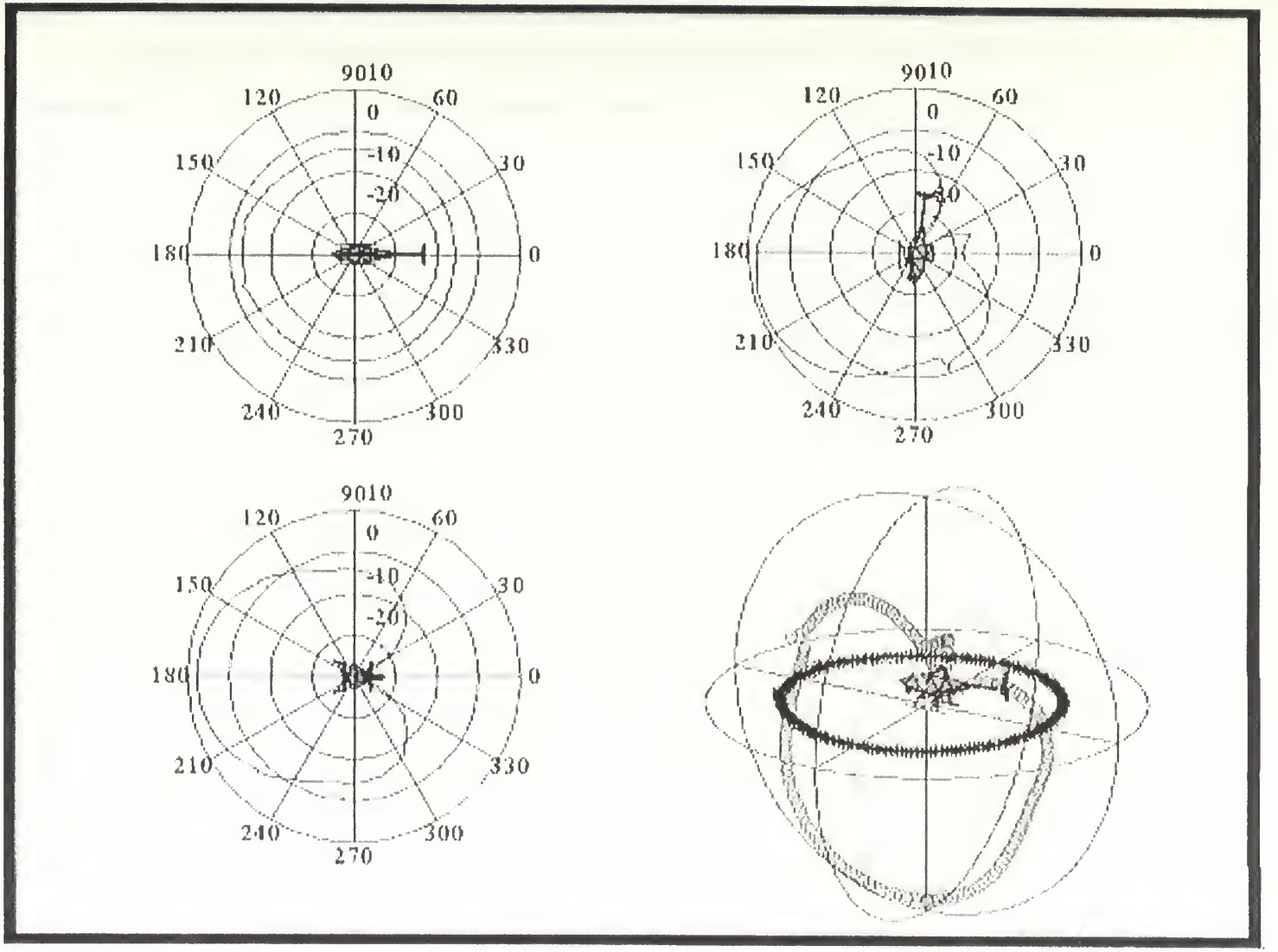

Figure 57: Yaw, pitch, roll and composite APATCH patterns for 130 MHz, antenna location C.

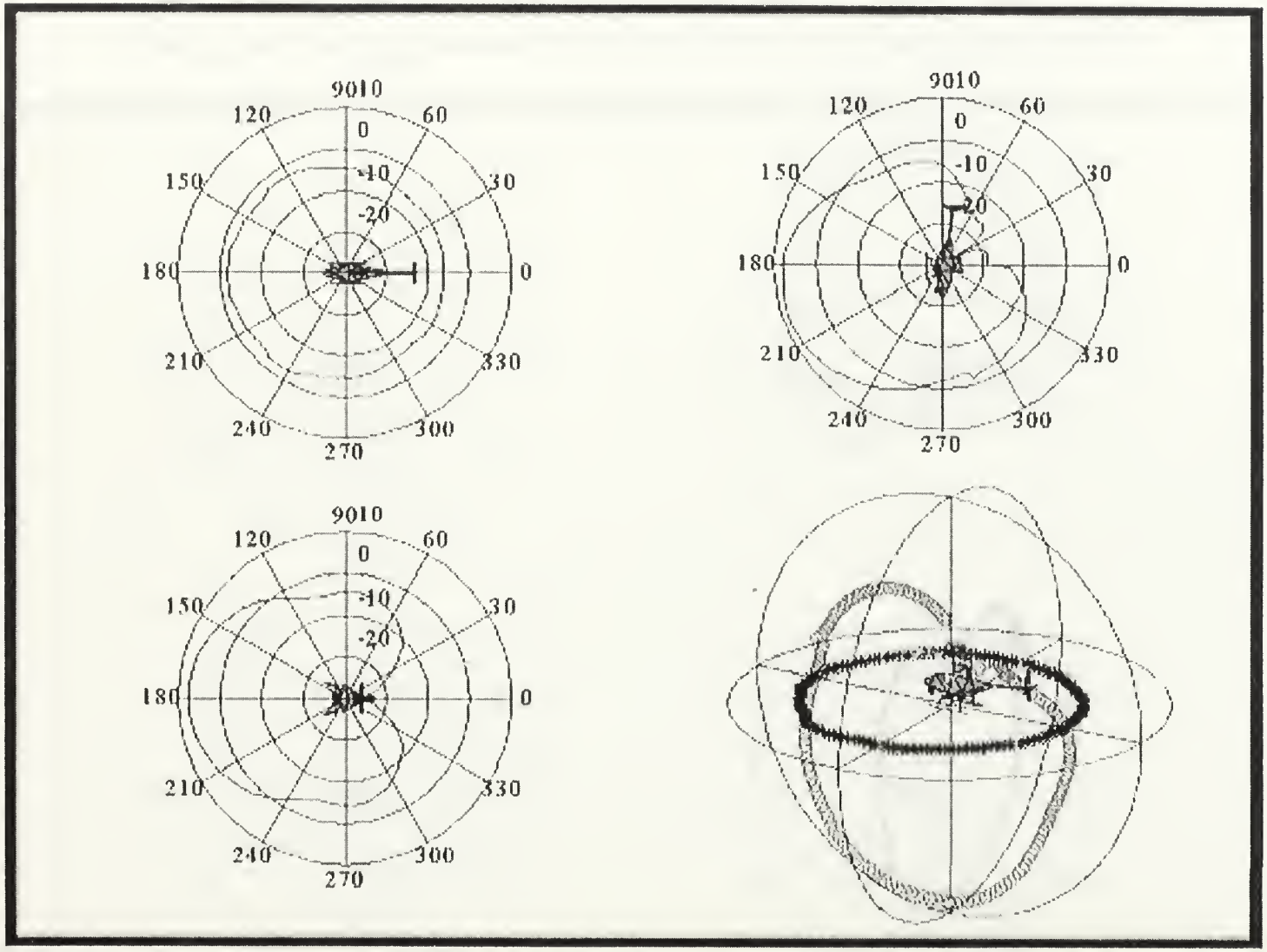

Figure 58: Yaw, pitch, roll and composite APATCH patterns for 275 MHz, antenna location C.

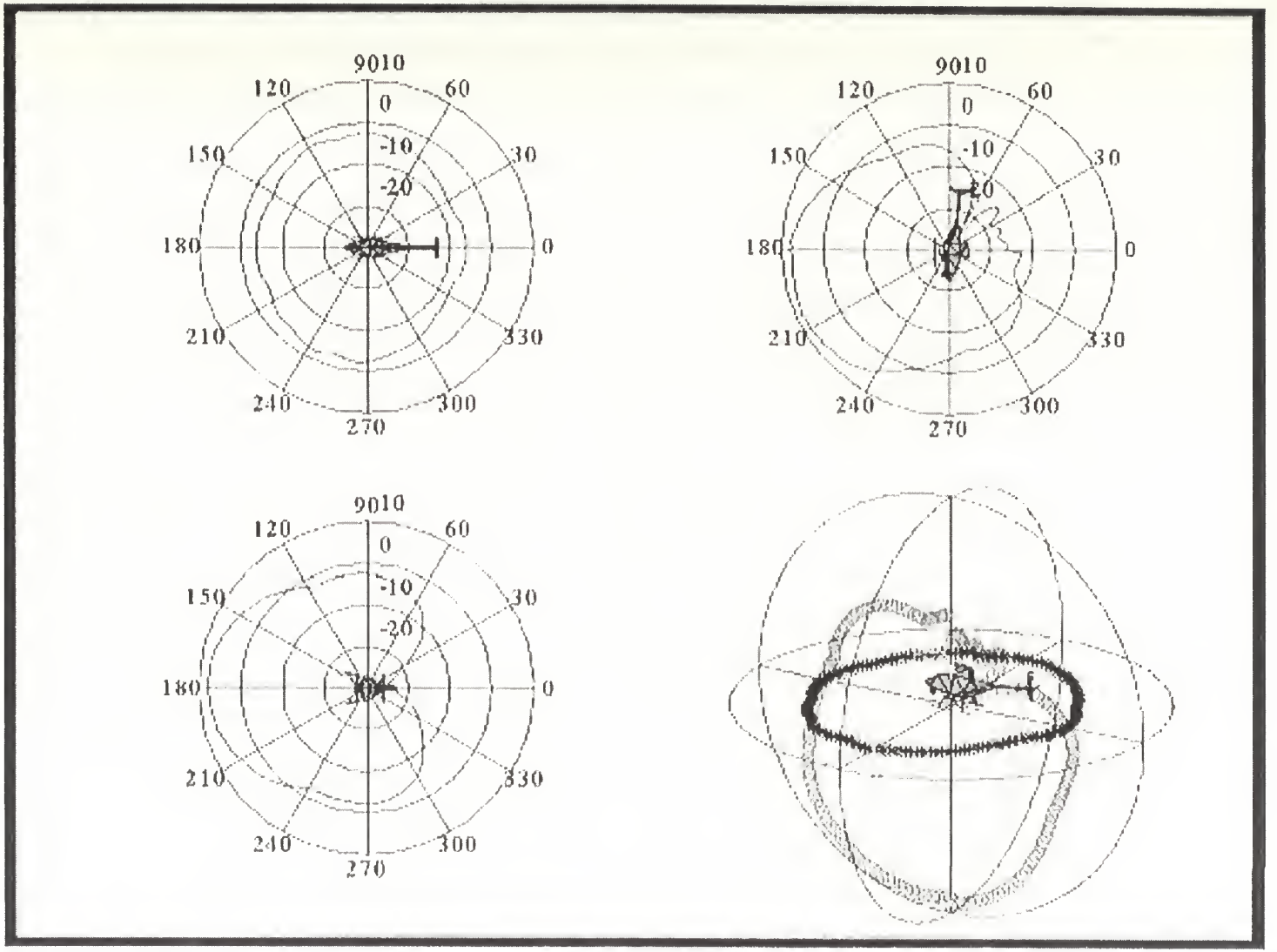

Figure 59: Yaw, pitch, roll and composite APATCH patterns for 460 MHz, antenna location C.

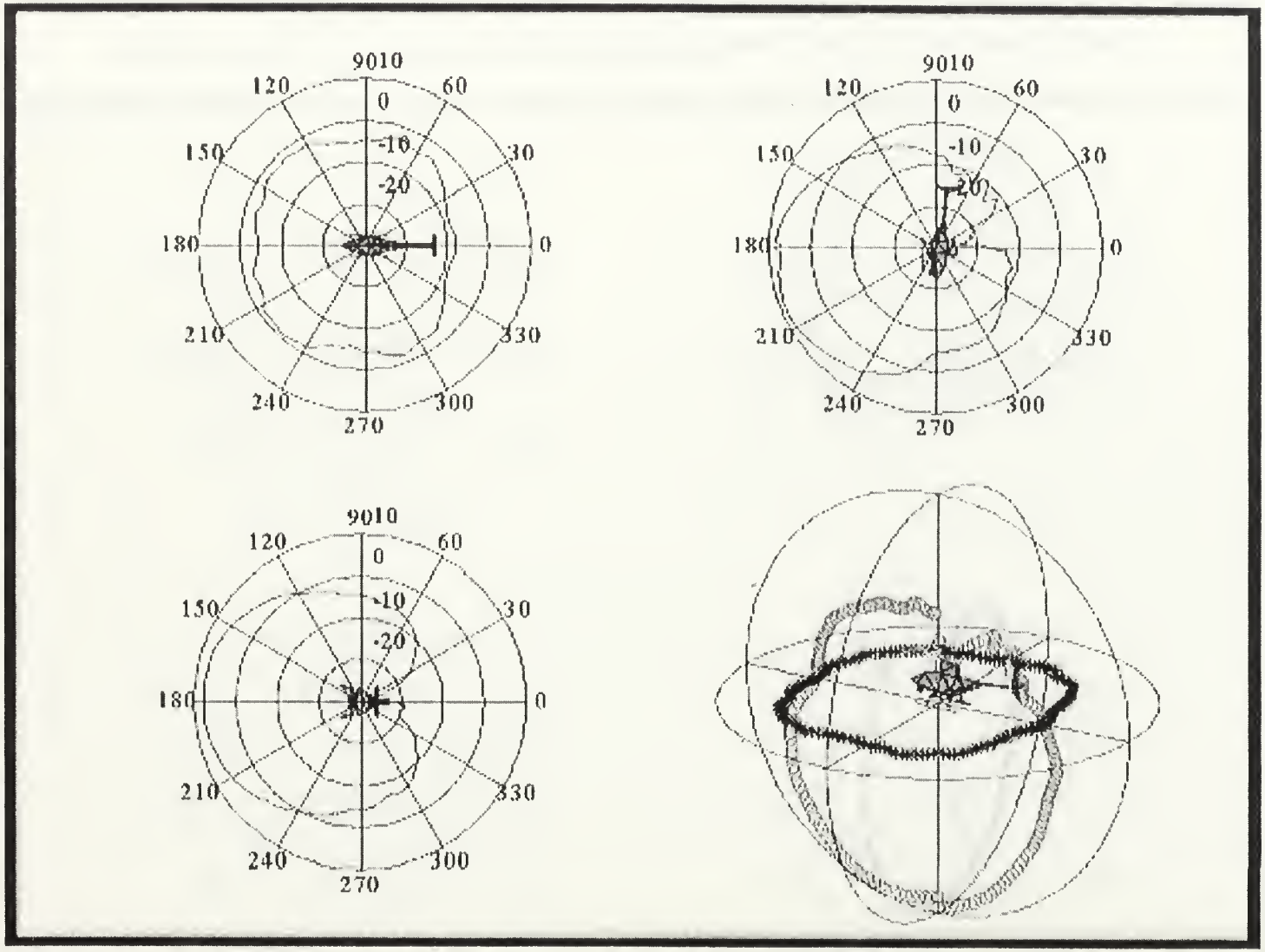

Figure 60: Yaw, pitch, roll and composite APATCH patterns for 810 MHz, antenna location C.

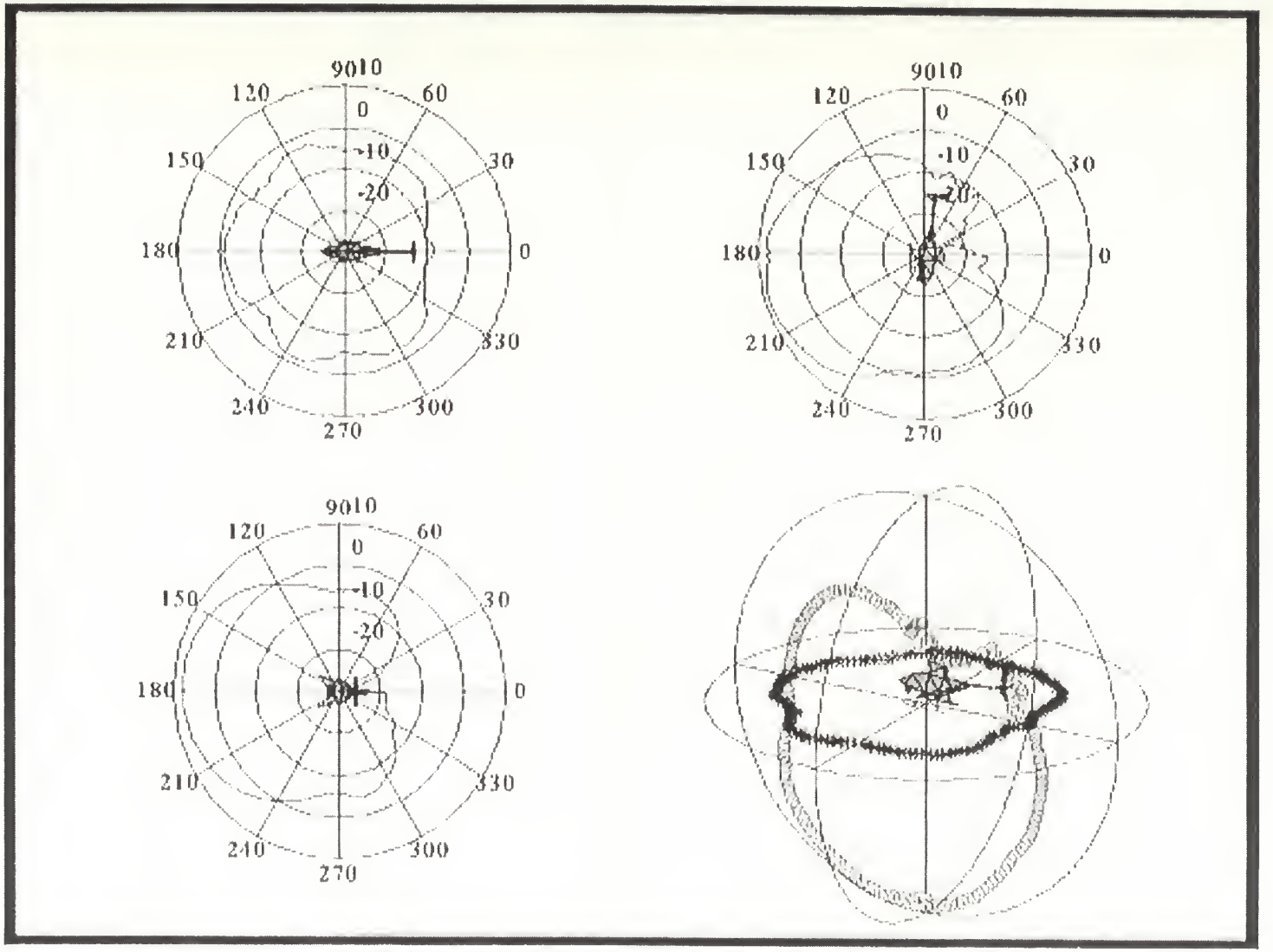

Figure 61: Yaw, pitch, roll and composite APATCH patterns for 960 MHz, antenna location C.

APPENDIX A: Relationship Between Sensitivity and Antenna Gain

The sensitivity is the minimum detectable signal for a given signal-to-noise ratio (SNR) expressed in either volts or watts. A formula relating the gain of the antenna to the receiver sensitivity can be derived based on the simple model shown in Figure A1. A receiver with a load impedance of $Z_L = R_L + jX_L$ is connected to the antenna terminals. The antenna impedance is $Z_a = R_a + jX_a = (R_\ell + R_r) + jX_a$, where R_ℓ is the loss resistance, R_r the radiation resistance, and X_a the antenna reactance. For convenience, let the antenna be lossless ($R_\ell = 0$).

The equivalent circuit of the antenna and receiver is also shown in Figure A1. The equivalent source voltage is $V_s = \bar{E}_i \bullet \bar{h}_e$ where $\bar{E}_i$ is the incident electric field vector and $\bar{h}_e$ the effective height [A1]. The voltage across the input of the receiver is (rms phasor quantities)

$$V_i = \frac{V_s Z_L}{Z_L + Z_a}$$

and the current into the receiver is

$$I = \frac{V_s}{Z_L + Z_a}.$$

Another figure of merit for antennas is the effective area, which is the power delivered to the load divided by the incident power density

$$A_e = \frac{P_L}{W} = \frac{I^2 R_L}{\left|\bar{E}_i\right|^2 / \eta_o}.$$

η_o is the impedance of free space. Substituting in the expressions for I and $\bar{E}_i$ into the above equation gives a relationship between the effective height and effective area:

$$\left|\bar{h}_e\right| = \sqrt{\frac{A_e \left|Z_L + Z_a\right|^2}{R_L \eta_o}}.$$

The effective area is related to the gain G by

$$G = \frac{4\pi A_e}{\lambda^2}$$

where λ is the wavelength. Solving this for effective area and using the result in the expression for effective height gives

$$|\bar{h}_e| = \sqrt{\frac{G\lambda^2 |Z_L + Z_a|^2}{4\pi R_L \eta_o}}.$$

Since the voltage at the input $V_s = \bar{E}_i \bullet \bar{h}_e$

$$|V_i| = \frac{|\bar{E}_i||Z_L|}{|Z_L + Z_a|}\sqrt{\frac{G\lambda^2 |Z_L + Z_a|^2}{4\pi R_L \eta_o}} \propto \sqrt{G}.$$

Therefore, if all other system parameters remain constant, including receiver sensitivity, the overall system sensitivity improves in direct proportion to the square root of the antenna gain.

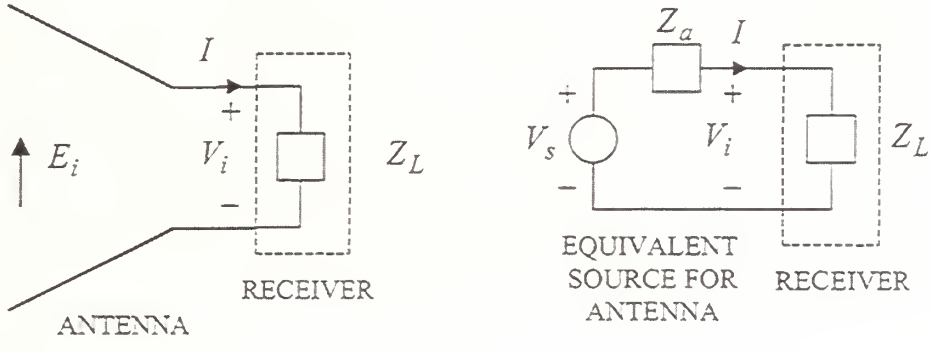

Figure A1: Antenna with a receiver and the equivalent circuit.

References

[A1] J. D. Kraus, *Antennas*, McGraw-Hill

APPENDIX B: Investigation of Rotor Effects on the Antenna Gain

Scattering by the helicopter rotor blades is a potential source of direction finding system error. The scattering from the blades is a form of multipath that results in an effective change in gain of the antenna relative to its gain in free space. Also, the rotation of the blades modulates the received signal, creating harmonics that are dependent on the angular frequency of the rotor and the total number of blades.

The first effect is the one primarily of interest in this study. Frequently the rotors are approximated by a solid conducting disk. This does not necessarily give accurate results when the rotor velocity is much less that the speed of light In fact, when this is the case the rotors can be considered approximately stationary. The scattered field from the helicopter and rotors can be computed at time "snapshots" and the time-varying quantities at observation points in the far field Fourier transformed to obtain the frequency components. The latter approach was taken in references [B1-B2].

The scattering from the rotors was calculated at four positions denoted 0, 30, 60 and 90 degress, as shown in Figure B1 (0 degrees corresponds to a blade along the tail boom). Frequencies of 275 MHz and 810 MHz were examined. In all cases the change in gain below the horizon (lower hemisphere) was less that 0.2 dB. However, the change in gain in the upper hemisphere was as large as 10 dB in a free isolated observation directions. Sample patterns for several rotor positions are shown in Figure B2 (275 MHz). Figure B3 plots the difference in gain (with rotor vs. without rotor) at 2 degree increments over all space. The data shows that the rotor scattering is not significant for observation points below the horizon.

References

[B1] T. Firestone, K. Cybert, M. McKaughan and D. Reuster, "The Effects of Rotor Modulation on a Sikorsky HH-60J Helicopter HF Communication Antenna," *Applied Computational Electromagnetics Society Symposium Digest,* March 2001.

[B2] A. Polycarpou, C. Balanis, and A. Stefanov, "Helicopter Rotor-Blade Modulation of Antenna Radiation Characteristics," *IEEE Trans. on Antennas & Propagation*, vol. 49, no. 5, May 2001.

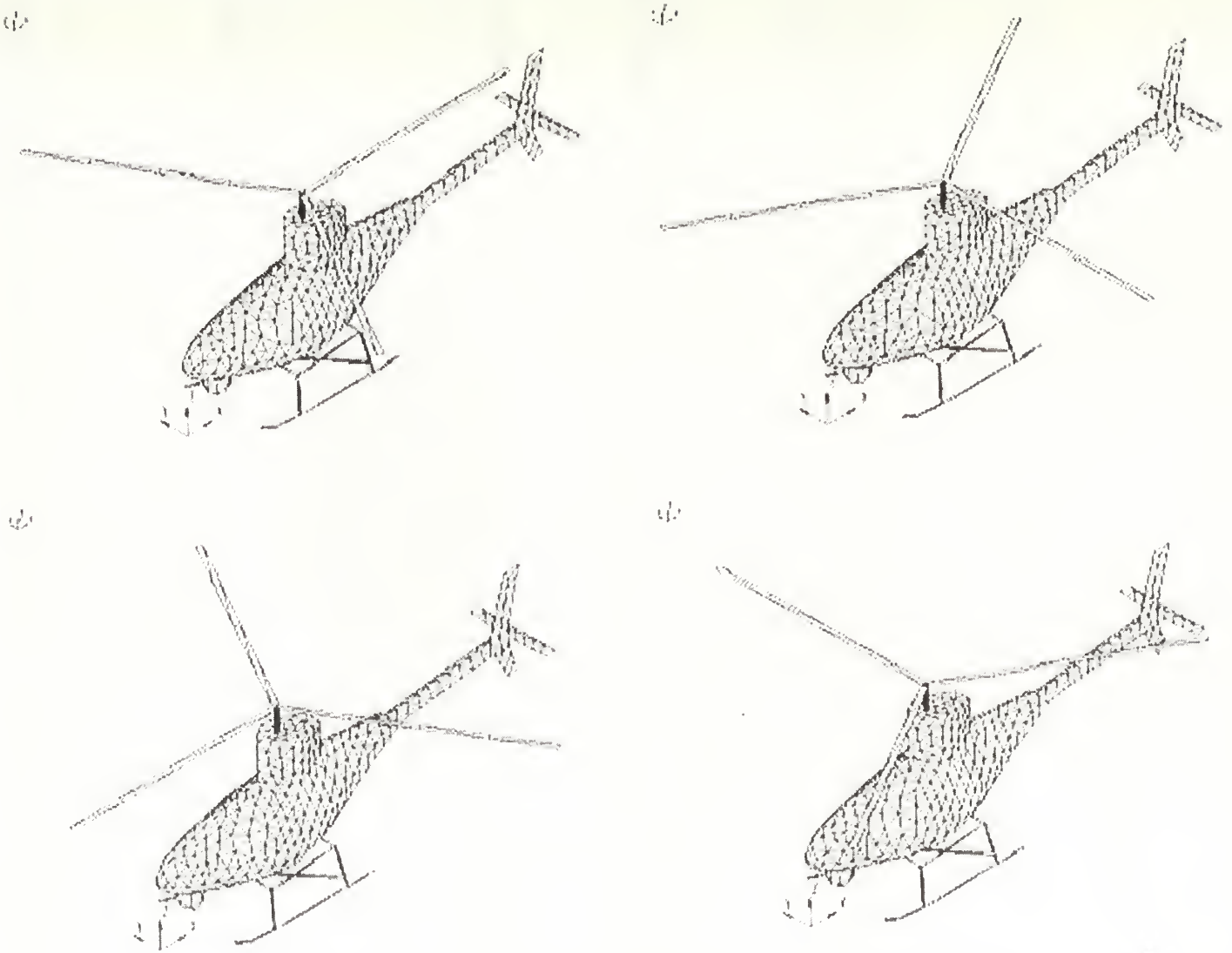

Figure B1: Rotor positions of (from upper left) 0, 30, 60 and 90 degrees.

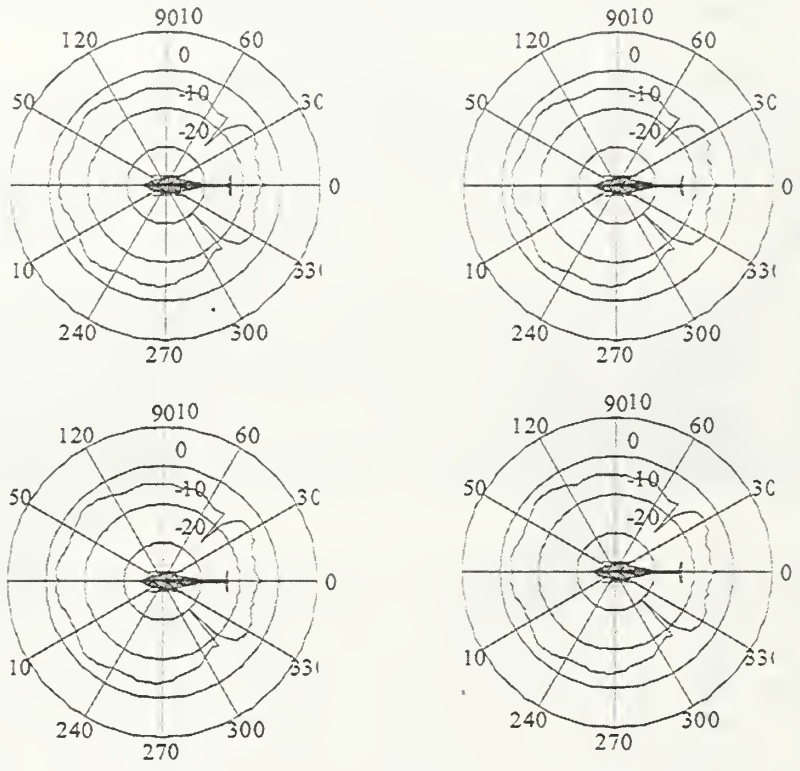

Figure B2: Sample yaw plane patterns (from upper left) for no rotor and rotor positions 0, 30, and 60 degrees, 810 MHz.

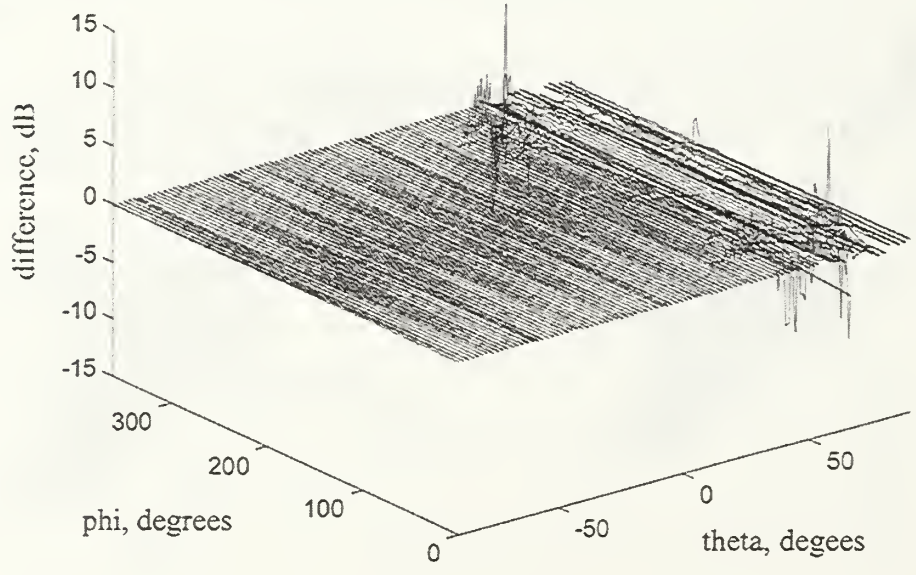

Figure B3: Difference between rotor and no rotor scattering (275 MHz, 30 degree rotor position).

Appendix C: Detection Range

The antenna gain affects the received signal level at the ground. Given a set of communication system parameters, the maximum slant range to a ground emitter can be computed. The geometry is shown in Figure C1. For a location on the ground $(x, y, 0)$ the following quantities can be computed for the helicopter at an altitude h:

$$R = \sqrt{x^2 + y^2 + h^2} = h / \cos\theta, \quad x = R\sin\theta\cos\phi, \quad y = R\sin\theta\sin\phi$$

Assume that the ground emitter has effective radiated power (ERP) of

$$\text{ERP} = P_t G_t = P_o |\sin\theta|$$

where P_o is a constant. The $\sin\theta$ shape is typical of a short monopole, which generally cannot be well matched. For example, it would not be unusual for the peak gain of the transmitting antenna to be –5 dBi (relative to an isotropic source) at 100 MHz. If the transmitter power is 1 W then

$$P_t G_t = (1)(0.316)|\sin\theta| = 0.316|\sin\theta|.$$

The received power at the antenna terminals is computed using the Friis transmission formula [C1,C2]

$$P_r = \frac{P_t G_t(\theta) G_r(\theta,\sigma)\lambda^2}{(4\pi R)^2}$$

Assuming thermal noise due to an effective system noise temperature T_e, the noise power is $P_n = kT_e B_n$ where B_n is the noise bandwidth. Therefore, the signal-to-noise ratio (SNR) is

$$\text{SNR} = \frac{P_r}{P_n} = \frac{P_t G_t(\theta) G_r(\theta,\phi)\lambda^2}{(4\pi R)^2 k T_e B_n}$$

If the minimum SNR for detection is denoted as $\text{SNR}_{\min}$ then the corresponding maximum detection range is

$$R_{\max} = \sqrt{\frac{P_t G_t(\theta) G_r(\theta,\phi)\lambda^2}{(4\pi)^2 k T_e B_n \text{SNR}_{\min}}}$$

The receiver antenna gain for the antenna on the helicopter $G_r(\theta,\phi)$ is computed by APATCH. However, the gain calculation assumes a lossless matched antenna (i.e., it is actually the directive gain that is calculated). Losses in the actual antenna will decrease the gain from the lossless value computed by APATCH.

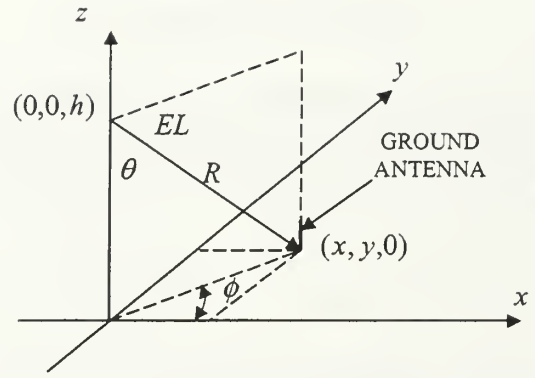

Figure C1: Geometry for computing detection range.

The Friis equation can be used to compute the maximum slant range for a given minimum SNR for detection. Assume the following parameters:

- transmitter power, 1W
- transmitter antenna gain, linear function in dB from -5 dBi at 100 MHz to 0 dBi at 1000 MHz[1]
- effective noise temperature of the receiver, 1000 K, noise figure, $F = 1 + T_e / T_o = 4.45$
- noise bandwidth, 10 kHz
- minimum SNR for detection is 10 dB

The maximum slant range at 100 MHz ($G_t = -5\,\text{dBi}, \lambda = 3\,\text{m}, G_r = 0\,\text{dBi}$) is

$$R_{\max} = \sqrt{\frac{(1)(0.316)(3)^2}{(4\pi)^2\left(1.38\times10^{-23}\right)(1000)\left(10\times10^{3}\right)(10)}} = 3{,}614 \text{ km}$$

and at 1000 MHz ($G_t = 0\,\text{dBi}, \lambda = 0.3\,\text{m}, G_r = 0\,\text{dBi}$):

$$R_{\max} = \sqrt{\frac{(1)(1)(0.3)^2}{(4\pi)^2\left(1.38\times10^{-23}\right)(1000)\left(10\times10^{3}\right)(10)}} \approx 640 \text{ km}$$

The results are unrealistic in that the maximum range would probably be limited to just over the radio horizon. At 5000 feet this would be about $R_{\max} \approx \sqrt{2h} = 100$ mi or 161 km ($R_{\max}$ is in miles, h is in feet [C3]).

References:

[C1] J. D. Kraus, *Antennas*, McGraw-Hill, 1950.
[C2] C. Balanis, *Antenna Theory*, Wiley, 1982.
[C3] R. Collin, Antennas and Radiowave Propagation, McGraw-Hill, 1985.

[1] This is typical of the performance of a "rubber ducky" antenna in this frequency band.

INITIAL DISTRIBUTION LIST

1. Defense Technical Information Center 2
   8725 John J. Kingman Road, Suite 0944
   Ft. Belvoir, VA 22060-6218

2. Dudley Knox Library 2
   Naval Postgraduate School
   411 Dyer Road
   Monterey, CA 93943-5101

3. Research Office, Code 09 1
   Naval Postgraduate School
   589 Dyer Road
   Monterey, CA 93943-5138

4. Chairman, Code EC 1
   Naval Postgraduate School
   833 Dyer Road
   Monterey, CA 93943-5121

5. D. C. Jenn, Code EC/Jn 5
   Department of Electrical and Computer Engineering
   Naval Postgraduate School
   833 Dyer Road
   Monterey, CA 93943-5121

6. Bert Donaldson 2
   SPAWAR PMW 189-4
   4301 Pacific Highway
   San Diego, CA 92110

7. George Alberti 1
   National Security Agency
   9800 Savage Road
   Suite 6435, Org S14
   Ft. Meade, MD 20755

8. David Kim 1
   National Security Agency
   9800 Savage Road
   Suite 6435, Org S14
   Ft. Meade, MD 20755

9. LCDR Michael Schachterle 1
Department of the Navy
Cruise Missiles and Joint Unmanned Aerial Vehicles
NAVY Unmanned Aerial Vehicles - PMA263
47123 Buse Road, Unit #IPT
Patuxent River, MD 20670-1547

10. Nils A. Anderson 1
Department of the Navy
Cruise Missiles and Joint Unmanned Aerial Vehicles
NAVY Unmanned Aerial Vehicles - PMA263-3
47123 Buse Road, Unit #IPT
Patuxent River, MD 20670-1547